SCUOLA DI DOTTORATO
UNIVERSITÀ DEGLI STUDI DI MILANO-BICOCCA

School of Medicine and Surgery

PhD program in Neuroscience - Cycle XXXIV

Curriculum in Experimental Neuroscience

Selected Growth Hormone Secretagogues (GHSs) as disease modifiers in models of neurodegenerative diseases and Amyotrophic Lateral Sclerosis: a proof-of-concept study

Meanti Ramona

Reg. N.: 751852

Tutor: Lucio Tremolizzo

Co-Tutor: Antonio Biagio Torsello

Coordinator: Rosa Maria Moresco

ACADEMIC YEAR 2020/2021

To myself:

Always! Never lose “joie de vivre”

Table of contents

ABSTRACT

Amyotrophic lateral sclerosis (ALS) is an idiopathic motor neuron disease characterized by progressive degeneration of upper and lower motor neurons, resulting in muscle atrophy, limb paralysis, and finally respiratory failure. About 5–10% of ALS is familial and among them the 20% show mutations in superoxide dismutase 1 (SOD1), which have been characterized to induce a toxic gain of function of enzyme. The pathophysiology of ALS seems multifactorial, involving excitotoxicity, mitochondrial dysfunction and dysregulation, impaired axonal transport, intracellular protein aggregates, and genetic mutations but remain largely unknown. Riluzole, an inhibitor of glutamate release, and edaravone, a free-radical scavenger, are the only two drugs approved for ALS. Symptomatic treatments remain the cornerstone of management for patients with ALS. There is a strong need to characterize new treatments not only alleviate symptoms, but also improve survival and quality of life.

In this research we focused on the potential therapeutic effects of three drugs belonging to the family of the growth hormone secretagogues (GHSs). The GHSs are endowed with several endocrine and extraendocrine effects that are at least in part mediated by binding to GHS-R1a, the receptor of ghrelin. In particular, we have selected three well-characterized compounds: (i) hexarelin, an agonist of GHS-R1a, which exerts cyto-protective effects at the mitochondrial level in cardiac and skeletal muscles, and could have neuroprotective effects; (ii) JMV2894, an agonist of GHS-R1a, which stimulates Ca^{2+} mobilization in vitro and growth hormone release in vivo, and modulates mitochondria functioning and ROS production; (iii) EP80317, an antagonist of GHS-R1a and agonist of CD36, which modulate the production of inflammatory cytokines, exerts anticonvulsant activities and has cardio-protective effects.

The first objective of this study was to determine the cyto-protective capacity of hexarelin, JMV2894 and EP80317 in Neuro-2A cells subjected to oxidative stress. Neuro-2A cells were incubated for 24 h with H_2O_2 or with the combination of H_2O_2 and GHSs to monitor their effects through the quantification of (i) cell viability, (ii) NO_2^- release, (iii) changes in cellular morphology, (iv) apoptotic response and (v) MAPK and Akt pathways. In a second group of experiments, the same treatments were used on SH-SY5Y human neuroblastoma cells overexpressing the wild type (WT) SOD1 enzyme, or the $SOD1^{G93A}$ mutated protein. In both Neuro-2A and SH-SY5Y cell lines H_2O_2 induced in a dose-dependent manner (i) a reduction of cell viability, (ii) the activation of caspase-3, caspase-

7 and Bax, and (iii) a down-regulation of the anti-apoptotic Bcl-2. Moreover, H_2O_2 induced an increased production of NO_2^- and drastic changes in cellular morphology (loss of cell/field, de-ramification and reduction of process length, loss of cellular complexity and shape, as well as reduction of cell size). In Neuro-2A and SH-SY5Y cells, both hexarelin and JMV2894 were effective in antagonizing the effects of H_2O_2 by (i) increasing cell viability, (ii) reducing NO_2^- release and (iii) restoring cell morphology. Hexarelin and JMV2894 reduced mRNA levels of caspase-3 and caspase-7, and modulated mRNA levels of the BCL-2 family. Hexarelin and JMV2894 also modulated the expression of mitogen-activated protein kinase (MAPK) ERK 1/2 and p38, and phosphoinositide-3-kinase (PI3K)/Akt, two pathways primarily involved in the regulation of cell growth, differentiation, and response to cellular stress, whose activation contribute to neuronal dysfunction. The specificity of GHS effects is demonstrated by the absence of significant effects of EP80317 treatments on all the previous parameters in the previous three cellular models. In SH-SY5Y WT cells, hexarelin was more effective than JMV2894 in antagonizing the effects of H_2O_2. Interestingly, In SH-SY5Y $SOD1^{G93A}$ cells, the effects of hexarelin and JMV2894 were blunted compared to those measured in SH-SY5Y WT cells. It is possible that in these cells the levels of oxidative stress induced by the combination of H_2O_2 treatment and $SOD1^{G93A}$ mutation was too high to be counteracted by hexarelin and JMV2894 treatments.

In the next series of experiments, we have studied the role of cellular communication between neurons and glial cells in modulating the onset and progression of neurodegeneration. In fact, the involvement of microglia in ALS exacerbation and propagation is still under debate. To this aim, we have treated N9 microglial cells with hexarelin or JMV2894 for 48 h and then isolated extracellular vescicles (EVs) from the conditioned culture media. Both GHSs treatment induced a higher release of EVs from N9 cells. EVs were subsequently incubated for 24 h with SH-SY5Y WT and $SOD1^{G93A}$ in presence of H_2O_2. In SH-SY5Y WT cells, EVs-derived from hexarelin-treatment significantly inhibited the increase of levels of caspase-7 and Bax induced by H_2O_2, whereas for caspase-3 there was a trend toward a reduction. EVs-derived from JMV2894-treated N9 cells significantly inhibited the increase of caspase-3 and caspase-7 induced by H_2O_2, and a trend toward a reduction for Bax levels. In SH-SY5Y $SOD1^{G93A}$, EVs derived from hexarelin and JMV2894 treatments significantly reduced the mRNA of Bax compared to H_2O_2-treated cells, but did not exert any beneficial effects to other apoptosis marker. These preliminary results suggest that EVs released from cells stimulated with specific

GHSs may have potential beneficial effects for neuronal survival and could be a promising strategy for the modulation of oxidative stress.

In conclusion, our results demonstrate neuroprotective and anti-apoptotic effects of hexarelin and JMV2894, suggesting that new GHS analogues could be developed for their neuroprotective effects. Further studies are needed to better investigate the anti-inflammatory and neuroprotective effects of EVs-derived from conditioned media of microglial cells stimulated with selected GHSs.

INTRODUCTION

1. Amyotrophic Lateral Sclerosis

Amyotrophic Lateral Sclerosis (ALS) was first identified in 1874 by the French neurologist Jean-Martin Charcot, who described it as a severe adult pathology due to progressive degeneration of motor neurons in the primary cortex, corticospinal tract and spinal cord (1). ALS has heterogeneity at the clinical, genetic and neuropathological levels, and results in severe muscle atrophy, paralysis, and eventual respiratory insufficiency, which typically leads to death within 3-5 years from the onset (2,3).

To date, ALS is recognized as a fatal multisystem neurodegenerative disorder that belongs to Motor Neuron Disease (MND), and characterized by rapid deterioration of both upper and lower motor neurons. Upper motor neurons (UMN) originate from the cerebral cortex, extend towards the periphery and reach the spinal cord, establishing contact with lower motor neurons. Lower motor neurons (LMN), starting from the anterior horns of the spinal cord, extend and reach the muscles, with which make contact in the neuromuscular plate (Figure 1). Being responsible for the voluntary muscles' contraction primarily involved in movement, swallowing, speaking and breathing, motor neurons degeneration in ALS spared only sensory, sexual, sphincter and, in most cases, cognitive functions.

Therefore, the term "amyotrophic" referred to (i) muscle atrophy, (ii) loss of strength, and (iii) appearance of fasciculation, which are typical manifestations of LMN pathologies. Indeed, "lateral sclerosis" is attributed to (i) hardness of the lateral portion of the spinal cord on palpation of autopsy specimens, (ii) hyperactive tendon reflexes, and (iii) Hoffman and Babinski signs, characteristic of the UMN diseases (1).

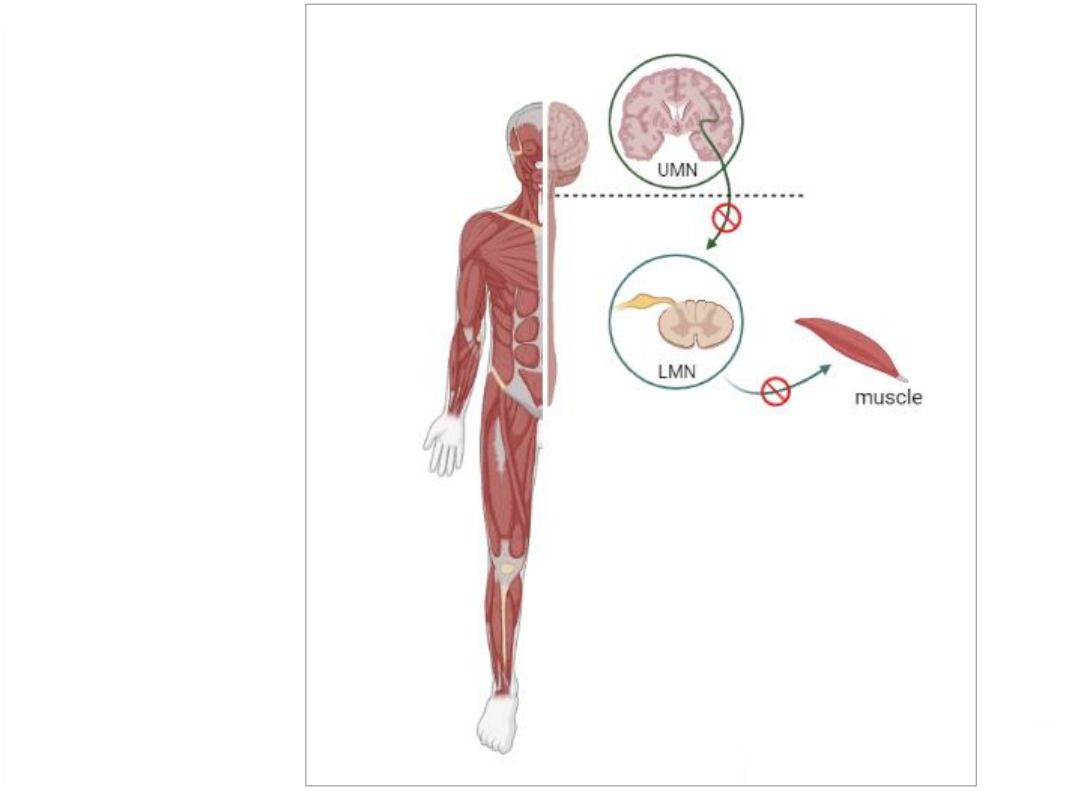

Figure 1. *The role of upper and lower motor neurons in ALS.*
ALS patients present signs of both upper motor neurons (UMN) and lower motor neurons (LMN) degeneration, which leads to progressive muscles weakness and atrophy. Created with BioRender.com.

1.1 Epidemiology

ALS worldwide incidence is estimated at 1.6 cases per 100.000 persons annually but with significant geographical, ethnical and gender differences (3–5). For example, in Europe the estimated prevalence is 10-12 per 100.000 persons per year, where established risk factors are age, family history, higher latitudes, cigarette smoking, and accumulation of heavy metals (4,6,7). In Japan, Guam and South West New Guinea, ALS prevalence is 50-100 times higher, probably due to environmental factors, such as the consumption of neurotoxic non-protein amino acid β-methylamino-L-alanine (BMAA) contained in the seeds of cycad *Cycas micronesica* (8).

The average age of onset varies between 60 and 75 years of age, and typically peaks at 64 years old in Caucasian adults. Only 5% of cases are under the age of 30 (4,8,9). Moreover, the lifetime risk of ALS is higher for men than for women (1.5:1), probably due to protective hormonal factors in women (10–12).

Finally, some evidences have demonstrated that athletes appear to have a higher risk of developing the disease than the general population, probably due to the greater likelihood of trauma, and as a result of exogenous factors that could alter some genes related to physical

activity, like *ciliary neurotrophic factor*, *leukaemia inhibitory factor* and *vascular endothelial growth factor* (13,14).

1.2 Aetiology

ALS is categorized in two different forms: the most common sporadic (sALS, 90-95%), which has no obvious genetically inherited component and the familial-type (fALS, 5-10%), associated mainly to genetic autosomal dominant inheritance and rarely to recessive and X-linked ones (15). Even though sALS and fALS are clinically indistinguishable and both exhibit the same pathogenetic mechanisms, among which oxidative stress, glutamate excitotoxicity, mitochondrial dysfunction, protein aggregation, altered axonal transport and inflammation (16), fALS occurs due to mutations in specific genetic loci (8) (Figure 2).

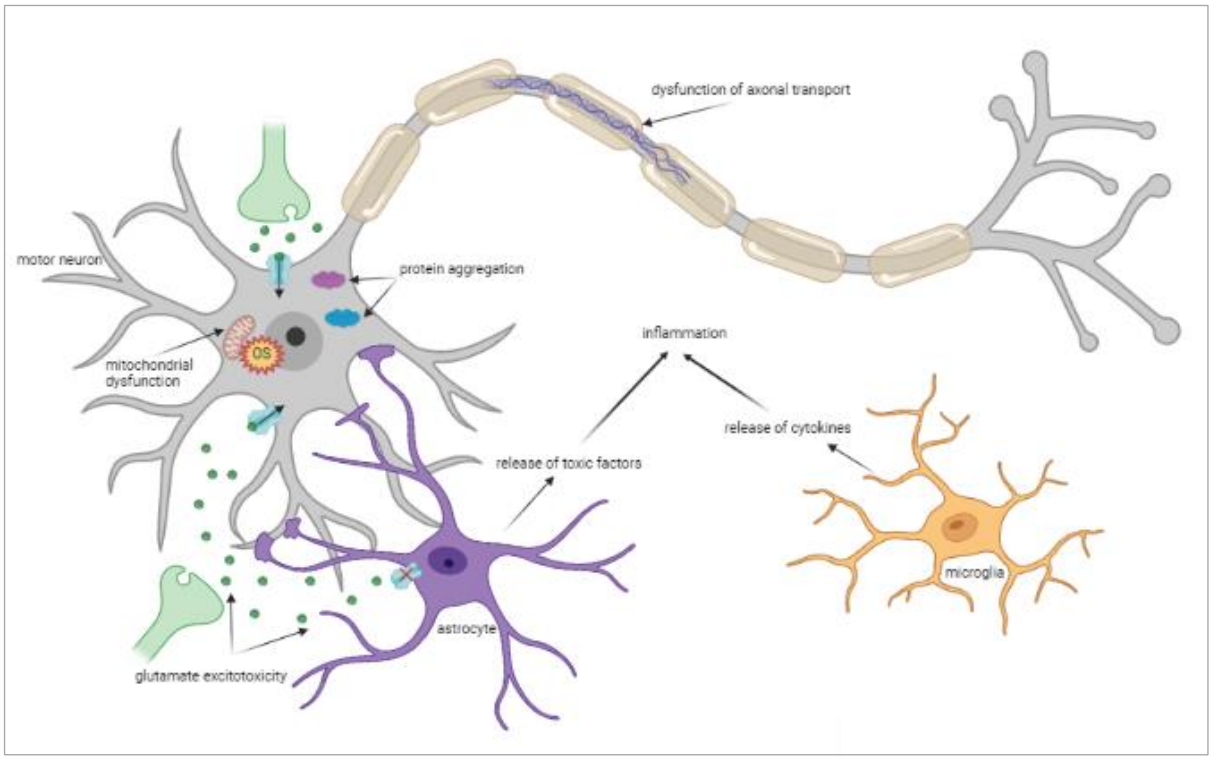

Figure 2. *Pathogenetic mechanisms mediating neurodegeneration in ALS.*
The underlying mechanisms of neurodegeneration in ALS are multifactorial and include (i) glutamate excitotoxicity, (ii) oxidative stress and mitochondria dysfunction, (iii) aggregates of mutant misfolding proteins, (iv) impaired axonal transport, and (v) release of pro-inflammatory cytokines by activated astrocytes and microglia cells. Created with BioRender.com.

1.2.1 Molecular mechanisms

The pathophysiological mechanisms underlying the development of ALS are multiple and multifactorial, with the involvement of a complex interaction of genetic, molecular and environmental factors.

The main hypotheses for molecular pathogenesis of ALS include damage linked to glutamate excitotoxicity, structural and functional abnormalities of mitochondria, free radical-mediated oxidative stress, cytoplasmic aggregates of misfolded proteins, impaired axonal structure and transport defects (8,16,17).

1.2.1.1 Glutamate excitotoxicity

Glutamate excitotoxicity was one of the first hypotheses proposed as a pathogenic mechanism of ALS (18,19). Glutamate is the predominant excitatory neurotransmitter of CNS, synthesized in the presynaptic terminals and stored in synaptic vesicles.

By presynaptic neuron depolarization, vesicles release glutamate in the synaptic cleft. Here, this neurotransmitter acts on different receptors on postsynaptic neurons, such as α-amino-3-hydroxyl-5- methyl-4-isoxazole-propionate (AMPA) and N-methyl-D-aspartate (NMDA) receptors. The depolarization of membrane after activation of neuronal glutamate receptors activates voltage-dependent calcium channels, allowing calcium (Ca^{2+}) entry and generation of free radicals (20). The signal is interrupted by glutamate removal from synaptic cleft by excitatory amino acid transporters (EAATs) on glial and neuronal cells (21). This procedure is finely regulated to avoid excitotoxicity that occurs when glutamate receptors are excessively stimulated, which could result in degeneration and death of the involved neurons (22). Glutamate receptors and transporters could have a key role in the excitotoxic mechanism of ALS. In fact, the level of EAATs is found to be largely reduced in the motor cortex and in the spinal cord of ALS patients (23). In particular, aberrant mRNA of the isoform 2 of the astroglial glutamate transporter (EAAT2) was subsequently detected in ALS patients, explaining the reduction in EAAT2 protein levels (24). Low EAAT2 expression leads to an increase of extracellular concentration of glutamate, with a consequent overstimulation of glutamate receptors and neuronal degeneration (8).

In vitro studies have demonstrated that administration of glutamate uptake blockers, i.e. threohydroxyaspartate (THA), mimics the chronic excitotoxicity mediated by defective glial and/or neuronal glutamate transport, as in ALS (25,26). To ascertain whether the loss of functional EAAT2 in ALS was a primary cause of motor neuron degeneration, Guo and colleagues generated a transgenic mutant SOD1 mice overexpressing EAAT2

(EAAT2/G93A double transgenic mice). In this study, mice with an increased EAAT2 expression showed a delay in motor neuron degeneration and disease progression, but there was no increase in survival, compared to $SOD1^{G93A}$ mice (27). Moreover, the vulnerability of motor neurons to glutamate excitotoxicity in ALS may be due to higher membrane permeability for Ca^{2+}, caused by a continue activation of AMPA receptors (28). Different studies have demonstrated that the mRNA of the subunit 2 of glutamate AMPA receptors (GluR2) could have an abnormal editing, contributing to neuronal death in ALS patients (29). To demonstrate this, the use of AMPA receptor selective blockers lead to a reduction of neuronal death (28).

Given the major role of glutamate in the pathogenesis of the disease, the Food and Drug Administration (FDA) has approved riluzole, a drug that inhibits the release of glutamate through the activation of voltage-gated sodium (Na^{2+}) channels on glutamate nerve terminals.

1.2.1.2 Mitochondrial defects

The key role of mitochondria in cell survival, metabolism, intracellular energy production, Ca^{2+} homeostasis and control of apoptosis is widely recognized (30,31).

Increasing observations suggest that mitochondria morphological and biochemical abnormalities could correlate with ALS pathogenesis. This mitochondrial hypothesis has gained more relevance from 2014 after the identification, both in *in vitro* and *in vivo* models of early pathology, of mutations in proteins encoded mitochondrial DNA (mtDNA), such as the protein CHCHD10, which determines the loss of crests of the inner membrane and consequent alteration of mitochondrial functionality (32,33).

In fact, histopathological observations have disclosed that mitochondria dysfunction could correlate with abnormalities in their morphology: fragmented network, swelling, augmented cristae in soma and proximal axons, and vacuolization were found in mitochondria from ALS patients and transgenic mouse models (8,34,35).

Interestingly, morphological alterations and defective role of mitochondria were not confined only to CNS, but also in skeletal muscles and in spinal motor neurons of ALS patients (36,37). In fact, in both skeletal muscle biopsies and in spinal cord of ALS patients have been reported ATP production deficits due to the alteration in the complex I, II, III and IV of the electron transport chain (38).

These defects cause damage to endoplasmic reticulum, determining alteration in intracellular Ca^{2+} homeostasis: higher Ca^{2+} concentrations lead to lowering of ATP production and to an increase in reactive oxygen species (ROS).

Finally, chronic mitochondrial alterations induce apoptosis, by the cytochrome C release and the pro-apoptotic gain-of-function of B-cell lymphoma 2 (Bcl-2) family proteins, which directly contribute to neuromuscular degeneration and neuronal dysfunction (39) (Figure 3).

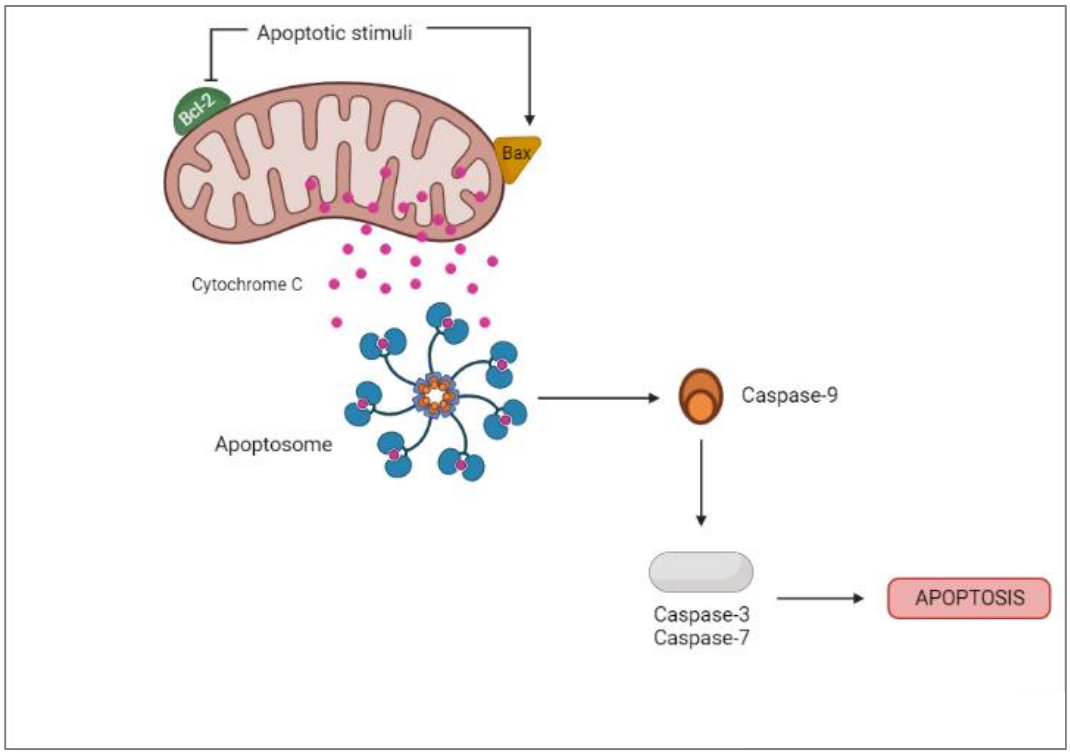

Figure 3. *Mitochondrial involvement in apoptosis pathway.*
In response to apoptotic stimuli, pro-apoptotic proteins, such as Bax, induce the permeabilization of the outer mitochondrial membrane, leading to release of cytochrome c from the mitochondrial intramembranous space. Cytochrome c is then bound to Apaf-1, resulting in the formation of a multimeric Apaf-1/cytochrome c complex that recruits procaspase-9 forming the apoptosome. Consequently, procaspase-9 is activated through proteolysis, and subsequently dissociated from this complex. Once activated, caspase-9 activates executioner caspases-3 and/or -7, which eventually lead to apoptosis. Created with BioRender.com

1.2.1.3 Free radical-mediated oxidative stress

A direct consequence of mitochondrial dysfunction is oxidative stress (OS), determined by the imbalanced ratio of reactive oxygen species (ROS) and free radicals produced by the normal metabolism of oxygen (O_2), and the antioxidant cellular mechanisms (30,40). All different species of ROS [hydrogen peroxide (H_2O_2), superoxide anion (O_2^-), highly reactive hydroxyl radical (HO•)], and the reactive nitrogen species (RNS) [nitric oxide (NO), nitric monoxide (NO•)], contribute to the deterioration of cell DNA, RNA, lipids and proteins (41).

Oxidative stress is largely involved in aging and neurodegenerative disorders (42) and could promote the formation of unfolded protein aggregates, increase the oxidation of proteins and lipids, and became a cause-consequence of mitochondria abnormalities (43). Indeed, elevation of free radicals and oxidative damage were found in post mortem-tissues (44), CSF, serum and urine of ALS patients (8). In addition, *in vitro* culture of ALS patient's fibroblast shows increased sensitivity to oxidative damage controls (45). However, from current knowledge, oxidative stress cannot be the only pathogenetic determinant of ALS, but it likely participates in a vicious circle that involves several molecular pathways.

Given the role of mitochondrial dysfunction and oxidative stress in the pathogenesis of the disease, edaravone has been proposed as a potential drug for the treatment of ALS, even though actually has been proven the lack of its effectiveness: benefits are not superior to its risks.

1.2.1.4 Cytoplasmic aggregates of misfolded proteins

Another cause involved in ALS onset is deposits of protein aggregates. The formation of cytoplasmic aggregates occurs as (i) a primary consequence of mutations at gene level, or (ii) following post-translational modifications of protein. There is a direct correlation between the degree of conformational instability of the protein induced by the mutations and the rate of clinical progression of the disease; in fact, at the late stages of the disease, dense aggregates of ubiquitinated proteins are visible, often associated with eosinophilic aggregates described as *Bunina bodies* (46,47).

The main proteins involved in the formation of inclusion bodies are (i) superoxide dismutase 1 (SOD1), (ii) trans-active response (TAR) DNA-binding protein 43 (TDP43) and (iii) fused in sarcoma/translocated in liposarcoma (FUS/TLS). Normally localized in the nucleus, altered proteins translocate to cytoplasm of motor neuron, neuron, glial cells and spinal cord of ALS patients, where clustered in inclusion bodies (48–50).

1.2.1.5 Impaired axonal transport

Motor neurons are highly polarized cells, endowed of long axons that transmit nervous impulses and transport organelles, RNAs, proteins and lipids. Defects in anterograde and retrograde (51) axonal transport are one of early pathophysiological events in ALS. Starting from the observation of specimens from post-mortem ALS patients, different studies have demonstrated an abnormal accumulation of neurofilaments, mitochondria, lysosomes and axonal spheroids in both proximal and distal axons of motor neurons (51,52). Subsequent in vitro and in vivo studies, using models of ALS, revealed a reduction in slow and fast axonal

transport and, consequently, significant spinal motor neurons loss, lower myelinated fibre densities and muscle pathology (16,53).

An efficient axonal transport for the trafficking and docking of mitochondria is particularly relevancy in areas with high demand of ATP and Ca^{2+} homeostasis. In fact, different studies have demonstrated that mitochondrial damage combined with reduced axonal transport are an important feature in ALS pathology (54).

1.2.2 Environmental factors

Different epidemiologic studies have suggested that environmental toxins, like chemicals, heavy metals and electrical magnetic fields could be a potential contributing cause of ALS (8).

The exposure to pesticides (i.e., insecticides, fungicides, herbicides and rodenticides), fertilizers and formaldehyde, principally in professional farmers, through oral, dermal and inhalation routes, can cause neurological damage, through the inducement of oxidative stress, mitochondrial dysfunction and neuronal loss (55).

The role of heavy metals, such as lead, selenium and mercury in motor neuron degeneration has been widely explored (55). High concentration of lead, especially in welders, determines an increase in ALS risks, because of lead's ability to substitute intracellular calcium and to led mitochondrial damage, oxidative stress, and strengthen glutamate's excitotoxicity (56). The potential role of selenium in developing ALS is demonstrated by the presence of seleniferous drinking water in South Dakota and in Northern Italy and the increase in ALS cases in these areas (57). Finally, evidence that mercury is involved in ALS pathogenesis is based only on animal and cell cultures studies, in fact there is no evidence of it in epidemiological case-control studies (55,57).

The most consistent non-genetic risk factor for ALS and link between chemicals and heavy metals is cigarette smoking: cigarettes contained heavy metals and formaldehyde and has been found to increase the probability of developing ALS through inflammation, oxidative stress, and neurotoxicity. Moreover, ALS risk is highest with start smoking younger age (8).

Lastly, *in vitro* and *in vivo* studies have demonstrated that radiation and extremely low-frequency electromagnetic fields (ranging from 3 Hz to 3,000 Hz) produce oxidative stress and disables cellular antioxidant properties, but further studies are needed, since only low level of association has been found (58).

1.2.3 Genetics of ALS

As mentioned above, sALS and fALS have similar clinical and pathological presentation, even though fALS mainly occurs due to mutations in specific genetic loci and inheritance, which follows Mendelian pattern, is primarily autosomal dominant (8).

Therefore, besides molecular and environmental factors' role in ALS onset, genome-wide association studies (GWAS), next-generation sequencing (NGS) and other classical genetically analysis have allowed to map the genes whose alterations are involved in ALS (59). Indeed, the current diagnosis of ALS includes the gene analysis of the four most robust and common genes: C9*orf*72, SOD1, TARDBP and FUS. Moreover, some studies have reported also the identification of susceptibility variants that further increased the risk of ALS and disease progression (including ATXN2, UNC13A, ANG, SMN1 and SMN2 genes) (60).

1.2.3.1 ALS1: SOD1 mutations

The superoxide dismutases (SOD) are ubiquitous antioxidant enzymes that defend cells against oxidative stress (OS), reactive oxygen species (ROS) and superoxide anion radicals through the dismutation of superoxide anions.

At present, in mammals have been identified three distinct and highly compartmentalize SOD isoforms: (i) SOD1, or Cu/Zn-SOD, (ii) SOD2, or Mn-SOD, and (iii) SOD3, or EC-SOD.

SOD2 is a mitochondrial enzyme, existing in a tetramer form, which requires manganese to catalyze reactions, while SOD3 is the extracellular enzyme most recently characterized, constitute of a copper and zinc-containing homodimer (61).

SOD1 was the first enzyme to be characterized and is found almost exclusively in intracellular cytoplasmic spaces. The human SOD1 gene consists of 5 exons and 4 introns, is localized in 21q22.1 chromosome and encodes for the superoxide dismutase Cu/Zn, a protein of 153aa (16kDa).

The evidence of mutations in chromosome 21 in ALS pathogenesis arose in 1991, and was confirmed by Rosen in 1993 (62). Nowadays, it is known that SOD1-related ALS (ALS1) determines the 20% of fALS and the 5% of sALS, and more than 170 mutations in this gene have been identified (63). All mutations are autosomal dominant, with the exception of the D90A, which can occur in both dominant and recessive forms.

Mutations of SOD1 cause oxidative stress and mitochondria alterations, modifications of gene expression and abnormal protein interactions, formation of intracellular aggregates of

misfolded SOD1 peptide, neurofilaments disorganization and cytoskeletal abnormalities, glutamate excitotoxicity, activation of caspases and apoptosis (64).

Moreover, different mutations in SOD1 cause different syndromes which differ in penetrance, age of disease onset, survival and clinical manifestation (65).

The A4V mutation is the most common in North America (50% of patients), and is associated with patient death within 12 to 18 months after symptom onset (66). D90A is the most frequent in Europe, especially in northern Sweden and Finland; it shows both autosomal dominant and recessive patterns of inheritance in different populations, has slowly progressive course, and may cause ataxia (38). I113T is the mutation most common in United Kingdom, characterized by late onset, long survival and reduced penetrance (67). G93A is a relative rare mutation, but it has been studied very thoroughly by *in vitro* models of fALS, obtained by transfecting, for example, human neuroblastoma cell line SH-SY5Y with plasmids directing constitutive expression of either wild-type SOD1 or the mutant $SOD1^{G93A}$ (68), and by the transgenic mouse model $SOD1^{G93A}$ (69). *In vitro* models expressing $SOD1^{G93A}$ show a significant decrease in mitochondrial membrane potential, a major cellular source of H_2O_2 and net increase of cytosolic Ca^{2+}, which results in mitochondrial swelling, uncoupling of oxidative phosphorylation, lipoperoxidation, nitric oxide (NO)-derived radicals and apoptosis (68).

At first, the impair antioxidant enzyme activity, which in turn led to accumulation of toxic superoxide anions, was supposed to be the mechanism underlying motor neuron damage caused by $SOD1^{G93A}$. This theory was dismissed experimentally by the use of "knock-out" mice for $SOD1^{G93A}$, which does not cause any motor neuron abnormalities.

Therefore, rather than a loss-of-function, SOD1 mutations would seems to cause a gain-of-function: in fact, mutations in the SOD1 gene change the affinity of enzyme to the natural and abnormal substrates, impair ability of enzyme to bind zinc or increase the enzyme aggregation in neurons (61). Despite this, the mechanism by which mutated SOD1 causes toxicity has not yet been fully understood.

Table 1. Genetic aetiology of ALS

Type	Gene	Gene Name	Chromosomal location	Protein	Form	Age	Site of Onset	Variant type	Characteristics
ALS1	SOD1	Superoxide Dismutase 1	21q22.11	Superoxide dismutase [Cu-Zn]	fALS+saLS	Adult	Spinal>Bulbar>FTD	Substitution Insertion Deletion Polymorphism Frameshift	The SOD1 gene encodes superoxide dismutase-1, a major cytoplasmic antioxidant enzyme that metabolizes superoxide radicals to molecular oxygen and hydrogen peroxide, thus providing a defense against oxygen toxicity.
ALS2	ALS2	alsin Rho guanine nucleotide exchange factor ALS2	2q33.1	Alsin	fALS	Juvenile	Spinal>Bulbar	Substitution Deletion	Alsin interacts with the chromosome 21 open reading frame 2 (C21orf2) in DNA damage repair. Variants in ALS2 can be causative of a number of juvenile/infantile onset MNDs including Infantile-onset ascending hereditary spastic paralysis, Juvenile primary lateral sclerosis and Autosomal recessive juvenile amyotrophic lateral sclerosis. These phenotypes are inherited in an autosomal recessive manner.
ALS3	-	-	18q21	-	fALS	Adult	-	-	ALS3 is a genetic locus spanning 8Mb on chromosome 18q21, identified using linkage analysis in a European family with autosomal dominant adult-onset ALS. There has been no gene identified at this locus.
ALS4	SETX	senataxin	9q34.13	Helicase senataxin	fALS+saLS	Juvenile	-	Substitution	SEXT mutations cause juvenile ALS, which symptoms appear during adolescence.
ALS5	SPG11	SPG11 vesicle trafficking associated, spatacsin	15q21.1	Spatacsin	fALS	Juvenile	Spinal+Bulbar	Substitution Insertion Deletion Frameshift	Mutations in SPG11 determine alteration in endolysosomial system and loss of motort neuron assons. This juvenile form of ALS has onset in the first decade of life.
ALS6	FUS	FUS RNA binding protein	16p11.2	RNA-binding protein FUS	fALS+saLS	Adult	Spinal>Bulbar>Other	Substitution Deletion Frameshift Insertion	FUS encodes for a nucleoprotein implicated in the metabolism of DNA and RNA and which is involved in tumongenesis.
ALS7	-	-	20p13	-	fALS	-	-	-	ALS 7 is a genetic locus on chromosome 20p13, identified using linkage analysis. There has been no gene identified at this locus.
ALS8	VAPB	VAMP associated protein B and C	20q13:32	Vesicle-associated membrane protein-associated protein B /C	fALS	Adult	Spinal	Substitution	ALS8 is determined by eterozygous mutations in VAPB gene located in chromosome 20q13.3, and includes both sexes equally. Alteration in vescicles-associated membrane proteins led to the formation of intracellular aggregates, altered axonal transport and motor neuron degeneration.
ALS9	ANG	angiogenin	14q11.2	Angiogenin	fALS+saLS	Adult	Spinal>Bulbar	Substitution Polymorphism	ALS9 is a genetic locus on chromosome 14q11.2, whose mutations mainly affects European individuals.
ALS10	TARDBP	TAR DNA binding protein	1p36.22	TAR DNA-binding protein 43	fALS+saLS	Adult	Spinal>Bulbar	Substitution	TARDBP encode for TDP-43, a RNA-DNA-binding protein involved in the regulation of gene expression and splicing. Inclusion bodies of TDP-43 had been found in autopsy specimens.
ALS11	FIG4	FIG4 phosphoinositide 5-phosphatase	6q21	Polyphosphoinositide phosphatase	fALS+saLS	Adult	Bulbar>Spinal	Substitution	Also known as SAC3, FIG4 is located on the cytosolic surface of late endosome membranes and regulates lipid signaling. Mutations in this gene cause cell vacuolation.
ALS12	OPTN	optineurin	10p13	Optineurin	fALS+saLS	Adult	Spinal>Bulbar>Other	Substitution Deletion Frameshift Silent	OPTN mutations, both homozygous and heterozygous, were detected in Japanese patients born from consanguineous marriages.
ALS13	ATXN2	ataxin 2	12q24.12	Ataxin-2	sALS	Adult	Spinal>Bulbar>Other	Repeated expansions	Intermediate-length (CAG) expansions (encoding 27–33 glutamines, polyQ) represent a risk factor for ALS, increasing the risk of about 10 fold, and are a modifier of ALS clinical presentation, being associated to a spinal phenotype and a more aggressive clinical course.

Type	Gene	Gene Name	Chromosomal location	Protein	Form	Age	Site of Onset	Variant type	Characteristics
ALS14	VCP	valosin containing protein	9p13.3	Transitional endoplasmic reticulum ATPase	fALS	Adult	Spinal>Bulbar	Substitution	ALS14 is associated with the formation of inclusion body myopathy, early onset of Paget's disease and frontotemporal dementia.
ALS15	UBQLN2	ubiquilin 2	Xp11.21	Ubiquilin-2	fALS+sALS	Adult	FTD>Spinal>Bulbar	Substitution	ALS15 is caused by an X-linked dominant mutation in UBQLN2 on chromosome Xp11. The ubiquilin-2 protein regulates the degradation of ubiquitinated proteins and its mutation causes the formation of aggregates.
ALS16	SIGMAR1	sigma non-opioid intracellular receptor 1	9p13.3	Sigma non-opioid intracellular receptor 1	fALS	-	Spinal	Substitution	Sigma 1 receptor (Sig1R), a gene product of SIGMAR1, is a chaperone protein highly expressed in spinal motor neurons and specifically localized at an interface of the endoplasmic reticulum (ER) and mitochondria. SIGMAR1 regulates various functions including lipid metabolism, autophagy initiation, and $Ca2+$ transfer from ER to mitochondria.
ALS17	CHMP2B	charged multivesicular body protein 2B	3p11.2	Charged multivesicular body protein 2b	sALS	Adult	Bulbar	Substitution	CHMP2B is inherited in an autosomal dominant manner and it typically starts between ages 46 and 65 years with subtle personality changes and slowly progressive behavioral changes, dysexecutive syndrome, dyscalculia, and language disturbances.
ALS18	PFN1	profilin 1	17p13.2	profilin 1	sALS	Adult	Spinal>Other	Substitution	Profilin 1 is a small 140 amino acid protein that is essential for the polymerization of monomeric G-actin to filamentous-actin. Although it mainly acts by stimulating actin polymerization, Profilin 1 and its ligands are involved in other processes, including vesicle trafficking, axonal transport, glutamate neuromodulation, endocytosis and nuclear export.
ALS19	ERBB4	erb-b2 receptor tyrosine kinase 4	2q34	Receptor tyrosine-protein kinase erbB-4	fALS	Adult	Spinal>Bulbar	Substitution	ErbB4 is a member of the epidermal growth factor (EGF) family, which regulate the cellular survival, proliferation, differentiation or death. ErbB4 is abundantly expressed in rat spinal motor neurons and also localized at neuromuscular junctions, where plays an important role in the development and modulation of the neuromuscular junction.
ALS20	HNRNPA1	heterogeneous nuclear ribonucleoprotein A1	12q13:13	Heterogeneous nuclear ribonucleoprotein A1	fALS+sALS	-	-	Substitution	ALS20 is caused by heterozygous mutation in the HNRNPA1 gene on chromosome 12q13. HNRPA1 shuttles continuously between the nucleus and cytoplasm and contains a 38-amino acid domain, termed M9, that acts as both a nuclear localization and nuclear export signal.
ALS21	MATR3	matrin 3	5q31.2	Matrin-3	fALS	Adult	Spinal	Substitution	Mutant MATR3 (S85C) had been previously associated with an autosomal dominant distal myopathy with vocal cord and pharyngeal weakness (VCPDM); however, in 2014, three different mutations (F115C, P154S, or T622A) in MATR3 were identified in cases of both fALS and sALS.
FTD/ALS1	C9orf72	C9orf72-SMCR8 complex subunit	9p21.2	Guanine nucleotide exchange C9orf72	fALS+sALS	Adult	Spinal>Bulbar>FTD	Repeated expansions	FTD/ALS1 is caused by a heterozygous hexanucleotide repeat expansion (GGGGCC) in a noncoding region of the C9orf72 gene on chromosome 9p21. Unaffected individuals have 2 to 19 repeats, whereas affected individuals have 250 to over 2,000 repeats. However, some individuals can show symptoms with as few as 20 to 22 repeats.
FTD/ALS2	CHCHD10	coiled-coil-helix-coiled-coil-helix domain containing 10	22q11.23	Coiled-coil-helix-coiled-coil-helix domain-containing protein 10, mitochondrial	fALS	Adult	Spinal>Bulbar	Substitution	The transmission pattern of FTD-ALS2 is consistent with autosomal dominant inheritance. CHCHD10 mutations led to fragmentation of the mitochondrial network as well as major ultrastructural abnormalities, similar to those observed in patient cells. The findings implicated a role for dysfunctional mitochondria in the pathogenesis of late-onset frontotemporal dementia with motor neuron disease.

Table created based on OMIM data and http://alsod.iop.kcl.ac.uk/.

1.3 Symptoms

ALS manifests silently, with nonspecific symptoms over several years, until when the progressive loss of motor neurons exceeds their survival compensatory capacity. As mentioned, the main clinical characteristic of ALS is the combination of both upper and lower motor neuron damage, which involves brain stem and spinal cord. Specifically, the involvement of upper motor neurons impairs limb function, leading to spasticity, weakness and deep tendon reflexes; on the other hand, lower motor neurons degeneration causes fasciculation, atrophy and weakness. Moreover, as the disease progresses and the degeneration involves motor neurons in brainstem, ALS patients' manifest difficulties in swallowing and speech.

ALS onset could be distinguished in (i) spinal and (ii) bulbar. Spinal manifestation affects 70% of patients, who show principally muscle weakness and focal atrophy given the compromise of motor neurons in spinal cord (70). In bulbar onset (25% of patients), the main signs of ALS are dysarthria, dysphagia, swallowing difficulties and facial weakness, which determines the impossibility in closing lips, due to upper motor neurons damage (45).

Despite this clinical distinction, the two beginnings often overlap and about 5% of patients present an onset with respiratory weakness (nocturnal hypoventilation, dyspnoea and orthopnoea), sleep disturbances, headaches, anorexia, decreased ability to concentrate and irritability (71).

Clinical progression is extremely heterogeneous and varies from patient to patient depending on the speed of worsening, the extent of paralysis and the muscles affected: for example, the earliest manifestations of muscle atrophy could involve muscles of the hands, forearms and shoulders in the upper limbs, or of the feet and thighs of the lower ones (72).

Regardless the type of onset, with disease progression ALS patients manifest weakness and fasciculation, spasticity, spastic or flaccid dysarthria (8), Hoffman and Babinski's signs with muscle cramps and fatigue, and involuntary muscle contractions (73–75). In the most cases, ALS spares neurological functions (76,77), but some ALS patients manifest frontotemporal cognitive dementia (FTD), supranuclear gaze palsy, weight loss, bladder dysfunction and multisystem involvement (45,74). Pain, distinguished in acute or chronic, exacerbates in about 70% of patients and it is mostly associated with musculoskeletal conditions (cramps, spasticity and atrophy), and because of bones, tendons, ligaments and nerves' damages (78,79).

Eventually, ALS patients undergo assisted ventilation (80) and could develop a state of paralysis known as "totally locked-in state", which involves paralysis of all voluntary

muscles and oculomotor impairment. Life expectancy in patients with late diagnosis does not exceed 30 months from symptoms onset, while only 20% of patients survive in a time interval ranging from 5 to 10 years (81). The leading cause of death in ALS is respiratory failure, as a result of pulmonary complications.

1.4 Diagnosis

ALS diagnosis is still difficult because of the lack of biological markers, the high variability of symptoms, and its overlap with other neurodegenerative diseases, which led to have a delay of 13-18 months from the appearance of the first symptoms to the diagnosis confirmation (82,83).

Diagnosis of ALS occurs by excluding other motor neurons pathologies, starting from patient's history, through laboratory, electrodiagnostic, neuroimaging and genetic investigations (8,84). In fact, ALS diagnosis requires (i) the presence of signs of second motor neuron degeneration, including electromyography (EMG) signs in clinically unaffected muscles, (ii) signs of degeneration of the first motor neuron on clinical examination and (iii) progressive spread of signs or symptoms to one region or other regions. At the same time, is necessary an absence of (i) electrophysiological or pathological evidence that could explain the signs of degeneration of the second and/or first motor neuron, and of (ii) neuroradiological evidence of other diseases (82,84).

Therefore, there is no single or absolute test for ALS, but an extensive workup that encompasses blood tests (erythrocyte sedimentation rate, C-reactive protein, haematological screen, liver function tests, electrolytes, thyroid function tests, vitamins, serum protein electrophoresis and immunoelectrophoresis), cerebrospinal fluid tests (cell count, protein, glucose, oligoclonal bands), neurophysiology investigations (electroencephalography (EEG), nerve conduction studies (NCS) with electromyography (EMG), and evoked potentials (EP)) and imaging studies (magnetic resonance imaging (MRI), computed tomography (CT), and positron emission tomography (PET)) (8,17).

Definitive diagnosis of ALS requires evidence of upper and lower motor neuron degeneration, progression or increase in neurological symptoms, and manifestation of Hoffman and Babinski signs (85); moreover, electrophysiological, laboratory, and neuroimaging results should not highlight other pathologies that could justify the clinical picture and rule out ALS as a cause (84). For instance, EMG and nerve conduction studies of ALS patients must show fasciculation potentials, indicative of spontaneous denervation discharges and subsequent re-innervation.

Finally, the application of (i) El Escorial, first published in 1994 by the World Federation of Neurology for inclusion standards for patients entering research studies and clinical trials (86), (ii) Airlie House Criteria, defined in 1998 to underlie the importance of laboratory exams as diagnostic tools (84), and (iii) Awaji algorithm, incorporated in 2000 which successfully increase the ability to detects ALS patients without increasing the number of false-positives (87), makes possible to distinguish (82,84,88,89):

1. Definite ALS, presence of upper motor neuron and lower motor neuron signs in the bulbar region and at two of the other spinal regions;
2. Probable ALS, presence of upper motor neuron and lower motor neuron signs in at least two regions with upper motor neuron signs rostral to lower motor neuron signs;
3. Probable ALS (laboratory results supported), presence of upper motor neuron and lower motor neuron signs in one region with evidence by EMG of lower motor neuron involvement in another region;
4. Possible ALS, presence of upper motor neuron and lower motor neuron signs in one region or upper motor neuron signs in two or three regions, such as monomelic ALS, progressive bulbar palsy, and primary lateral sclerosis.

As result, patients can benefit from treatment and the corresponding results of clinical trials.

1.5 Therapies

Despite the growing knowledge of ALS aetiology, the complexity of this disease has compromised identification of resolutive modifying or neuroprotective agents. The current standard of care involves only the drugs, riluzole and edaravone. Other interventions aim to improve the quality of life of patients and their caregivers, but they are only symptomatic and palliative treatments (15).

1.5.1 Disease modifying drug treatments

1.5.1.1 Riluzole

In 1995, FDA approved riluzole as the standard treatment for ALS patients. Approval was based on the results of two independent trials that demonstrated a prolonged survival, or, a two-to-three-month delay in the need of tracheostomy in the riluzole-treated group compared to controls (90,91). These benefits were mainly reported in patients with moderate functional impairment (17,92).

Riluzole is a neuroprotective drug that inhibits presynaptic release of glutamate, inactivates NMDA receptors, and triggers extracellular glutamate uptake (92,93). The drug is generally well tolerated at the dose of 50 mg twice daily, but racial, gender and individual metabolic variations may lead to absorption variability and enhanced toxicity (Rilutek, prescribing information, 2018). The most common side effects are hepatotoxicity, asthenia, nausea, gastrointestinal upset and decreased lung function, that leads in some patients to interstitial lung disease (Rilutek, prescribing information, 2018) (94,95).

1.5.1.2 Edaravone

Edaravone is an antioxidant, and scavenger of free radicals, first approved in Japan in 2001 for the treatment of cerebral embolism and acute ischemic stroke (92,95,96). Given the presence of excessive oxidative stress and the involvement of SOD1 gene in pathogenesis of ALS, edaravone was initially tested in $SOD1^{G93A}$ mice, an experimental model in which it slowed motor decline and SOD1 protein aggregations, promoting cell survival and inhibiting apoptosis (97,98).

Edaravone was approved by the FDA in 2017, although its exact mechanism of action is still unknown, and its clinically positive effects are still a matter of debate. In fact, it was tested in a highly selected cohort of patients, characterized by an early onset and rapidly progressive disease (99,100).

Edaravone is an expensive treatment with a complex dosage: 60 mg IV administration for 14 days followed by 14 days without drugs (95). Nevertheless, this drug is well tolerated, in fact the primary adverse events are contusion, headache and dermatitis (101).

1.5.2 Treatment of specific symptoms

1.5.2.1 Dietary supplementation

Dysphagia and hypermetabolism are two key conditions of ALS prognosis that lead patients to dehydration, worsening of weakness and fatigue, and to weight loss. Therefore, the presence of a nutritionist is essential from onset of the disease. The first approach to nutritional management is the modification of food consistency, with the use of thickeners or creamy ready meals, accompanied by the use of appropriate adaptive eating utensils to promote independence as long as possible, and the pharmacological reduction of sialorrhea (102). When the patient becomes unable to eat independently, the same measures are carried out by assisted feeding until nutrition status is compromised by loss of 5-10% of usual body weight. In this case, and when the body mass index is lower than 20 kg/m 2 and/or forced vital capacity is <50%, percutaneous endoscopic gastrostomy (PEG) is indicated (103,104).

1.5.2.2 Emotional lability and psychological support

Emotional lability, also known as pseudobulbar affect (PBA), is the tendency of 20-50% of patients to laugh or cry inappropriately. PBA is an involuntary emotional expression, probably determined by corticobulbar involvement, and not associated with mood disorders or depression (102,105). Normally, especially in patients without cognitive impairment, emotional lability is a transient phenomenon, which resolves over several months, but it could be treated with tricyclic antidepressant or the combination of dextromethorphan and quinidine (95).

Starting from the communication of the diagnosis, and for the entire duration of the disease, psychological support is crucial; a good relationship patient-psychologist mitigates a patient's sense of abandonment that may arise at the beginning, and allows establishing the "timing". Timing process is characterized by setting a support relationship, also with the caregiver and the family, managing emotions and supporting the patient's decision processes.

As a consequence of the patient's awareness of their progressive, disabling and terminal illness, it is common for the patient to experience depression and anxiety. Although supportive counselling is important, the use of drug therapy is essential, even if it has to take into account other symptoms and side effects (105). Drugs mainly used are tricyclic

antidepressants and inhibitors of serotonin reuptake (amitriptyline, escitalopram and mirtazapine), bupropion and benzodiazepines (17).

1.5.2.3 Exercise

Muscle cramps, fatigue and spasticity are some of the symptoms that progressively worsen in ALS patients. These symptoms, that are in part caused by the pathology and are side effects of riluzole treatment, could be controlled by levetiracetam, baclofen, tizanidine, and botulinum toxin (102,105,106).

Although the role of physical activity is controversial, involvement of a physiotherapist and a physiatrist are essential in the multidisciplinary team. The use of rehabilitative and physiotherapeutic personalized projects, with modulated exercises for the different stages of pathology, retard the progressive loss of strength and mobility, prolong patient autonomy, and provide instruction on special postural changes and techniques that ameliorate feeding, articulation and reduce panic attacks (45,105).

1.5.2.4 Respiratory symptoms

Respiratory failure is the outcome of ALS, with or without pneumonia. The atrophy of respiratory muscles is determined by combined degeneration of central and peripheral respiratory centres, and by motor neurons degeneration.

The appearance of respiratory problems could emerge at the beginning of the disease or by its progression, with manifestation of dyspnoea, orthopnoea, daytime somnolence, morning headache, lack of restorative sleep and frequent nocturnal waking (105).

Clinical and instrumental assessment of respiratory functionality must be done every 2-4 months by spirometry, arterial blood gas analysis and nocturnal saturation. Using these diagnostic exams, the pulmonologist evaluates the forced vital capacity (FVC), vital capacity (VC) and the sniff nasal inspiratory pressure (SNIFF), and determines the correct management of respiratory function (8).

Starting from physical techniques, such as breath stacking and assisted cough, and the use of bronchodilators and anti-cholinergic agents (107), the worsening of respiratory conditions lead to more aggressive management. When desaturation on overnight oximetry increases while FVC is <80%, or SNIFF is <40cmH_2O (17), current guidelines suggest the use of non-invasive ventilation (NIV). NIV improves survival, slows the decline of FVC, and improves the quality of life in ALS patients, but with bulbar impairment is no longer sufficient.

Invasive mechanical ventilation through tracheostomy is the last method that could prolong survival, but at the same time contributes to severe loss of quality life ("locked-in" condition) (17,105,108).

1.5.3 Cellular therapies

Given the central role of neuroinflammation and astrogliosis in ALS, different ongoing or completed clinical trials are focused on microglia/macrophages molecules and on new therapies aimed at modulating astrocyte biology (109,110).

For instance, it has been observed that the progression of the disease could be slowed down by transplanting astrocyte precursors into the cervical spinal cord of $SOD1^{G93A}$ mice (109,111). Moreover, cell therapy is arousing significant interest among clinicians and researchers due to extensive progress in both preclinical and early phase clinical trials, since stem cells may intervene on several mechanisms simultaneously. In fact, stem cell therapy could sustain neuroprotection, both by replacing damaged cells and by providing trophic support to the injured environment and also by actively participating in the regulation of neuroinflammatory processes (112,113).

2. Microglia

Microglia are the immune cells permanently resident in the central nervous system (CNS) that represent ~10-15% of the total population of cells within the brain and ~5-20% of total glial cells, and are critical for proper brain development and maintenance health in the mature brain, rapidly adapting their function to physiological or pathophysiological needs (114,115).

Microglia was first identified in the 19th century by neuroscientists Rudolf Virchow, Santiago Ramón y Cajal and Pío del Río-Hortega, who described the basic morphological features of microglia using a silver staining technique, and hypothesized their phagocytic function.

Owing to phenotypic similarities to peripheral monocytes/macrophages and dendritic cells (DCs), microglia were proposed to be of myeloid in origin and derived from the hematopoietic system (114). However, unlike meningeal, choroid plexus, and perivascular macrophages, microglia originate from embryonic yolk sac (YS) and populate the CNS prior to its vasculogenesis. The concept of microglial derivation from the YS was first suggested in the early 1990s by Cuadros et al., (116) and further supported by Alliot et al., (117): through the use of chimera between chick embryos and quail YS, was found that primitive myeloid cells invade the brain rudiment independently of the blood supply during development. Moreover, in the YS there is the presence of microglia precursors and later the brain rudiment of the developing embryo by embryonic day 8 (E8).

Recently has been identify linfo-erythromyeloid precursors as the genuine microglia progenitors on a stem cell level: these cells continue their physiological and morphological development from the YS to the developing brain, where the mature cells finally reside and build the ultimate pool of microglia (118). Therefore, during neonatal development, myeloid precursors differentiate into microglia drive by transcription factors, growth factors, chemokines, matrix metalloproteinases (MMPs), and microRNAs, while in the adult CNS, microglia are maintained under steady-state conditions via a balance between mitosis and apoptosis (114,119).

As mentioned above, microglial cells are key players in both degeneration and regeneration of the brain. In adult healthy brain, microglia are in “resting” state, a highly dynamic population, with a small cell body and highly ramification morphology, which actively screen their microenvironment with motile processes, exerting a crucial role in maintaining homeostasis, and participating to physiological functions, like synaptic pruning, adult neurogenesis and modulation of neuronal networks (120–123). Upon detection of specific

factors generated by parenchymal injury, degeneration, or infection, microglia undergo morphological transformations and respond rapidly through induction of genetic programs designed to overcome and repair CNS insults.

2.1 M1/M2 phenotype

In face of loss brain homeostasis, resting microglia activate and rapidly change morphology: cellular processes complexity is reduced, with less and thinner ramification, and size soma increases, reverting microglial to amoeboid form. Moreover, "activated" microglia become more motile and move to the injured site, where proliferate, eliminate the brain homeostasis-disrupting agent and provide to tissue regeneration.

In this sense, "activated" microglia is not a unidirectional way to identify microglial activity, but represents a highly regulated process by which microglia pass from a "resting" to the "executive" form, assuming specific morphological, molecular and functional features.

In fact, the term "activation" has been associated with at least two distinct phenotypes: (i) M1, toxic and pro-inflammatory, and (ii) M2, protective and anti-inflammatory (124).

M1-phenotype represent the "classically activated" microglia and is characterized by (i) the release of pro-inflammatory molecules such as interleukin-1α (IL-1α), IL-1β, IL-6, tumor necrosis factor-α (TNF-α) and interferon-γ (INF-γ), (ii) specific markers, as inducible nitric oxide (NO) synthase (iNOS) and major histocompatibility complex class II (MHC-II), and (iii) reactive oxygen species (ROS) release (125–127).

M2-phenotype is the "alternatively activated" microglia, which is induced by anti-inflammatory cytokines, such as IL-4 and IL-10, and exert protective role, suppressing inflammation, phagocyting cellular debris and supporting neuronal survival through the release of trophic factors (124,128).

However, this type of classification represents only the extremes of a wide spectrum of possible forms of activation (129) and has now turned out to be somewhat reductive, although is consistent with what has been described for macrophages (130,131). In fact, M2-phenotype includes (i) M2a associated with the production of anti-inflammatory cytokines and trophic factors (125), (ii) M2b considered to be a combined M1/M2a subtypes (132), and (iii) M2c associated with phagocytosis and suppression of the innate immune system (132,133). Furthermore, "acquired deactivation" represents another M2 anti-inflammatory phenotype and it is mainly induced by the uptake of apoptotic cells or exposure to anti-inflammatory cytokines, such as IL-10 and transforming growth factor-β (128,134).

2.2 Neuroinflammation and microglial activation in ALS

Neuroinflammation in ALS has been reported both in animal models and in patients in the very early stages of the disease (109) and it is characterized by activated microglia, astrogliosis and infiltration by immune system cells into the sites of neuronal injury.

Despite recent evidence suggesting the involvement of a complex crosstalk between the CNS and peripheral immune cells, the specific influence of the peripheral immune system in ALS pathogenesis is still under investigation (135). A deregulation of the communications between motor neurons and glial cells seem be implicated in the damage of motor neurons (20) and alterations of brain homeostasis may result from both central (microglia and astroglia actions) and peripheral activation (peripheral lymphocyte and macrophage activities) of immune system elements (136,137). Monocytes and macrophages may induce CNS inflammation mainly by regulating the status of T cells, dendritic cells, or natural killer cells in lymph nodes, spleen, or peripheral circulation (138); microglia may be principally involved in CNS neuroinflammation. This hypothesis, however, has been undermined as peripheral monocytes have been shown to actually migrate into the CNS (135). Neuroinflammation in ALS consists of two phases. The initial neuroprotective phase is characterized by an anti-inflammatory compensatory response by adjacent glial and/or peripheral immune cells; by contrast, the cytotoxic phase is linked to neurodegeneration (130). In particular, *in vitro* exogenous $SOD1^{G93A}$ mutation induced microglial morphological and functional activation, increasing the release of pro-inflammatory cytokines and ROS (139). Similarly, during the early stages of disease in the $SOD1^{G93A}$ mouse, microglia become neuroprotective (M2), with attenuated toll-like receptor 2 (TLR2) response to controlled immune challenge and an overexpression of anti-inflammatory IL-10 (140). Only in the late phase microglia convert to the cytotoxic phenotype (M1) (136,141).

In patients with ALS, microgliosis occurs specifically with motor neuron injury in the motor cortex, along the corticospinal tract, and in the ventral horn of the spinal cord (130). These stages may account for the two phases of ALS mentioned above (Figure 4).

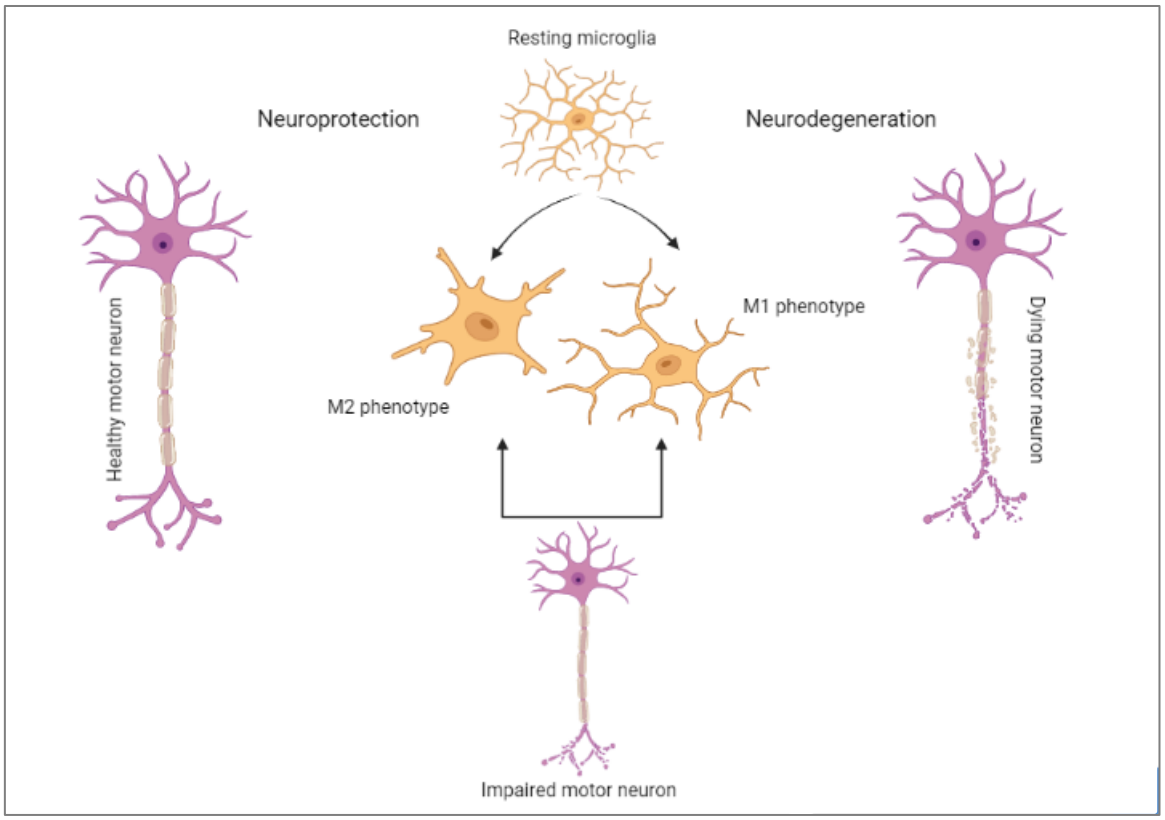

Figure 4. *Microglial polarization during ALS.*
During ALS progression, activated microglia represent a continuum between the toxic M1-phenotype, which produces cytokines and increase inflammation, and M2-phenotype, which promotes tissue repair. Created with BioRender.com.

Monocytes, macrophages and T lymphocytes are also similarly neuroprotective in the early phases of ALS but transform into their neurotoxic phenotypes in the later phases (130). In peripheral blood of ALS patients, alterations in T lymphocytes, monocytes, complement activation and cytokines have all been documented (135). Activated macrophages, as well, have been shown to increase in number in the ventral root and sciatic nerve of ALS mice (142); these findings suggest that inflammation may also participate in neuromuscular junction (NMJ) dissociation during ALS progression. It is of some significance that in the sciatic nerve, macrophage activation and the inflammatory response occur as early events, which precede the onset of symptoms or clinical signs of motor weakness; thereafter, macrophage activation and inflammation progressively increase through to end stage (143). These findings are reinforced by a recent demonstration of activated inflammation and abnormal glial cell responses in the limb muscle of a fALS rat model, specifically near denervated NMJs (144). Indeed, *in vitro* co-culturing of different-aged $SOD1^{G93A}$ microglia with wild-type (WT) motor neurons has shown that $SOD1^{G93A}$ early-activated microglia

exhibit neuroprotective features, enhancing neuronal survival, while end-stage $SOD1^{G93A}$ microglia show toxic properties and increase motor neuron death (134,145).

Despite this, the microglial phenotype is not so strictly and uniquely correlated with the progression of the disease: recently, different studies have highlighted the co-existence of M1/M2 during ALS progression. For instance, $SOD1^{G93A}$-expressing microglia do not display a significant prevalence of M1 or M2 phenotypes at any time point during disease progression (146). In fact, Lewis and colleagues have demonstrated an increased expression of both iNOS (M1 marker) and arginase 1 (Arg1; M2 marker) in activated microglia of $SOD1^{G93A}$ mice (147). Moreover, transcriptome analysis of $SOD1^{G93A}$ microglia confirmed that the activation of genes involved in anti-inflammatory pathways, including insulin growth factor-1 (IGF-1) gene, coexists with the upregulation of genes related to potentially neurotoxic factors, among which proinflammatory cytokines (146).

For instance, IGF-1, which is a beneficial component of inflammation, is over expressed by $SOD1^{G93A}$ microglia not only in pre-symptomatic stage, as usually with M2 protective environment, but also in end-stage (134,148).

On this basis, the possibility to modulate microglial phenotypes could be a promising therapeutic strategy for ALS, i.e. shifting the balance towards M2 phenotype through the use of trophic factors. In fact, several findings have suggested that the delivery of IGF-1 to CNS could extends lifespan and slows the progression of disease in ALS animal models, even when delivered at the time of overt disease symptoms (134,149,150).

3. Extracellular vesicles

Extracellular vesicles (EVs) are a wide family of cell-derived spherical particles enclosed by a phospholipid layer implicated in cell communication. Despite the initial hypothesis which described EVs secretion as a cellular mechanism for discarding useless materials from the cells (151), EVs are involved in many physiological and pathological processes, such as homeostasis maintenance, immune response, inflammation, cancer progression and neurodegenerative diseases (132,152–154).

EVs are present in most of bodily fluids, including blood, urine, saliva, breast milk, amniotic and cerebrospinal fluids, and in culture medium of cell cultures (132,155), and are deputed to transfer membrane and cytoplasmic proteins, lipids and nucleic acids between cells, becoming an integral part of the intercellular microenvironment.

According to their biogenesis, morphology, protein and lipid composition and size (ranging from 30 nm to 1000 nm in diameter), EVs can be broadly classified in three subclasses: (i) apoptotic bodies, (ii) microvesicles, and (iii) exosomes (152,156).

Apoptotic bodies (ABs) are formed only during programmed cell death, by budding, blebbing, or fragmentation of the plasma membrane. ABs range from 1000 to 5000 nm and are characterized by the presence of organelles within the vesicles (157), besides DNA fragments and histones, cytosol and degraded proteins (158). The principal role of ABs is a more efficient clearance of apoptotic cells and a fine control of immune responses.

Microvesicles (MVs) are released by budding from the plasma membrane, through a Ca^{2+}-mediated process (159). MVs vary in size from 150 to 1000 nm in diameter (160) and are surrounded by a phospholipid bilayer, usually associated with lipid rafts and cholesterol, sphingomyelin, ceramide and phosphatidylserine, containing proteins, lipids, and nuclei acids depending on the cell of origin (19,159).

Exosomes (EXOs) are the smallest EVs, with a diameter from 30 to 150 nm, and have the characteristic “cup shaped” morphology, visualizable by transmission electron microscopy (TEM) (19,152,154). EXOs are surrounded by a phospholipid bilayer, that provide a rich source of biomarkers and antigens, and contain proteins, lipids, DNAs, mRNAs, microRNAs, long non-coding RNAs, viral and prion genetic materials, depending on cellular origin and target function (154) (Figure 5).

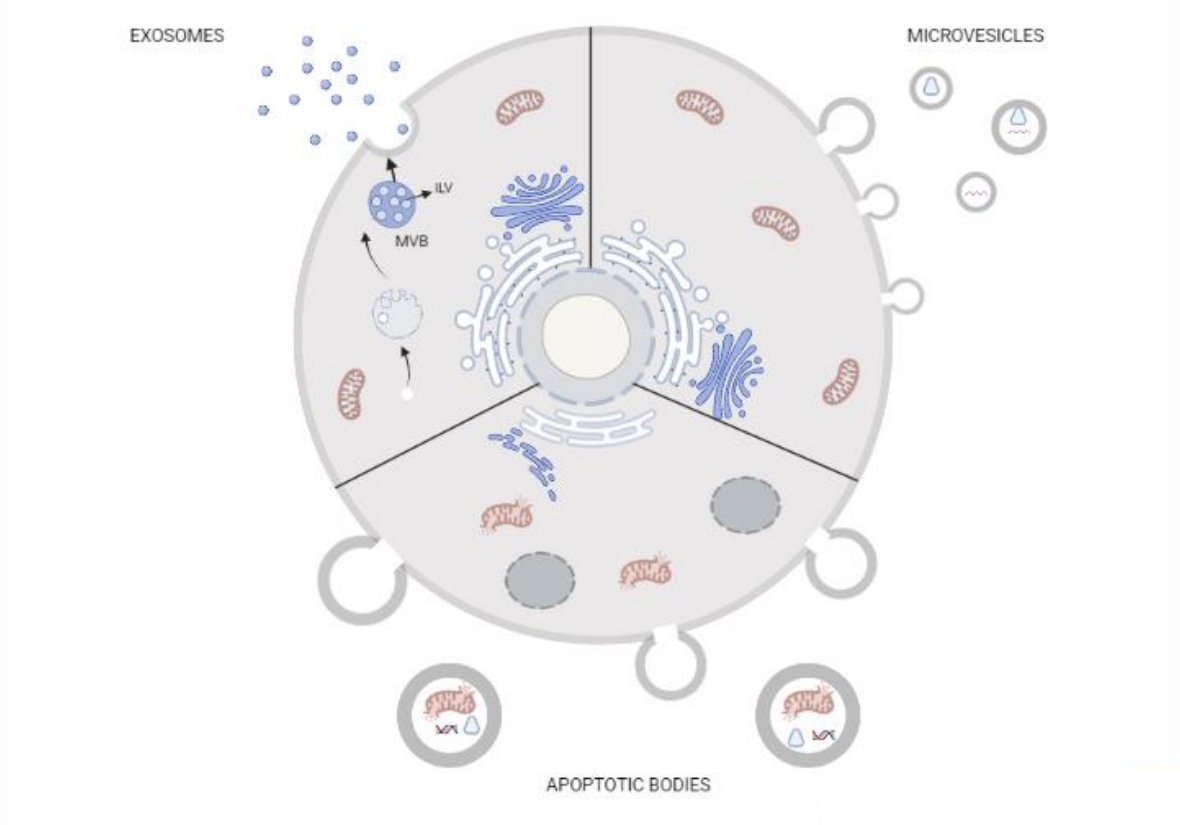

Figure 5. *Biogenesis and biological composition of various forms of EVs.*
(i) Apoptotic bodies range from 1000 and 5000 nm, originate from apoptosis pathway and carry proteins, lipids, nucleic acids and organelles. (ii) Microvesicles generate through blebbing of plasma membrane, range between 150 and 1000 nm and contain proteins, lipids and nucleic acids. (iii) Exosomes are generated through multivesicular bodies (MVB) and intraluminal vesicles (ILV) formation, range 30-150 nm, and carry nucleic acids, small proteins and lipids. Created with BioRender.com.

3.1 Biogenesis

Despite their similar functions, MVs and EXOs have different biogenesis, all involving membrane-trafficking processes: MVs are released by budding from plasma membrane through a process dependent on intracellular Ca^{2+} concentration, EXOs originate from invagination and endocytosis of the plasma membrane, and undergo a series of transformations independent from cell Ca^{2+} influx (19).

Even though the biogenesis of MVs is far less defined as compared to exosomes, different mechanisms are found to be responsible for the shedding of MVs, including the repositioning of phosphatidylserine to the outer leaflet, the contraction of the actin-myosin machinery and Ca^{2+} influx (19,157,161).

The canonical mechanism hypothesized sees ADP-rybosylation factor 6 (ARF6) as the initiator for the activation of phospholipase D (PLD). PLD recruits the extracellular signal-regulated kinase (ERK) to the plasma membrane where, once phosphorylated, activates the myosin light chain kinase (MLCK). In turn, MLCK phosphorylates and activates the myosin light chain allowing MVs release (157,161). Furthermore, external factors can induce MVs release, i.e., the influx of Ca^{2+} induces the redistribution of phospholipids in the plasma membrane, resulting in increased release of MVs (159,162).

On the contrary, EXOs' generation is based on an endosomal system, which could be (i) endosomal sorting complex required for transport (ESCRT)-dependent or (ii) ESCRT-independent (158).

In both cases, the process initiates with the invagination and endocytosis of the plasma membrane, mediated or not by clathrin, and results in the formation of early endosome (EEs) (163–165). By the interaction with Golgi complex, and the participation of ESCRT (ESCRT-dependent pathway), or lipids and tetraspains (ESCRT-independent mechanism), EEs mature in late endosomes (LEs) also known as multivesicular bodies (MVBs). Therefore, EXOs can present typical endosome-associated proteins (as GTPase and Alix) or membrane proteins (as tetraspain, CD36 and Hsp70), depending on the mechanism involved in their biogenesis, transport and fusion (163).

MVBs and their EXOs content can be (i) degraded in lysosomes (degradative exosomes) or (ii) fused with the plasma membrane, releasing EXOs in the extracellular environment (exocytic exosomes) which can act in a paracrine or endocrine manner, through endocytosis, fusion or binding with specific receptors (19,163).

3.2 Biological content

Even though different studies have tried to characterize the biochemical composition of EVs, the actual composition of each subtype of EVs is unknown.

Nevertheless, the biologically active molecules of EVs comprise (i) proteins, (ii) lipids, and (iii) nucleic acids, all reflecting the status of the parental cells.

Initial proteomic studies showed that EVs contain a specific subset of cellular proteins, some of which depend on the cell type that secretes them, others are found in most EVs regardless of cell type. The latter include proteins from endosomes, plasma membrane and cytosol, depending on the mechanism of EVs origin (166).

Endolysosomal EVs tend to be more enriched in major histocompatibility complex class II (MHC II) and tetraspanins (CD9, CD37, CD63, CD81 and CD82) (167); ESCRT-dependent EVs present also Alix and chaperones (Hsp70 and Hsp90), irrespective of the cell type (155). Noteworthy, all these proteins, especially tetraspanins, ESCRT proteins, Alix and HSPs, are commonly used as general EV markers (155).

Fewer studies have analysed the lipid composition of exosomes (168–171), but have found an enrichment of sphingomyelin, phosphatidylserine, cholesterol, and generally of saturated fatty acids, in addition to the presence in EVs of lipid raft–associated proteins, GPI-anchored proteins and flotillins (168,172).

The presence of nucleic acids, in particular of mRNA and microRNA, in EVs was first identified in 2007. This finding led to think that exosomes could be ideal vectors for gene therapy, especially for their resistance to RNAse digestion (173).

Most studies have described small RNA (200 nucleotides less than the average of cellular fraction) in EVs , including mRNA, miRNA, and low levels of ribosomal 18S and 28S RNA, specifically in apoptotic cell-derived materials (156,166), mainly coding for transcription factors and genes involved in angiogenesis and adipogenesis.

3.3 Functions of EVs in intercellular communication

The main role of EVs is to deliver their cargo, protecting it against degradation, until the interaction with adjacent or distant recipient cells. As mentioned above, the uptake can occur (i) directly, by fusion with the target cell or by endocytosis, or (ii) indirectly, mediated by receptor binding.

For example, integrins and other lipidic molecules on EVs surface interact with intercellular adhesion molecules (ICAMs) of the recipient cells (174), leading to the fusion of EVs with the cellular plasma membrane and the consequent release of EVs cargo in the cytoplasm. Moreover, among different mechanisms for the uptake by endocytosis, clathrin-, caveolin-, lipid raft-mediated endocytosis, macropinocytosis and phagocytosis are mainly involved in CNS: clathrin-dependent endocytosis or phagocytosis has been described in neurons, macropinocytosis in microglia, and phagocytosis or receptor-mediated endocytosis in dendritic cells (161).

The cargo, as the EVs composition, depends on the cell of origin, but proteins and functional RNAs contained in the EVs are implicated in many biochemical and cellular processes, such as communication, inflammation, tissue repair, regeneration, cell differentiation and metabolism (19,175).

In CNS, neurons, microglia, astrocytes, and oligodendrocytes secrete EVs into the extracellular environment, playing a vital role in the regulation of synaptic communication and strength, and nerve regeneration (176,177), but also in the occurrence and progression of neurodegenerative diseases (154).

Since EVs can transfer biological information over long distance and EXOs are capable to cross the BBB, increasing attention has been paid to the use of EVs as a potential therapeutic tool in neurodegenerative diseases.

3.4 Exosomes in ALS and therapeutic perspectives

Different *in vitro* and *in vivo* studies have demonstrated that EVs could be considered as a potential biomarker of neuroinflammation and neurodegeneration, but also more easily a novel and efficient therapeutic tool (153).

Referring to ALS, given its complex pathogenesis and since EVs can act at the same time via multiple mechanisms, in the last years an increasing interest has been addressed to them as targets to modulate ALS disease (50,178).

Starting from the observation of Gomes and colleagues, which in 2007 have demonstrated the presence of WT and mutated SOD1 in the EXOs derived from the supernatant medium

of mouse motor neuron-like NSC-34 cells (179), different studies now suggest EXOs as targets to modulate ALS disease. In fact, EXOs derived from NSC-34 overexpressing $SOD1^{G93A}$ is a mechanism of cell-to cell transfer of mutant SOD1 toxicity.

Basso and colleagues have supported this *in vitro* study, demonstrating that in mice expressing $SOD1^{G93A}$, astrocytes have an up-regulation of $SOD1^{G93A}$ and are characterized by a bigger release of EXOs, which transfer mutant SOD1 to spinal neurons, inducing selective motor neuron death (178). The same ability to transfer mutant and misfolded SOD1 found both in *in vitro* and *in vivo* models, is also detected in the EXOs derived by spinal cord of ALS patients (50).

Starting from these evidences, Pinto and colleagues have investigated the influence of motor neuron-derived EXOs in the activation and polarization of the recipient microglia, in an *in vitro* co-culture model of NSC-34/N9 cells. The results of this study showed that EXOs cause M1 polarization, which turns after 24 hours in a switch to mixed M1 and M2 subpopulations (180).

At the same time, increasing evidence suggests that EXOs also display anti-inflammatory properties, reducing the number of activated inflammatory microglial cells, supporting oligodendrocytes and protecting neurons (181,182).

Some studies have demonstrated that EXOs of different origins could be a novel non-cell therapeutic approach for ALS treatment. In 2016, both Bonafede and Lee have shown that EXOs isolated from adipose derived stromal cells (ASCs) exert neuroprotective effects in an *in vitro* model of ALS and using H_2O_2 as pathological insult. The presence of EXOs increased cellular survival, probably counteracting apoptosis pathway, reducing mutant SOD1 and restoring mitochondrial protein function (19). Currently, by performing *in vitro* and *in vivo* studies, different authors have found a promising therapy for the treatment of spinal cord injury with M2-type microglia-derived EXOs, which reduce inflammation and apoptosis mainly through the downregulation of phosphatidylinositol-3-kinase (PI3K)/Akt/mTOR pathway (183,184).

4. Ghrelin and Growth Hormone Secretagogues (GHSs)

4.1 The history of ghrelin and GHSs

The discovery of ghrelin was obtained by reverse pharmacology, starting from met-enkephalin and its properties. In 1976 Bowers and colleagues identified a peptide derived from met-enkephalin, which devoid of opiate activity, and capable of stimulating growth hormone (GH) secretion from pituitary glands (185). Following this discovery, were developed new peptidyl and non-peptide molecules, among this (i) growth hormone-releasing peptide-6 (GHRP-6) (186), that selectively stimulated the release of GH, (ii) hexarelin, with marked lipophilicity and greater resistance to enzymatic degradation compared to GHRP6, and (iii) MK-0677, which allowed for the identification and cloning of the gene for GH secretagogues receptor (GHS-R) (187) and, a few years later, the identification of ghrelin as the endogenous ligand of GHS-R.

Ghrelin is an octanoylated 28-amino acid peptide produced by the oxyntic glands of the stomach, which stimulates growth hormone (GH) secretion and appetite, resulting in body weight gain. The human ghrelin gene sequence is located on chromosome 3p25-26 and the mature mRNA encodes a protein of 117 amino acids, called pre-pro-ghrelin. Through enzymatic processing and post-translational modifications (an esterification with an octanoic acid on the third serine residue) ghrelin is activated and acquire greater lipophilicity (188).

Plasma ghrelin is expressed in two different forms, acylated or unacylated. Acyl ghrelin is the active form of ghrelin, able to (i) bind GHS-R, (ii) to reach and cross the blood brain barrier (BBB), and (iii) is capable of increasing the secretion of growth hormone (GH) and glucagon, reducing the secretion of insulin, and contributing to the maintenance of plasma glucose levels. Furthermore, acyl ghrelin stimulates appetite, regulates gastrointestinal motility, cardiac function, osteoblast proliferation and myoblast outgrowth, and exerts a broad range of neuroprotective effects (189). Desacyl ghrelin, also called unacylated ghrelin, is an isoform of ghrelin lacking the acyl moiety and is unable to bind the GHS-R receptor. Although desacyl ghrelin was generally considered an inactive product of ghrelin degradation, it has emerged to be an active peptide, which in some cases presents ghrelin-like and extra-ghrelin like bioactivities.

Ghrelin is endowed with several endocrine and extra-endocrine effects, and a large number of synthetic analogues have been developed, called growth hormone secretagogues (GHS). GHS are a large family of synthetic compounds with a heterogeneous chemical structure, which includes peptidyl, peptidomimetic, and nonpeptidic moieties, originally developed in the late 1970s for their capability to stimulate GH secretion, both *in vitro* and *in vivo* (190).

Although the importance of GH effects in the CNS were first reported 60 years ago, only more recently has been hypothesized the role of GH as a neuroprotective factor (191). In fact, GH is involved in brain growth and development, and in contrasting aging; moreover, it has been observed a decrease of GH level related to neuronal death (192,193). Despite these evidences, neuroprotective GH mechanism of action is not fully understood. On the one hand it seems to act directly, for example reducing the production of ROS, on the other by stimulating the production of insulin-like growth factor 1 (IGF-1) (194,195).

Ghrelin and GHS not only stimulate GH secretion, but also improve cellular and systemic metabolism, exert neuroprotective, anticonvulsant and anti-inflammatory effects, and modulate cardiovascular function (185). Moreover, they increase food intake, body weight and influence regulation of skeletal muscle mass in animals and humans by stimulation of insulin-like growth factor 1 (IGF-1) production (196–198). The involvement of IGF-1 as a neuroprotective factor has been demonstrated by different *in vitro* studies that have shown how the addition of IGF-1 to the culture medium promotes neurotics formation and increases neuronal survival (199). Moreover, *in vivo* subcutaneous injection of IGF-1 in neurodegenerative disease models leads to regeneration of motor nerves and sciatic nerve, reduction of atrophy and loss of muscle strength (149).

Interestingly, in the cerebrospinal fluid of ALS patients, the levels of GH and IGF-1 are significantly reduced compared to controls (200), suggesting that a therapy capable of bringing the levels back to normal may have positive effects.

4.2 Ghrelin and GHSs receptor

GHS-R is encoded by a single gene located on human chromosome 3q26.2, but two distinct cDNAs have been isolated: (i) GHS-R1a, of 366 aa and a molecular weight of 41 kDa, that belongs to the superfamily of G protein-coupled receptors and has the classic seven-domain transmembrane structure with three intracellular and three extracellular loops; (ii) GHS-R1b, produced by an alternative splicing mechanism, which encodes a protein of 289 aa and 5 transmembrane domains. Given its "truncated" structure, GHS-R1b is not able to be bind by GHS or to activate the mechanisms of intracellular transduction, but it would seem that has a modulatory action on the signal transduction capacity of GHS-R1a (201).

GHS-R1a is expressed in the central nervous system (CNS), in the hypothalamus, pituitary, hippocampus and substance nigra, as well as in various peripheral tissues, such as the thyroid, lung, liver, spleen, adipose tissue, gonads, and myocardium (202,203).

The binding of ghrelin and GHSs to GHS-R1a activates $G\alpha_{q/11}$ protein, which leads to the formation of inositol triphosphate (IP3) and diacylglycerol (DAG). IP3 induces a release of calcium (Ca^{2+}) from intracellular deposits, while DAG activates protein kinase C (PKC). Increased intracellular Ca^{2+} inhibits voltage-gated potassium channels, allowing Ca^{2+} to enter even from the extracellular environment. Activation of GHS-R1a also leads to transactivation of the β and γ subunits of the tyrosine kinase pathway, leading to the activation of mitogen-activated protein kinases (MAPKs) and phosphoinositide 3-kinase (PI3K)/protein kinase B (Akt), both of which involved in cell survival (60,204–207) (Figure 6).

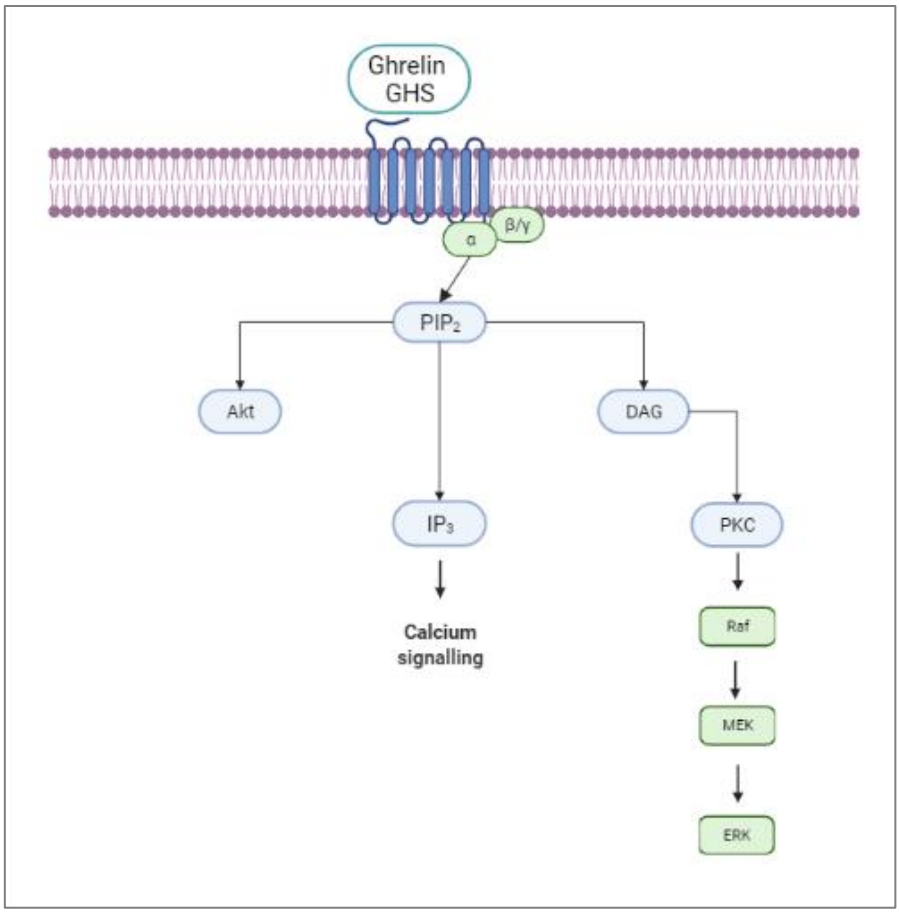

Figure 6. *Schematic representation of the major signaling pathways regulated by ghrelin and GHSs.* The activation of GHS-R1a receptor, by the binding with ghrelin or GHS, results in the generation of phosphatidylinositol phosphate PIP_2, that induces (i) the protein inositol 3 kinase (PI3K)/Akt pathway, (ii) the release of intracellular calcium, (iii) the activation of protein kinase C (PKC). This last, leads to the stimulation of mitogen-activated protein kinases (MAPKs) pathway. Created with BioRender.com.

4.3 Effects of GHSs

4.3.1 Ghrelin and GHS: neuroprotection, modulation of neuronal pathology and neuroinflammation

The presence of GHS-R1a in the CNS suggests that ghrelin and GHS may exert neuroprotective effects in the central nervous system (CNS) (185).

Recently, it has been shown that ghrelin and hexarelin are endowed with anti-oxidant, anti-inflammatory, and anti-apoptotic effects (207) in different *in vivo* and *in vitro* disease models, including stroke (208,209), Parkinson's disease (210,211), Alzheimer's disease (212), multiple sclerosis (213) and ALS (214–216). Different studies performed on hypothalamic neuronal and on human neuroblastoma SH-SY5Y cells have demonstrated the neuroprotective and anti-apoptotic effects of the hormone and its derivatives, even though the mechanisms are not yet fully understood and do not seem to be exclusively due to the link with GHSR-1a (210,217). Moreover, the presence of a ghrelin-specific receptor in the spinal cord suggests that ghrelin could have direct effects on spinal cord function. The spinal cord IGF-1 system may be involved in the neuroprotective effect of ghrelin which prevents apoptotic death of motoneurons (218). Ghrelin and GHS, such as hexarelin, modulate the PI3K/Akt and extracellular signal regulated kinase 1/2 (ERK1/2) pathways, both of which are involved in cell survival (60,209,219). Collectively, these findings suggest that ghrelin and GHS have the potential to become novel pharmacophores for the treatment of ALS (215).

In neurodegenerative diseases, neuroinflammation is frequently associated with reactive microglial and astroglial cells, infiltrating lymphocytes and macrophages, and activation of the complement system (220,221). Some evidence suggests that in ALS the immune system may dynamically balance between neuroprotection and neurotoxicity. Specifically, during periods of slow disease progression, the immune system exerts a protective effect by secreting anti-inflammatory factors that rescue and repair damaged tissue; by contrast, during accelerated disease progression the immune system exerts a strong proinflammatory and neurotoxic effect (130). Interestingly, astrocytes express the GHSR1a-receptor and are responsive to ghrelin. Ghrelin act as survival and anti-inflammatory factor through stimulation of ERK1/2, PI3K/Akt, and the anti-apoptotic protein B-cell lymphoma 2 (Bcl-2), as well as by inhibiting caspase-3 (222). In addition, ghrelin markedly attenuates inflammation and inhibits inflammatory factors, and microglial activation (216).

4.3.2 Ghrelin and GHS: role in skeletal muscle

Some studies have documented depressed IGF-1 levels in muscle from ALS patients [185]; by comparison, elevated levels of muscle IGF1 in mutant $SOD1^{G93A}$ mice was linked to improved muscle function and increased motor neuron survival (223–226). Promising results from preclinical studies with IGF-1 may open new perspectives in ALS management. IGF-1 is a key anabolic growth factor for regulating muscle hypertrophy, sharing some growth and development stimulatory properties with ghrelin and GHS. The myotrophic effects of ghrelin and GHS have been described in different pathological conditions. Muscle wasting is a co-morbidity associated with a wide range of disorders that severely increases morbidity and affects patient prognosis and quality of life. The loss of skeletal muscle, often accompanied by a reduction in appetite, increased catabolism, and loss in body weight, is a key adverse factor in cancer cachexia. Muscle wasting is a predisposing factor in the clinical decline of patients, is directly associated with increased mortality, and represents a negative predictor of treatment outcome (227). Ghrelin, hexarelin and JMV2894 in preclinical models of cisplatin-based chemotherapy improved not only anorexia and weight loss, but also strength and mass muscle, as well as increased patient survival (101,228,229). Ghrelin and GHS reduce muscle wasting through multiple mechanisms of action (228). Ghrelin, hexarelin and JMV2894 prevent muscle atrophy by mitigating inflammation and increasing Akt phosphorylation (230). Ghrelin and GHS have also been shown to prevent muscle atrophy induced by dexamethasone and angiotensin II (231–233).

4.4 Hexarelin, JMV2894 and EP80317

In this thesis has been used three different GHSs whose molecular mechanisms have not yet been fully characterized. In fact, it is possible that they act like ghrelin, binding to the GHS-R1a receptor, or to other receptors (like CD36), or even without any bond.

Hexarelin is a synthetic hexapeptide that binds not only to the GHS-R1a but also the CD36 receptor and manifests varied beneficial effects in diseases associated with muscle wasting (230,234,235), chronic heart failure (236), excitotoxicity, neurological disorders, epilepsy and diabetes (237). Despite the emerging biological importance of hexarelin, its signalling mechanisms have been only partially elucidated. Some studies have demonstrated that hexarelin modulates activation of different intracellular pathways, such as mitogen-activated protein kinases (MAPKs) and phosphoinositide 3-kinase (PI3K)/protein kinase B (Akt) (204,205), and, thereby, could indirectly influence intracellular calcium (Ca^{2+}) concentrations (238). Furthermore, hexarelin protects cells *in vitro* from apoptosis by

inhibiting NO synthesis and reactive oxygen species (ROS) release, modulating caspases activity as well as the expression of proteins belonging to the BCL-2 family (229,234,238–241).

Starting with hexarelin, with a series of modifications involving trisubstitutions of 1,2,4-triazole, new ligands of GHS-R1a were then obtained, including JMV2894 and EP80317 (242).

JMV2894 is a new peptidomimetic derivative of ghrelin, a complete agonist of GHS-R1a. JMV2894 stimulates GH secretion *in vivo* and *in vitro* (242,243). *In vivo* studies, in cachexia models, have shown that JMV2894 is able to partially counteract weight loss and increase in muscle damage, blocking atrophy. On the other hand, *in vitro*, it has been shown to be able to completely counteract the increase in intracellular Ca^{2+} concentration caused by the effects induced by cisplatin (230,234,244).

EP80317 is a hexapeptide, which differs from hexarelin in the loss of GH-releasing properties caused by the presence of substitutions to the first and third amino acid residues. EP80317 is pharmacologically active on macrophages and its activity is dependent on the activation of the peroxisome proliferator-activated receptor-γ (PPAR-γ). The activity of this GHS is mediated by the activation of the CD36 receptor (245–247), a target also of desacyl-ghrelin, involved in the internalization of low-density oxidized lipoproteins, which determine the initiation of the glial recruitment signal cascade (248).

AIM

Amyotrophic lateral sclerosis (ALS) is a fatal neurodegenerative disease characterized by the rapid loss of both upper and lower motor neurons in brainstem, motor cortex and spinal cord, which led ALS patients to manifest severe muscle atrophy and progressive paralysis of all skeletal muscles. Despite the growing knowledge about its aetiology, the pathogenetic mechanisms are still unclear even though (i) mutations of superoxide dismutase 1 (SOD1) and (ii) increased oxidative stress have been linked with several variants of familial ALS. SOD1 is a powerful antioxidant enzyme that protects cells from the damaging effects of superoxide radicals, whose mutations (in about 20% of familial and 5% of sporadic ALS) lead to gain/loss of function and enhance the accumulation of highly toxic hydroxyl radicals. Among SOD1 mutations, the substitution of glycine 93 to alanine ($SOD1^{G93A}$) is a mutation frequently studied, both in cellular and animal models. As a consequence of the pathological mechanisms, motor neurons are subjected to several cellular changes, including alterations of gene expression, abnormal protein interactions, activation of caspases, dysfunctions of mitochondria and cytoskeletal abnormalities.

The current standard of care involves only two drugs (riluzole and edaravone) that may be effective in slowing the progression of the disease but do not cure ALS, while all the other interventions aim to improve the quality of patients' life, but are only symptomatic and palliative. Therefore, a more effective drug therapy targeting the disease progression is still strongly needed.

Emerging evidences have suggested that ghrelin and growth hormone secretagogues (GHSs) exert different biological actions, as well as neuroprotection. Therefore, we have studied the potential neuroprotective effects of growth hormone secretagogues (GHSs) as possible candidates for the treatment of ALS.

GHSs are a large family of synthetic compounds, including short peptides, peptoid, and non-peptidic moieties, which have shown endocrine functions, through the stimulation of growth hormone release, and extra-endocrine properties, including stimulation of food intake and lean mass, at least in part by the binding to GHS-R1a, the receptor of ghrelin.

Among GHSs, we have selected three well-characterized compounds: (i) hexarelin, a hexapeptide that exerts cyto-protective effects at the mitochondrial level in cardiac and skeletal muscles, both in vitro and in vivo, and may also have important neuroprotective activities; (ii) JMV2894, an agonist of GHS-R1a, which stimulates Ca^{2+} mobilization in vitro and growth hormone release in vivo, and modulates mitochondria functioning and ROS

production; (iii) EP80317, an antagonist of GHSR-1a, which can bind to the CD36 receptor and modulate the production of inflammatory cytokines, exert anticonvulsant activities and cardioprotective functions.

In the first series of experiments, we will evaluate the cyto-protective effects of these selected GHSs in Neuro-2A cells, a mouse neuroblastoma cell lines widely used to study the oxidative stress mechanism in neurodegenerative diseases. Neuro-2A cells will be treated with various concentrations of H_2O_2, to identify the lowest concentration that reproducibly and significantly inhibits cell growth, or with the combination of H_2O_2 and GHSs, to investigate the protective effect of GHSs on H_2O_2-induced reduction of cell viability and increased oxidative stress.

Given that oxidative stress may directly induce morphological alterations and apoptosis pathways, we will characterize the capability of GHSs to antagonize H_2O_2 effects through the quantification of (i) cytoskeletal changes using Image J skeleton and fractal analysis procedures, and (ii) mRNA levels of caspase-3, caspase-7, Bax, and Bcl-2 by Real-Time PCR.

We will also investigate GHSs capability to modulate in Neuro-2A cells the mitogen-activated protein kinase (MAPK) ERK 1/2 and p38, and phosphoinositide-3-kinase (PI3K)/Akt, two pathways primarily involved in the regulation of cell growth, differentiation, and response to cellular stress, whose activation contribute to neuronal dysfunction.

In the second series of experiments, we will apply the same protocols and analyses to SH-SY5Y cells, a human neuroblastoma cell line transformed for (i) overexpressing the WT SOD1 enzyme or (iii) expressing $SOD1^{G93A}$ protein, two well-established simplified in vitro models of ALS. We have specifically chosen to use these cell models because SH-SY5Y $SOD1^{G93A}$ cells display remarkable biochemical abnormalities compared to the SH-SY5Y WT cells, including the increase of cytosolic Ca^{2+} concentrations, decrease ATP levels, and an increased cytosolic and mitochondrial ROS production.

The results will allow the evaluation of the neuroprotective, anti-oxidant and anti-apoptotic effects of GHSs, and identifying the most effective GHS among the three used.

Another aspect of the onset and progression of ALS is the neuroinflammatory response, characterized by activated microglia, astrogliosis and infiltrating immune cells in the sites of neuronal injury.

To better understand the complex communication between neurons and microglia, murine microglia N9 cells will be treated with the three GHSs, and their conditioned media will be used to isolate EVs.

EVs are involved in many physiological and pathological processes, and have the role to deliver their cargo, protecting it against degradation, until the interaction with adjacent or distant recipient cells. Different in vitro and in vivo studies have demonstrated that EVs could be considered as a novel and efficient therapeutic tool.

Therefore, isolated EVs will be (i) characterized in terms of size and concentration by NanoSight NS300, (ii) disaggregated with RIPA buffer to quantify protein by Micro BCA Protein Assay, or (ii) incubated with SH-SY5Y WT and $SOD1^{G93A}$ cells.

In particular, SH-SY5Y WT and $SOD1^{G93A}$ cells will be treated with the combination of H_2O_2 and EVs, and we will evaluate the apoptotic responses. The results will clarify if GHSs are capable to induce the release of potential neuroprotective EVs from microglial N9 cells. Taken together these results will be useful to better understand whether GHSs could be developed to become a therapeutic strategy for the treatment of ALS and other neurodegenerative diseases.

MATERIALS AND METHODS

1. Chemicals

Hexarelin, Dulbecco's Modified Eagle's Medium (DMEM)-high glucose, Dulbecco's Modified Eagle's Medium/Nutrient Mixture F-12 Ham (DME/F-12), Iscove's Modified Dulbecco's Medium (IMDM), G418 disulfate salt solution, hydrogen peroxide (H_2O_2), 3 (4,5 dimethylthiazol-2yl)-2,5-diphenyl tetrazolium bromide (MTT), Griess reagent, poly-D-lysine hydrobromide, 4',6-diamidino-2-phenylindole dihydrochloride (DAPI), fluoromount aqueous mounting medium, PKH26 (MINI26) and bovine serum albumin (BSA) were purchased from Sigma-Aldrich (St. Louis, MO, USA). Penicillin, streptomycin, L-glutamine, trypsin-EDTA, phosphate-buffer saline (PBS) and fetal bovine serum (FBS) were obtained from Euroclone (Pero, Milan, Italy). Alexa Fluor 488 Phalloidin was purchased from ThermoFisher Scientific (Waltham, MA, USA).

JMV2894 and EP80317 were synthetized by conventional solid phase from the laboratory of Prof. Jean-Alain Fehrentz, *Institut des Biolécules Max Mousseron,* University of Montpellier (France). Compounds were purified by high performance liquid chromatography (HPLC) (purity ≥ 98%).

Prior to assay, GHS were freshly dissolved in ultrapure water. Both GHS and H_2O_2 were diluted in culture media to final working concentrations for the experiments.

2. Cell cultures

2.1 Neuro-2A

Immortalized Neuro-2A murine neuroblastoma cells were obtained from Interlab Cell Line Collection (ICLC) and cultured in DMEM-high glucose (Sigma-Aldrich) supplemented with 10% heat-inactivated FBS, 100 IU/mL penicillin, 100 µg/mL streptomycin and 2 mM L-glutamine (Euroclone) and Mycozap Prophylactic (Lonza, Basel, Swiss) under standard cell culture conditions (37 °C, 5% CO_2 humidified incubator) (249,250).

2.2 SH-SY5Y

Human SH-SY5Y human neuroblastoma cells, either parental or constitutively expressing the G93A mutated SOD1, were a kind gift of Prof. Lucio Tremolizzo of the University of Milano-Bicocca. Briefly, monoclonal cell lines were obtained by transfection with plasmids directing constitutive expression of either wild-type SOD1 (WT) or mutant G93A ($SOD1^{G93A}$), as described by (68). SH-SY5Y cells were grown in DME-F12 (Sigma-Aldrich) supplemented with 10% heat-inactivated FBS, 100 IU/mL penicillin, 100 µg/mL

streptomycin (Euroclone) and Mycozap Prophylactic (Lonza), under standard cell culture conditions. WT and SOD1^{G93A} cells were grown in presence of 200 µg/mL G418, which was removed 2 days before performing the experiments.

After reaching confluence, Neuro-2A and SH-SY5Y cells were washed with PBS, detached with trypsin-EDTA solution (Euroclone), and seeded for experiments.
In each experiment, Neuro-2A cells were incubated with H_2O_2 alone or the combination of 100 µM H_2O_2 and 1 µM GHSs (hexarelin, JMV2894 or EP80317) for 24 h. Similarly, SH-SY5Y WT and SOD1^{G93A} cells were incubated for 24 h with H_2O_2 alone or the combination of 150 µM H_2O_2 and 1 µM GHSs.

2.3 N9

N9 immortalized murine microglia cells were grown in IMDM (Sigma-Aldrich) supplemented with 5% FBS, 2 mM L-glutamine, 100 IU/ml penicillin, 100 µg/ml streptomycin (Euroclone) and Mycozap Prophylactic (Lonza) at 37°C, under standard cell culture conditions (251).
N9 cells were incubated for 48 h with hexarelin or JMV2894 1 µM, and the conditioned culture media were collected and processed to isolate extracellular vesicles (EVs) as described below.

3. Cell viability

Neuro-2A and SH-SY5Y (WT and SOD1^{G93A}) cells were seeded in 96-well culture plates at the density of 4×10^4 cells/well and cultured for 24 h at 37 °C. The day after seeding, the cells were incubated with increasing concentrations (50–200 µM) of H_2O_2 or GHSs (10 nM–10 µM), or with a selected concentration of H_2O_2 (100 µM for Neuro-2A and 150 µM for SH-SY5Y) and a GHSs (1 µM). After 24 h of incubation, a 10 µL aliquot of 5 mg/mL MTT (Sigma-Aldrich) was added to each well and incubated at 37 °C for 3 h. Then, the culture medium was removed and a 200 µL aliquot of acidified isopropanol was added in order to dissolve the formazan crystals. Absorbance was read at 570 nm using the multilabel spectrophotometer VICTOR^3 (Perkin Elmer). Cell viability of control groups was set to 100% and the absorbances of experimental groups were converted to relative percentages (absorbance of experimental group/ absorbance of relative control) × 100 = % of viable cells.

4. Griess assay

NO production was evaluated in terms of the nitrite (NO_2^-) content of culture media measured with the Griess reaction. Briefly, Neuro-2A and SH-SY5Y (WT and $SOD1^{G93A}$) cells were seeded in 96-well culture plates and treated with H_2O_2 (100 µM for Neuro-2A, 150 µM for SH-SY5Y) and 1 µM GHSs for 24 h. At the end of the treatment, 100 µL aliquots of medium were transferred to a new 96-well plate and were mixed with 100 µL of Griess reagent 1X (Sigma-Aldrich), incubated 15 minutes in the dark at room temperature, and absorbance was measured at 540 nm with the VICTOR^3 spectrophotometer (Perkin Elmer). A standard curve with increasing concentrations of sodium nitrite (Sigma-Aldrich) was used for quantification. NO_2^- content of control groups were set to 100% and the absorbance of experimental groups were converted to relative percentages (absorbance of experimental group/ absorbance of relative control) × 100 = % of NO_2^-. The final nitrite concentration is proportional to the NO metabolite in the sample.

5. Actin staining assay

Neuro-2A and SH-SY5Y cells (2×10^5 cells/well) were seeded on coverslips coated with poly-D-lysine (Sigma-Aldrich) and incubated for 24 h. Cells were treated with H_2O_2 (100 µM for Neuro-2A, 150 µM for SH-SY5Y) for 24 h, with or without 1 µM GHSs (hexarelin, JMV2894 or EP80317), then washed with PBS and fixed with 4% paraformaldehyde (Titolchimica, Rome, Italy) for 10 min at room temperature. Cells were subsequently washed with PBS, incubated with cold acetone for 5 min at −20 °C, and blocked in PBS with 1% BSA for 30 min at room temperature. In order to stain actin, Neuro-2A and SH-SY5Y cells were incubated with 2 U/mL Alexa Fluor 488 Phalloidin diluted in PBS with 1% BSA at room temperature for 20 min, and then washed with PBS. Counterstaining of nuclei was made with 1 µg/mL DAPI for 10 min at room temperature. After washing with PBS, fluoromount aqueous mounting medium was added, and the cells were observed under a confocal laser scanning microscope (LSM 710, ZEISS, Jena, Germany); images were captured at 40x and 63x magnification by ZEN software (ZEISS).

6. Morphological analysis

Photomicrographs obtained at 40x magnification were used to evaluate the number of cells in the same area using a specifically designed macro with ImageJ software (National Institutes of Health, Bethesda, MD, USA) (252). The same photomicrographs were used for skeleton analysis (253). Skeleton analysis was applied to quantify the number of process endpoints and length normalized by the number of cells in the same area. Briefly, the photomicrographs were filtered to soften the background, enhance the contrast and remove noise, by using the application Fiji free software (https://imagej.net/fiji, accessed on 8 March 2021). All the images were then binarized, subsequently skeletonized and analysed with Analyze Skeleton (2D/3D) plugin (http://imagej.net/AnalyzeSkeleton, accessed on 8 March 2021). The overlay of skeleton to original image is reported to demonstrate that skeletons are representative of the original image; all the modification steps are illustrated in Figure 7.

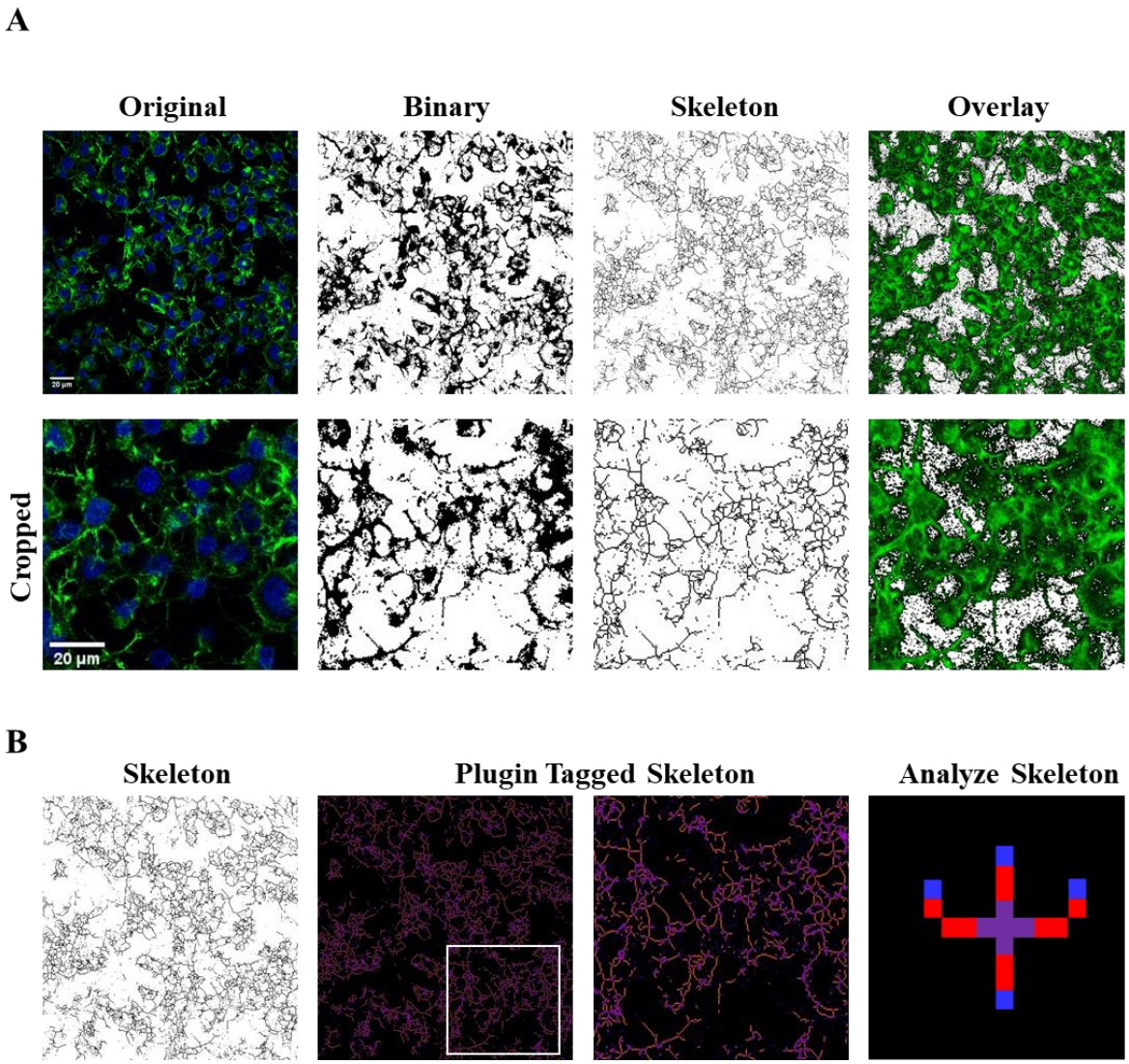

Figure 7. *Skeleton Analysis application to quantify cells morphology.*
(A) Representative photomicrograph (40x magnification) and the series of ImageJ plugin protocols of Neuro-2A cells, which were applied to each photomicrograph for skeleton analysis. Original photomicrograph was modified enhancing the background, removing noise and using with FFT filter prior to be converted to binary images. Binary image was skeletonized. The overlay of skeletonized and original images is reported; cropped photomicrographs show the image details. Scale bar: 20 µm. (B) The workflow used to Analyze Skeleton plugin: skeletonized process in orange, endpoint in blue, and junction in purple.

Moreover, we applied fractal analysis using FracLac plugin for ImageJ (https://imagej.nih.gov/ij/plugins/fraclac/fraclac.html, accessed on 8 March 2021), in order to evaluate the cellular shape and morphology by different parameters (fractal dimension, lacunarity, maximum span across the hull, perimeter and area) (254). Photomicrographs obtained with 63x oil immersion objective were modified similarly to skeleton analysis. Photomicrographs of cells were cropped and transformed to 8-bit grayscale images. Then, cell images were binarized and manually edited to obtain a single cell made of continuous set of pixels. To avoid bias, this modification was done taking into account the original image. Binary images were outlined and analyzed with Fractal Analysis plugin. All the modification steps and representative images of FracLac box counting analysis are shown in Figure 8.

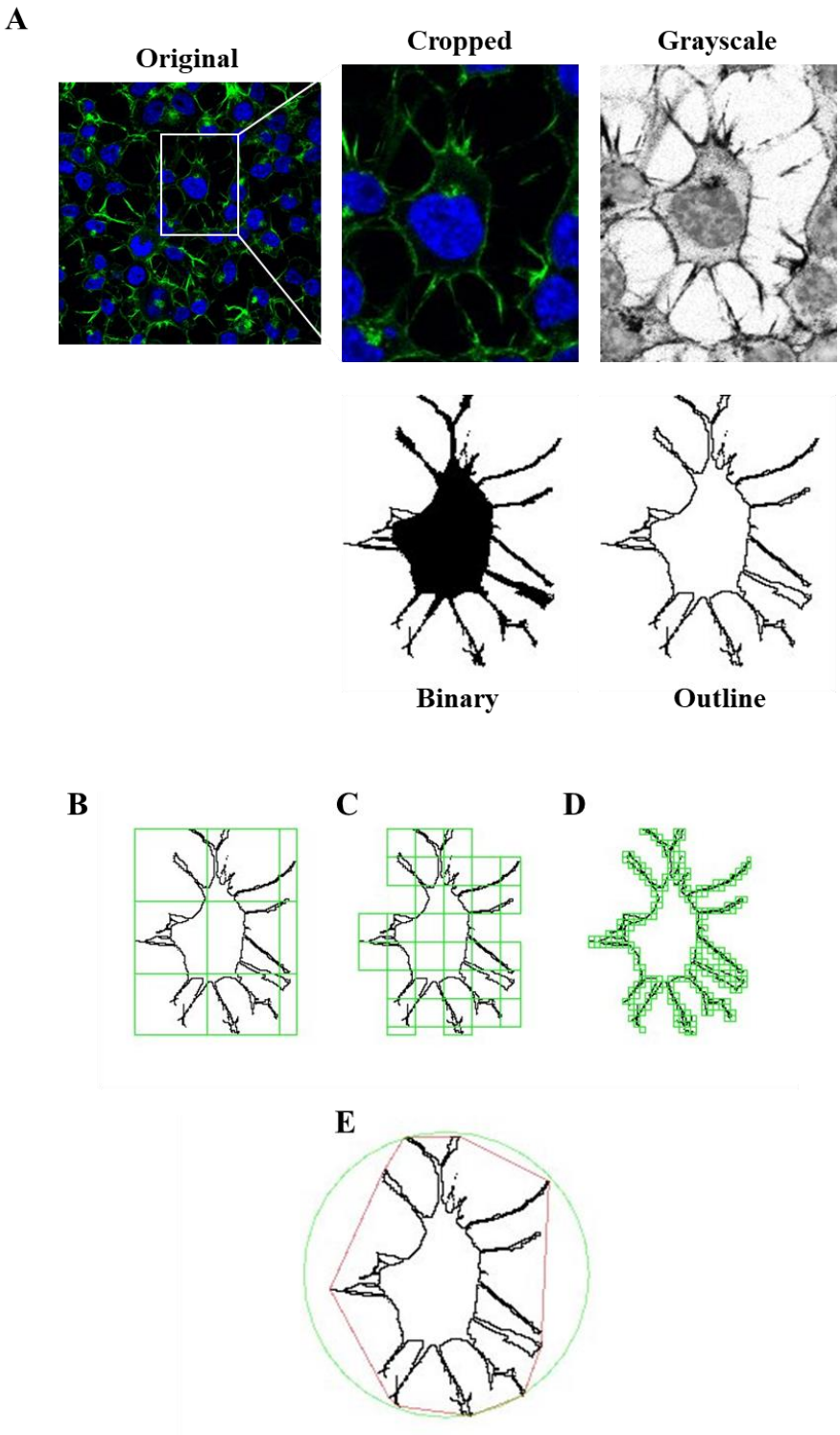

Figure 8. *FracLac Analysis application to quantify cellular morphology.*
(A) Representative process applied to obtain an outlined single cell for FracLac plugin. After selecting a cell in the photomicrograph (63x magnification), the image was cropped and modified to remove noise and enhance the background. The image was then processed to obtain an 8-bit grayscale microphotograph, and binarized. Binary image was manually edited to clear the background and to join all branches, and finally outlined. FracLac quantifies cell complexity and shape with a box counting method which permits to quantify fractal dimension (B), lacunarity (C), perimeter (D), and the maximum span across the convex hull (E) by drawing a convex hull (pink) and a bounding circle (green).

7. Isolation of EVs

N9 cells were plated in petri dishes and treated with 1 µM GHSs in a culture media without FBS for 48 h. To obtain EVs, conditioned medium was collected and subjected to the following series of centrifugations at 4 °C:

- 1000 ×g for 10 minutes, to remove dead cells;
- 1000 ×g for 20 minutes, to discard cell debris;
- 110.000 ×g for 70 minutes, to obtain EVs.

EVs were resuspended in 900 µL of PBS (Euroclone), splitted in 3 equal aliquot (300 µL) and centrifuged at 4 °C, at 110.000 ×g, for 70 minutes (255).

Finally, EVs were resuspended in 50 µL of (i) PBS (Euroclone) for the characterization and quantification with NanoSight NS300 (Malvern Panalytical), (ii) DME-F12 for in vitro experiments, and (iii) RIPA buffer (Cell Signaling Technology città nazione) for protein quantification, respectively.

8. Characterization and quantification of EVs

In order to treat SH-SY5Y WT and $SOD1^{G93A}$ with equal amount of N9-derived EVs, EVs were both characterized and quantified by NanoSight NS 300 (Malvern Panalytical), and by Micro BCA Protein Assay (Thermo Fisher Scientific) for the determination of protein contents.

Using the light scattering system, the NanoSight NS300 characterize (presence, size distribution and concentration) nanoparticles suspended in liquid, loaded into the laser module sample chamber and viewed in close proximity to the optical element.

Briefly, this instrument works basing on (i) the Brownian motion, which is the random motion of particles in a liquid suspension, and according to it the diffusion of different particles in a fluid is inversely proportional to their size; and on (ii) light scattering, the phenomenon by which photons change their direction after incidence on an object. Moreover, since the temperature of the sample and viscosity of the diluent can influence the motion of the particles, the laser module contains thermoelectric Peltier elements, allowing the sample temperature to be controlled, and permits to choose the type of diluent (aqueous), allowing the normalization of the results. Scattered light is visualized by a 20x magnification microscope onto which is mounted a video camera.

This is fully programmed using the nanoparticle-tracking analysis (NTA) Software Suite, which tracks EVs and generates digital images, and calculates dimension, concentration and distribution by using Stokes-Einstein equation.

EVs were tracked using the flow mode with syringe pump, which yields more EVs analyzed per video length, improved reproducibility due to better statistics, and allows fresh sample to be continuously introduced to sample chamber, with the following parameters:

- camera type: sCMOS;
- camera level: 15; FPS: 25.0;
- detect threshold: 5;
- temperature: 20 °C;
- dilution factor: 1:20;
- viscosity (water): 0.999-1.000 cP (centipoise);
- 3 videos for each analyzed sample.

Moreover, after isolation by ultracentrifugation, EVs were lysed in 50 µL of RIPA buffer (Cell Signaling Technology) and total protein concentrations were determined using the Micro BCA Protein Assay Kit (Thermo Fisher Scientific). This kit is a detergent-compatible bicinchoninic acid formulation for the colorimetric detection and quantitation of total protein, optimized for use with dilute protein samples. In our study, we have used a diluted albumin standard curve, ranging 0-200 µg/mL, with a test tube procedure mixed to the microplate ones.

SH-SY5Y WT and SOD1^{G93A} cells were treated for 24 h with i) 150 µM H_2O_2; ii) 1.5*10^9 EVs/mL (corresponding to 1 µg of total protein); or iii) the combination of H_2O_2 and EVs.

9. EVs labelling and assessment of preferential EVs cellular distribution

To assess the uptake and distribution of EVs by SH-SY5Y WT and SOD1^{G93A} cells, EVs derived from N9 cells treated for 48 h with GHSs were labelled with PKH26 red fluorescent cell linker kit (MINI26, Sigma) according to the procedures for general cell membrane labeling, with some modifications. Briefly, EVs resuspended in 50 µL PBS were mixed with 50 µL of PKH26 dye in diluent C (1:1 v/v) for 5 min at room temperature. This mixture was further diluted with 2.5 mL of PBS and centrifuged at 110.000 ×g for 70 min to precipitate the PKH26 labeled EVs. The EVs pellet was further washed twice with PBS by ultracentrifugation at 110.000 ×g for 70 min, to remove any free dye, and finally the EVs pellet was resuspended in 50 µL PBS. Then, labelled EVs were added either to SH-SY5Y WT and to SH-SY5Y SOD1^{G93A} on coverslips for 24 h. Cells were fixed with 4% (w/v) paraformaldehyde in PBS and stained with phalloidin and DAPI, as mentioned above.

Fluorescence images were obtained by confocal laser scanning microscope (LSM 710, ZEISS), and captured at 40x and 63x magnification by ZEN software (ZEISS).

10. Real-time PCR analysis

In order to monitor the apoptosis pathway, Neuro-2A and SH-SY5Y cells were plated in 24-well culture plates at a density of 2×10^5 cells/well, and treated for 24 h according to previously described protocols. Following treatment, cells were washed with PBS and total RNA was extracted using EuroGOLD Trifast reagent (Euroclone), according to the manufacturer's instructions and quantified using a Nanodrop ND-1000 spectrophotometer (Thermo Fisher Scientific). Reverse transcription was performed using iScript cDNA Synthesis Kit (Bio-Rad) using140 ng of RNA for each sample. Amplification of cDNA (21 ng) was performed in a total volume of 20 μL of iTaq Universal Probes Supermix (Bio-Rad), using Real-Time QuantStudio7 Flex (Thermo Fisher Scientific). After 2 min at 50 °C and 10 min at 94.5 °C, 40 PCR cycles were performed using the following conditions: 15 s at 95 °C and 1 min at 60 °C. Relative mRNA concentrations of the target genes were normalized to the corresponding β-actin internal control and calculated using the $2^{-\Delta\Delta Ct}$ method.

11. Western blot analysis

Neuro-2A and SH-SY5Y cells were plated in 6-well culture plates at a density of 8×10^5 cells/well, incubated at 37 °C for 24 h and then treated as previously described. Following treatment, cells were rinsed with ice-cold PBS and lysed in RIPA buffer (Cell Signaling Technology), supplemented with a protease-inhibitor cocktail (Sigma-Aldrich), according to the manufacturer's protocol. Total protein concentrations were determined using the Pierce BCA Protein Assay Kit (Thermo Fisher Scientific). Equal amounts of protein (20 μg) were heated at 95 °C for 10 min, loaded on precast 4–12% gradient gels (Invitrogen, Waltham, USA), separated by electrophoresis, and transferred to a polyvinylidene difluoride (PVDF) membrane (Thermo Fisher Scientific). Non-specific binding was blocked with 5% dried fat-free milk dissolved in phosphate-buffered saline (PBS) supplemented with 0.1% Tween-20 (PBS-T) for 1 h at room temperature. After 3 washes in PBS-T, membranes were incubated with the primary antibody overnight at 4 °C (Anti-cleaved caspase-3 (Asp175) (5A1E) rabbit antibody, #9664, Cell Signaling Technology, 1:1000; anti-cleaved caspase-7 (Asp198) rabbit antibody, #9491, Cell Signaling Technology, 1:1000; anti-Phospho-p44/42 MAPK (Erk1/2) (Thr202/Tyr204) rabbit antibody, #9101, Cell Signaling Technology, 1:1000; anti-p44/42 MAPK (Erk1/2) rabbit

antibody, #4695, Cell Signaling Technology, 1:1000; anti-Phospho-p38 MAPK (Thr180/Tyr182) rabbit antibody, #4511, Cell Signaling Technology, 1:1000; anti-p38 MAPK rabbit antibody, #9212, Cell Signaling Technology, 1:1000; anti-Phospho-Akt rabbit antibody, #4060, Cell Signaling Technology, 1:2000; anti-Akt rabbit antibody, #4685, Cell Signaling Technology, 1:1000; anti-actin rabbit antibody, #A2066, Sigma Aldrich, 1:2500), and then with a peroxidase-coupled goat anti-rabbit IgG (#31460, Thermo Scientific, 1:5000) for 1 h at room temperature. Signals were developed with the extra sensitive chemiluminescent substrate LiteAblot TURBO (Euroclone) and detected with Amersham ImageQuant 800 (GE Healthcare, Buckinghamshire, UK). Image J software was used to quantify protein bands.

12. Statistical analysis

Statistical analysis was performed using the program GraphPad Prism (GraphPad Software, San Diego, California). Values are expressed as the mean ± standard error of the mean (SEM). Experiments were independently replicated at least three times. One-way ANOVA followed by Tukey's t-test was used for multiple comparisons. A p-value of less than 0.05 was considered significant.

RESULTS

1. Effects of H_2O_2 on cell viability

Neuro-2A and SH-SY5Y (WT and $SOD1^{G93A}$) cells were treated with increasing concentrations of H_2O_2 (50–200 µM) for 24 h in order to assess its effects on cell replication and to identify the lowest concentration that reproducibly and significantly inhibited cell growth. As shown in Figure 9, H_2O_2 reduced cell replication in a concentration-dependent manner in all the different cell lines tested.

Figure 9A shows the effect of H_2O_2 treatment on cell viability in Neuro-2A cells: even though the concentration of 80 µM already determined a significant decrease of cell viability ($p < 0.001$), 100 µM H_2O_2 induced a significant and reproducible reduction of cell survival (20.41 ± 3.12%, $p < 0.001$) compared with control.

H_2O_2 caused a significant inhibition of cell growth also in SH-SY5Y WT and $SOD1^{G93A}$ (Figures 9B,C). In particular, 150 µM was the lowest concentration of H_2O_2 that induced a significant decrease of cell viability compared to the control group (WT: 23.67 ± 2.49%, $p < 0.01$; SOD1: 26.21 ± 3.88%; $p < 0.01$).

As H_2O_2 at 100 µM and 150 µM significantly and reproducibly decreased cell replication compared with control, they were used in subsequent experiments for Neuro-2A and SH-SY5Y (WT and $SOD1^{G93A}$) cell lines, respectively.

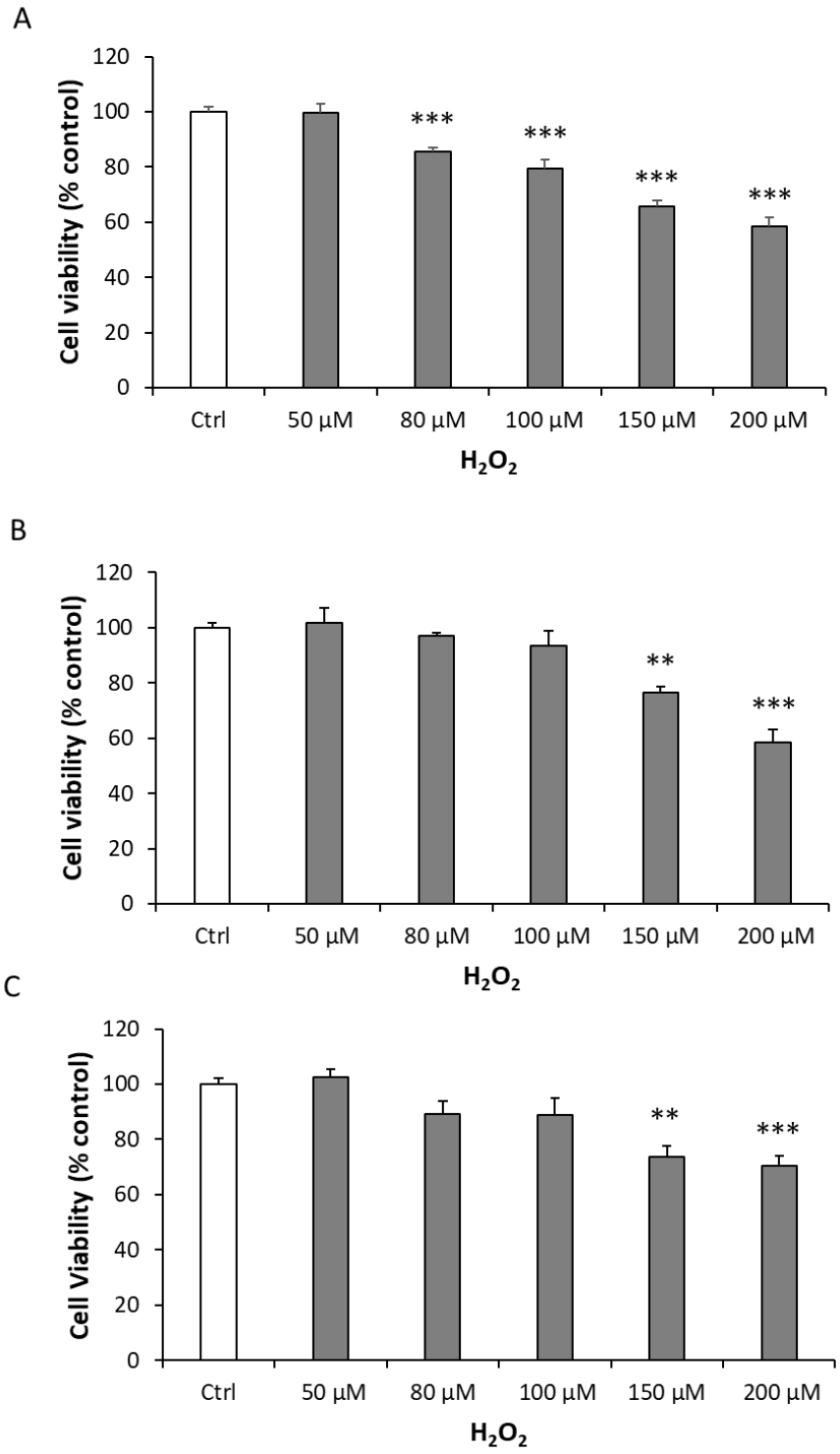

Figure 9. *Effects of increasing concentration of H_2O_2 on Neuro-2A, SH-SY5Y WT and SH-SY5Y SOD1^{G93A} cell viabilities.*

(A) Neuro-2A, (B) SH-SY5Y WT and (C) SH-SY5Y SOD1^{G93A} cells were treated for 24 h with different concentrations of H_2O_2 (0, 50, 80, 100, 150, 200 µM) and cell viability was assessed by MTT assay. Results were obtained in at least three independent experiments (n = 21). Statistical significance: ** $p < 0.01$, and *** $p < 0.001$ vs. Ctrl.

2. Effects of GHSs on cell viability

Several cell viability assays were performed to verify the cytotoxicity of GHSs and to identify the concentrations to be used in subsequent experiments. To these aims, we have treated Neuro-2A and SH-SY5Y (WT and $SOD1^{G93A}$) cells with increasing concentrations of GHSs (10 nM–10 μM) for 24 h (Figure 10, 11, 12).

As shown in Figure 10, exposure of Neuro-2A cells to increasing concentrations of hexarelin, JMV2894 and EP80317 for 24 h did not reduce cell viability.

Also in SH-SY5Y WT cells, incubation with hexarelin and JMV2894 for 24 h did not reduce cell viability, while 10 μM EP80317 significantly decreased cell survival ($p < 0.05$; Figure 11). Treatment of SH-SY5Y $SOD1^{G93A}$ with increasing concentrations of EP80317 and JMV2894 for 24 h did not affect cell replication, but 10 μM hexarelin induce a significant reduction of cell viability ($p < 0.05$; Figure 12).

Given the results obtained and previous experimental data, 1 μM was the concentration of GHSs selected for the subsequent experiments.

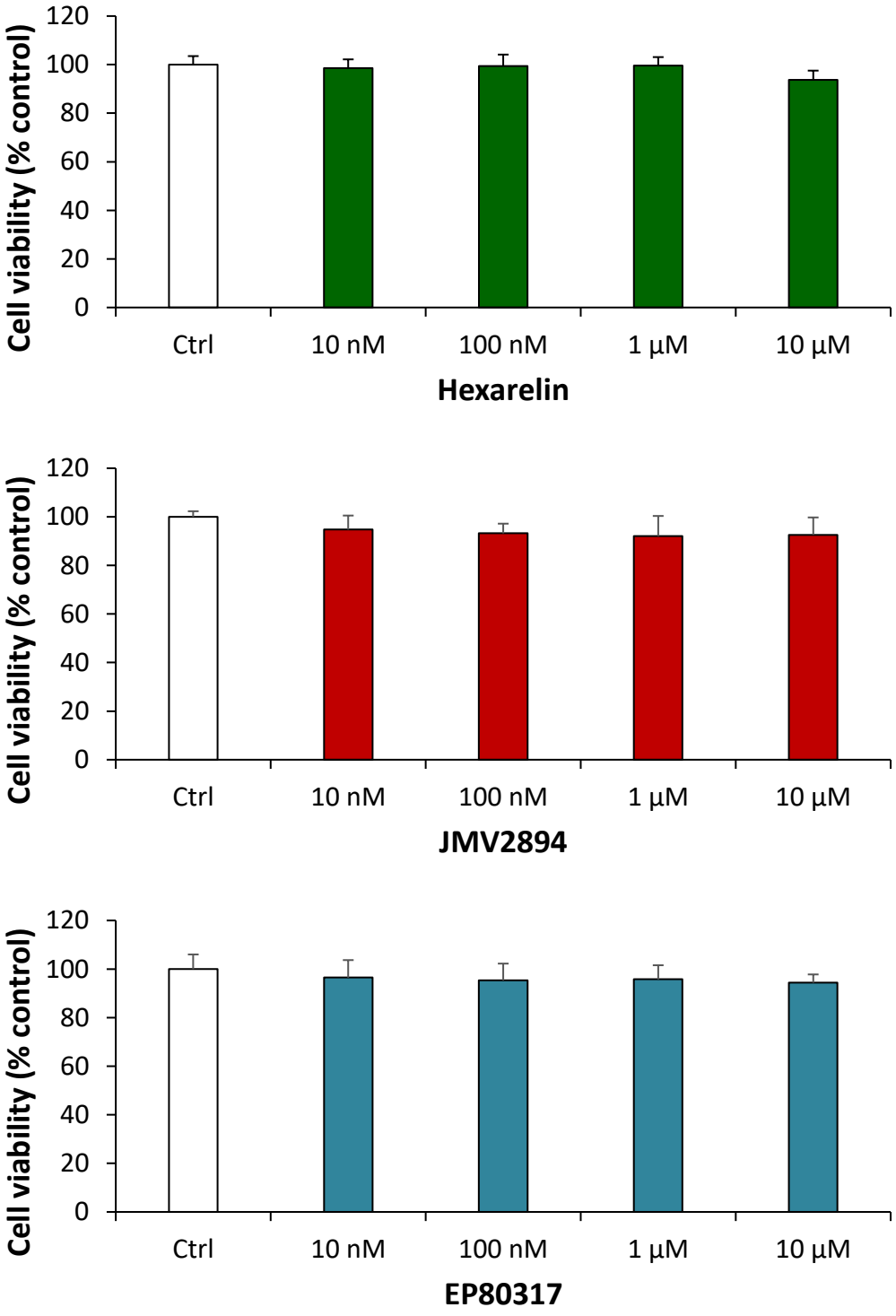

Figure 10. *Effects of increasing concentrations of GHSs on viability of Neuro-2A cells.* Neuro-2A, cells were treated for 24 h with increasing concentrations of GHSs (0, 10 nM, 100 nM, 1 µM and 10 µM) and viability was assessed with MTT assay. Results were obtained in at least three independent experiments (n = 21).

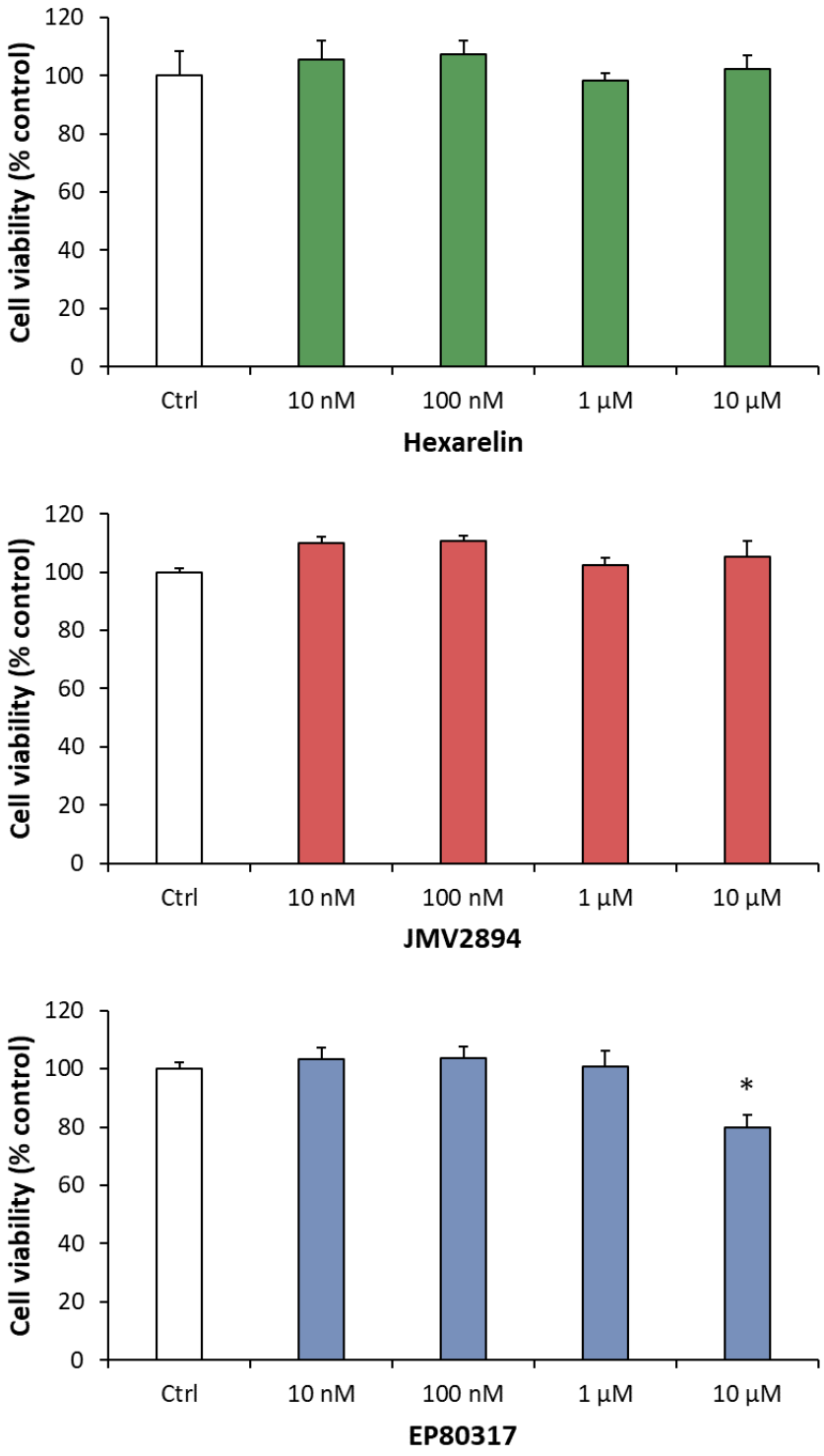

Figure 11. *Effects of increasing concentrations of GHSs on viability of SH-SY5Y WT cells.* SH-SY5Y WT cells were treated for 24 h with increasing concentrations of GHSs (0, 10 nM, 100 nM, 1 µM and 10 µM) and cell viability was assessed with MTT assay. Results were obtained in at least three independent experiments (n = 21). Statistical significance: * $p < 0.05$ vs. Ctrl.

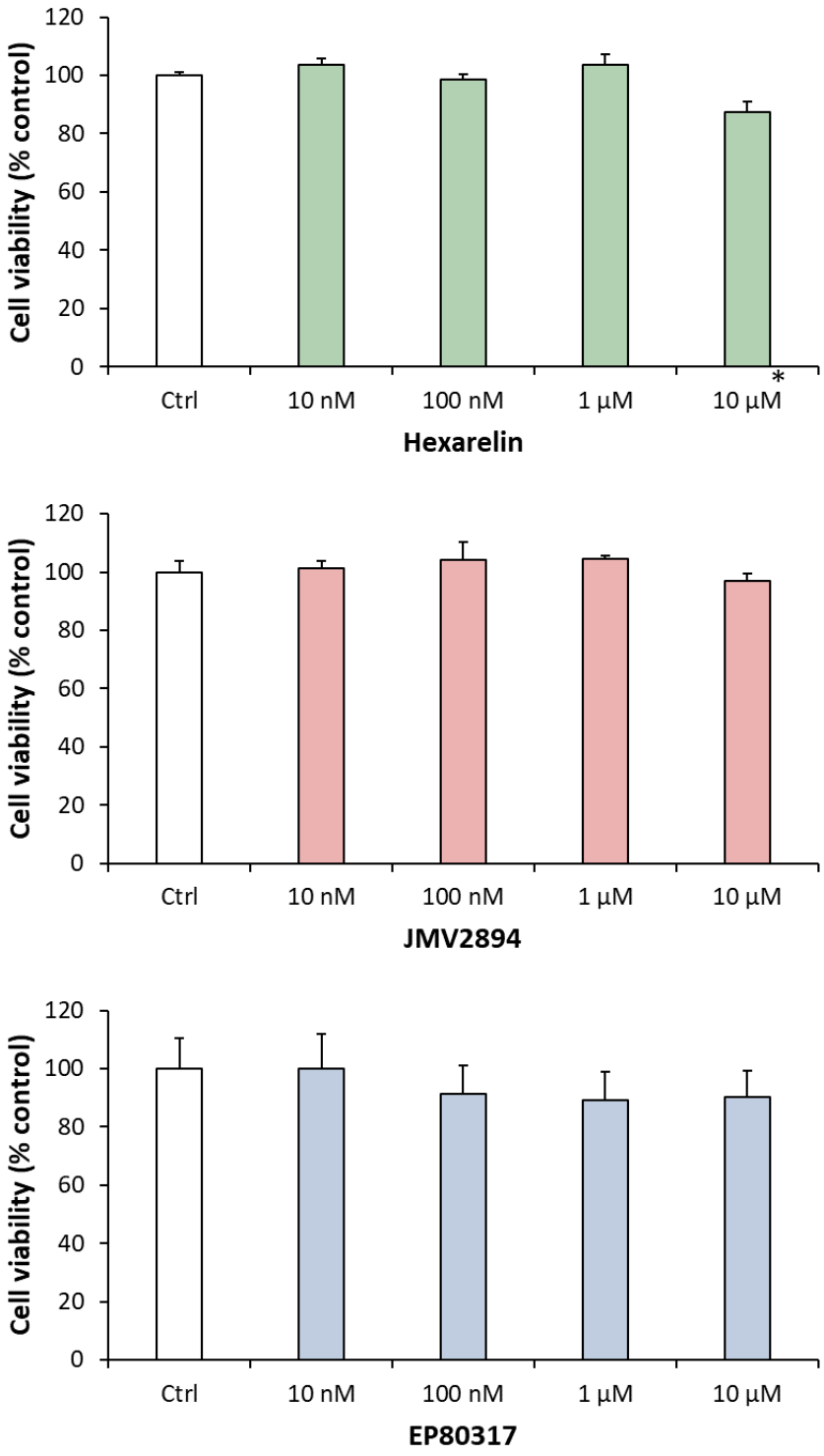

Figure 12. *Effects of increasing concentrations of GHSs on viability of SH-SY5Y SOD1^{G93A} cells.* SH-SY5Y SOD1^{G93A} cells were treated for 24 h with increasing concentrations of GHSs (0, 10 nM, 100 nM, 1 µM and 10 µM) and cell viability was assessed with MTT assay. Results were obtained in at least three independent experiments (n = 21).). Statistical significance: * $p < 0.05$ vs. Ctrl.

3. Effects of GHSs on H_2O_2-induced toxicity

To investigate the protective effect of GHSs on H_2O_2-induced damage, cultured Neuro-2A and SH-SY5Y (WT and $SOD1^{G93A}$) cells were incubated for 24 h with 100 and 150 µM H_2O_2 (respectively for Neuro-2A and SH-SY5Y), 1 µM GHSs or the combination of H_2O_2 and GHSs (Figure 13).

As expected, in Neuro-2A cells 100 µM H_2O_2 induced a significant growth reduction compared with control cells ($p < 0.001$), whereas GHSs alone did not induce any effect. In Neuro-2A cells hexarelin and JMV2894 significantly antagonized the reduction in cell viability caused by H_2O_2 (22.05 ± 3.28%, $p < 0.05$ and 12.60 ± 2.25%, $p < 0.05$, respectively) (Figure 13A).

The viability of SH-SY5Y (WT and $SOD1^{G93A}$) was significantly decreased following incubation with 150 µM H_2O_2 ($p < 0.001$) for 24 h. In SH-SY5Y WT, only 1 µM hexarelin significantly protected the cells from H_2O_2 reduction of cell viability (14.30 ± 2.40%, $p < 0.05$) (Figure 13B). As shown in Figure 13C, in SH-SY5Y $SOD1^{G93A}$ cells, the three GHSs failed to antagonize the reduction of cell viability induced by H_2O_2.

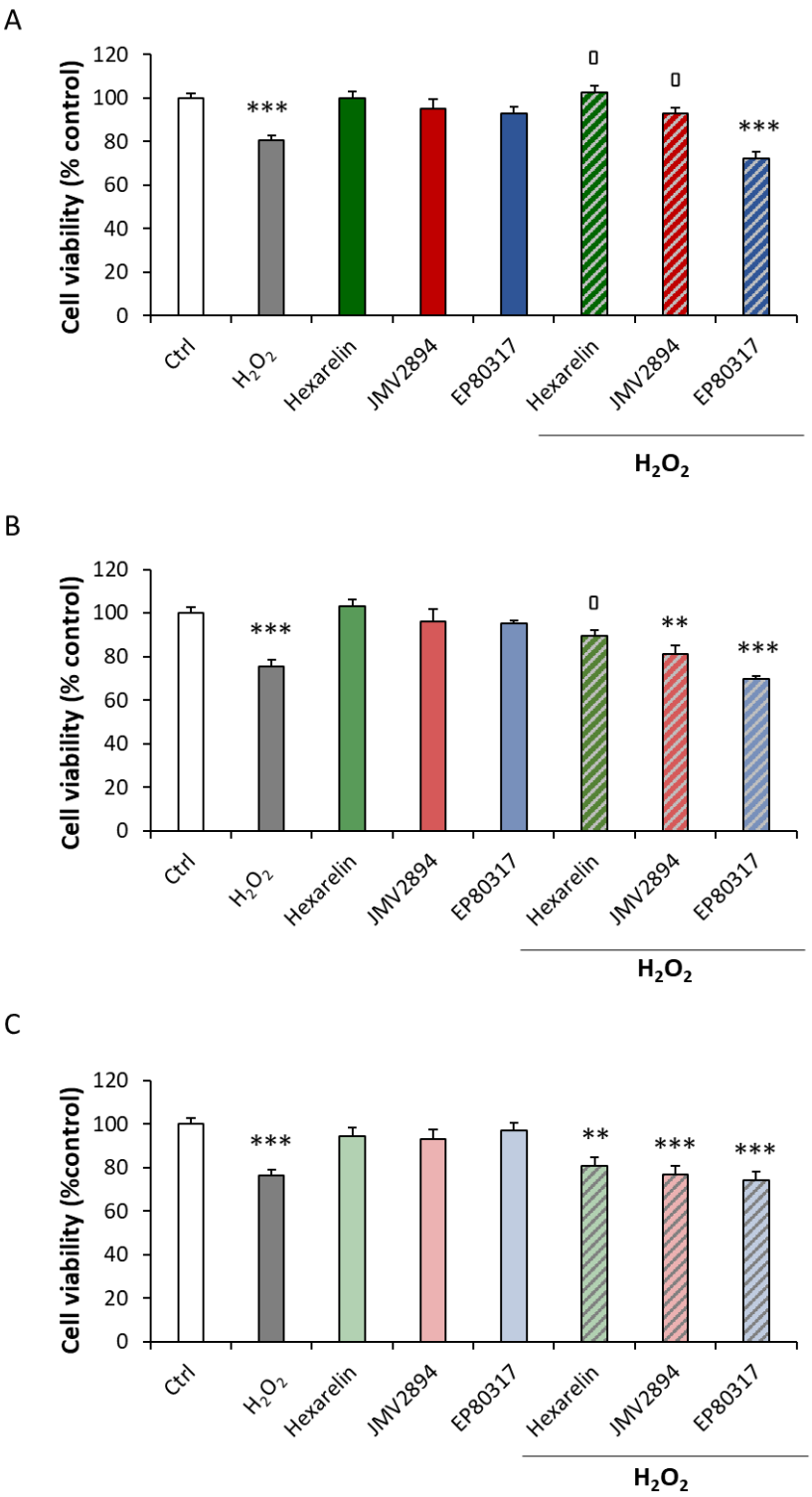

Figure 13. *Protective effects of GHSs in Neuro-2A, SH-SY5Y WT and SH-SY5Y SOD1^{G93A} cells.* (A) Neuro-2A, (B) SH-SY5Y WT and (C) SH-SY5Y SOD1^{G93A} cells were treated for 24 h with or without GHSs (1 µM) and H_2O_2 (100 µM for Neuro-2A, 150 µM for SH-SY5Y WT and SOD1^{G93A}) and cell viability was assessed with MTT assay. Results were obtained in at least three independent experiments (n = 21). Statistical significance: ** $p < 0.01$, *** $p < 0.001$ vs. Ctrl; ° $p < 0.05$ vs. H_2O_2.

4. Effects of GHSs on NO_2^- production in Neuro-2A and SH-SY5Y cells treated with H_2O_2

Nitric oxide (NO) is a highly reactive cytotoxic free radical, whose synthesis can be induced by oxidative stress. Extracellular nitrite (NO_2^-) concentrations, proportional to NO formation induced by H_2O_2, were measured in the culture medium by the Griess assay.

The NO_2^- levels in Neuro-2A media are shown in Figure 14A. The amount of NO_2^- released by Neuro-2A cells increased significantly when exposed to 100 µM H_2O_2 (increase: 33.86 ± 10.90%, $p < 0.05$), and the treatment with GHSs significantly decreased the H_2O_2-induced NO_2^- production. Briefly, treatment with 1 µM hexarelin significantly reduced the release of NO_2^- induced by 100 µM H_2O_2 (reduction: 85.60 ± 7.99%, $p < 0.001$ vs H_2O_2). Similarly, 1 µM JMV2894 effectively antagonized H_2O_2, whereas 1 µM EP80317 did not reduce the increase of NO_2^- concentrations caused by H_2O_2.

In the same way, to assess the potential of GHSs to modulate NO release in SH-SY5Y (WT and $SOD1^{G93A}$) cells, NO_2^- levels were measured in the culture supernatants of H_2O_2-treated cells, in absence or presence of GHSs. The results shown in Figure 14B and C demonstrated that 150 µM H_2O_2 significantly stimulated ($p < 0.001$) NO_2^-production by SH-SY5Y WT and $SOD1^{G93A}$ cells. Similarly to Neuro-2A cells, hexarelin and JMV2894 significantly inhibited NO_2^- increase stimulated by H_2O_2 ($p < 0.05$) in SH-SY5Y WT, while in SH-SY5Y $SOD1^{G93A}$ GHSs-treatments induced only a trend toward a reduction of NO_2^- levels.

These results suggest that the anti-apoptotic effects of GHSs, in particular those of hexarelin and JMV2894, could be mediated by an antioxidant mechanism.

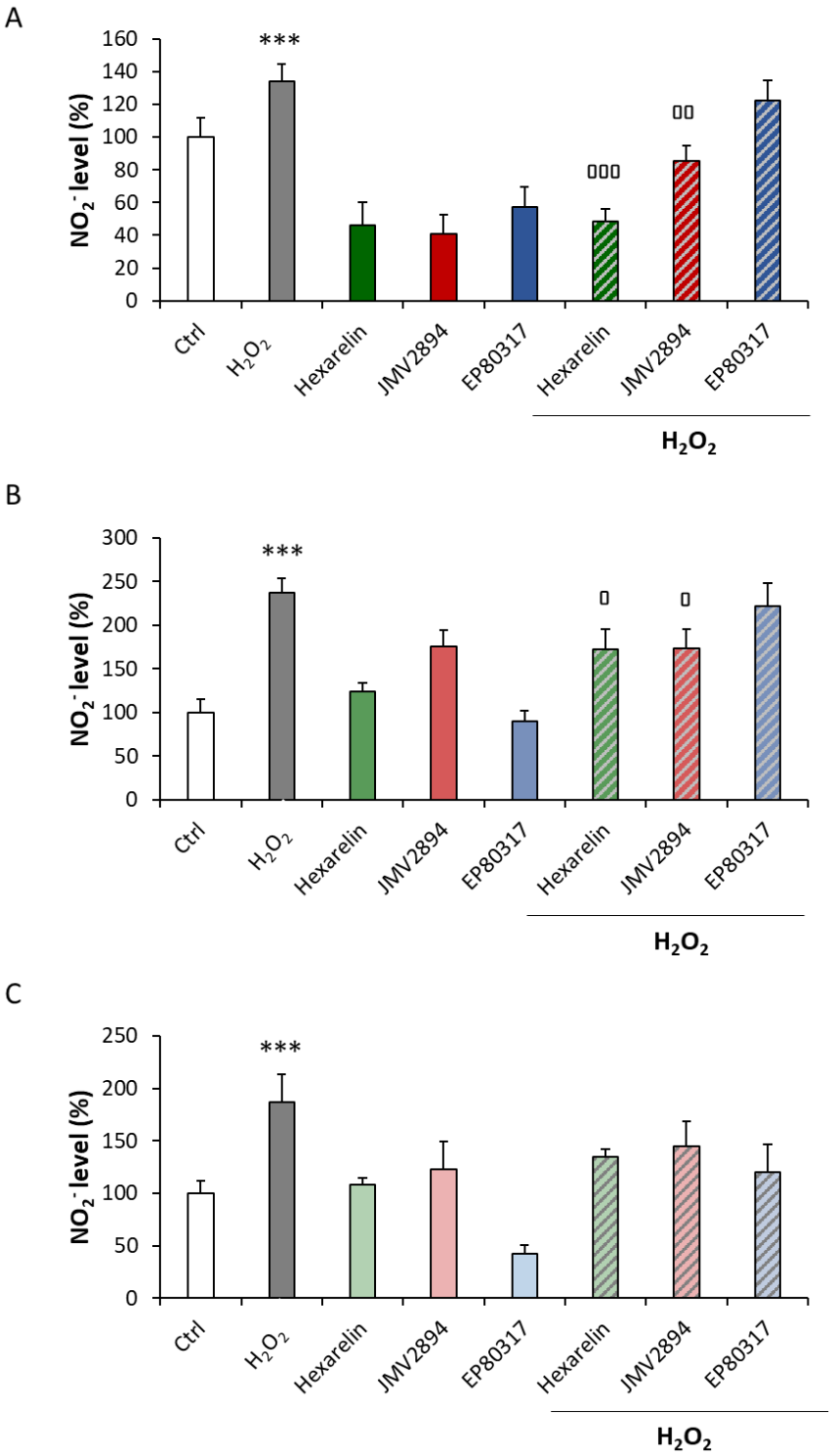

Figure 14. *GHSs effects on the extracellular NO_2^- release induced by H_2O_2.*
(A) Neuro-2A, (B) SH-SY5Y WT and (C) SH-SY5Y SOD1^{G93A} cells were treated for 24 h with or without GHSs and the selected concentration of H_2O_2 (100 µM for Neuro-2A, 150 µM for SH-SY5Y WT and SOD1^{G93A}). Culture media were used for Griess reaction to measure NO_2^- extracellular release. Data are expressed as mean ± SEM (n = 24). Statistical significance: *** $p < 0.001$ vs. Ctrl; ° $p < 0.05$, °° $p < 0.01$, and °°° $p < 0.001$ vs. H_2O_2.

5. Effects of GHSs on morphological changes induced by H_2O_2-treatment

Cells were stained as described in Materials and Methods and observed with a confocal laser-scanning microscope (LSM 710, ZEISS) in order to characterize morphological changes induced by treatments. Representative photomicrographs for each treatment of all cellular line are shown in Figure 15A, 16A and 17A (Neuro-2A, SH-SY5Y WT and SH-SY5Y $SOD1^{G93A}$ cells respectively). First, we quantified the number of Neuro-2A and SH-SY5Y (WT and $SOD1^{G93A}$) cells in a fixed area by the use of a specific macro for ImageJ software (252). The number of cells in each field was used for normalizing data of skeleton analysis, which in turn was used to quantify endpoints and process length (253,256), since the loss of ramifications is a typical characteristic of morphological cytoskeletal changes in apoptosis. Briefly, Analyze Skeleton Plugin was applied to skeleton images obtained after a series of ImageJ plugin protocols of original photomicrographs, as described in Material and Methods, and shown in Figure 7. Process length (Figure 7B, orange) indicate the measure of processes elongation, while endpoints (Figure 7B, blue) are the termination of cellular ramifications.

As shown in Figure 15B, 100 µM H_2O_2 induced a significant reduction ($p < 0.001$) in the number of Neuro-2A cells per field compared with control; interestingly, cell numbers were significantly greater only in group treated with the combination of H_2O_2 and 1 µM hexarelin ($p < 0.01$). Figure 15C and D show that H_2O_2 treatment alone caused a reduction of both cellular process endpoints and summed process length per cell, compared with controls ($p < 0.001$ and $p < 0.001$, respectively); the effects of H_2O_2 alone were significantly inhibited by co-incubation with hexarelin ($p < 0.001$) or JMV2894 ($p < 0.001$).

In SH-SY5Y WT cells, the reduction in the number of cells per field and that of cellular process endpoints caused by H_2O_2 ($p < 0.01$ and $p < 0.001$, respectively) were significantly counteracted by the treatments with hexarelin or JMV2894 ($p < 0.05$ and $p < 0.001$, respectively). In contrast, EP80317 enhanced the effects of H_2O_2 (Figure 16B,C). H_2O_2 treatment induced also the reduction of summed process length per cell compared with control ($p < 0.001$); in this case the co-incubation with GHSs significantly antagonized this effect of H_2O_2 ($p < 0.001$, Figure 16D).

As expected, the morphological analysis of SH-SY5Y $SOD1^{G93A}$ revealed that H_2O_2 significantly reduced the (i) number of cells per field ($p < 0.001$, Figure 17B), (ii) cellular process endpoints ($p < 0.001$, Figure 17C), and (iii) summed process length per cell ($p < 0.01$, Figure 17D) compared with control. These morphological changes were counteracted by the treatment with GHSs; in fact, hexarelin similarly to JMV2894 restored the number of

cells, elongations and end-point of SH-SY5Y SOD1^{G93A} cells to control levels (Figure 17B, C and D), while EP80317 increased only the number of cellular endpoints (Figure 17D).

We used FracLac for ImageJ to investigate and quantify morphological changes of cells as a consequence of treatments. Examples of cropped photomicrographs, binary and outline transformations of Neuro-2A, SH-SY5Y WT and SOD1^{G93A} cells are shown in Figures 18A, B and C, respectively. We have quantified by fractal analysis the following parameters:

1- Fractal dimension (D), an index of cell complexity pattern, which is used to identify cellular forms ranging from simple rounded to complex branched (Figure 8B) (254,256).
2- Lacunarity, a property of the soma based on the heterogeneity or translational and rotational invariance in a shape (Figure 8C); lower lacunarity values indicate a loss of shape heterogeneity (254,256).
3- Maximum Span Across the Convex Hull (MSACH), which is the maximum distance between two points across the convex hull (Figure 8E).
4- Perimeter, calculated as the number of pixels on the outline cell shape (Figure 8D).
5- Area, quantified as the total number of pixels present in the filled shape of cell image (Figure 8A "Binary").

As shown in Figure 19A, in Neuro-2A cells H_2O_2 induced a significant reduction ($p < 0.001$) of D compared with the controls, indicating a reduced branch complexity, according to skeleton analysis. Conversely, Neuro-2A cells treated with the combination of H_2O_2 and 1 µM GHSs exhibited a significantly greater D value ($p < 0.001$ for hexarelin and JMV2894 groups, $p < 0.01$ for EP80317) compared with cells treated with H_2O_2 alone, with values similar to the D value of controls.

The lacunarity values of cells treated with 100 µM H_2O_2 alone were significantly smaller than those of the control group. Hexarelin and JMV2894 antagonized the effects of H_2O_2, since cells treated with hexarelin or JMV2894 and H_2O_2, showed values significantly greater ($p < 0.001$) compared to those of cells treated with H_2O_2 alone (Figure 19B). Finally, H_2O_2 treatment alone significantly reduced MSACH, perimeter and area ($p < 0.001$ for all); this reduction was blunted by co-incubations with GHSs (Figures 19C, D and E).

In SH-SY5Y WT and SOD1^{G93A} cells, H_2O_2 did not induce any significant modification of D values (Figures 20A and 21A) but, similarly to Neuro-2A cells, 150 µM H_2O_2 significantly decreased lacunarity ($p < 0.01$) compared to controls (Figures 20B and 21B). GHSs antagonized this effect in both SH-SY5Y WT and SOD1^{G93A} cells: Figures 20B and 21B show that lacunarity values are greater in cells treated with GHSs+H_2O_2 than those in cells treated with H_2O_2 alone; however, differences reached statistical significance only in SH-

SY5Y WT cells ($p < 0.001$ for hexarelin and JMV2894; $p < 0.05$ for EP80317). MSACH, perimeter and area values of SH-SY5Y WT and $SOD1^{G93A}$ cells treated with H_2O_2 alone were significantly smaller than control group. As shown in Figures 20C, D, E and Figures 21C, D, E, this reduction was attenuated by co-incubation with GHSs.

The morphological results obtained with skeleton and fractal analysis are summarized in a 3D scatter plot (Figure 22A,B and C). We have chosen to represent endpoints/cell, fractal dimension and lacunarity because they are independent variables and allow better appreciation of apoptosis-induced cytoskeletal changes.

A

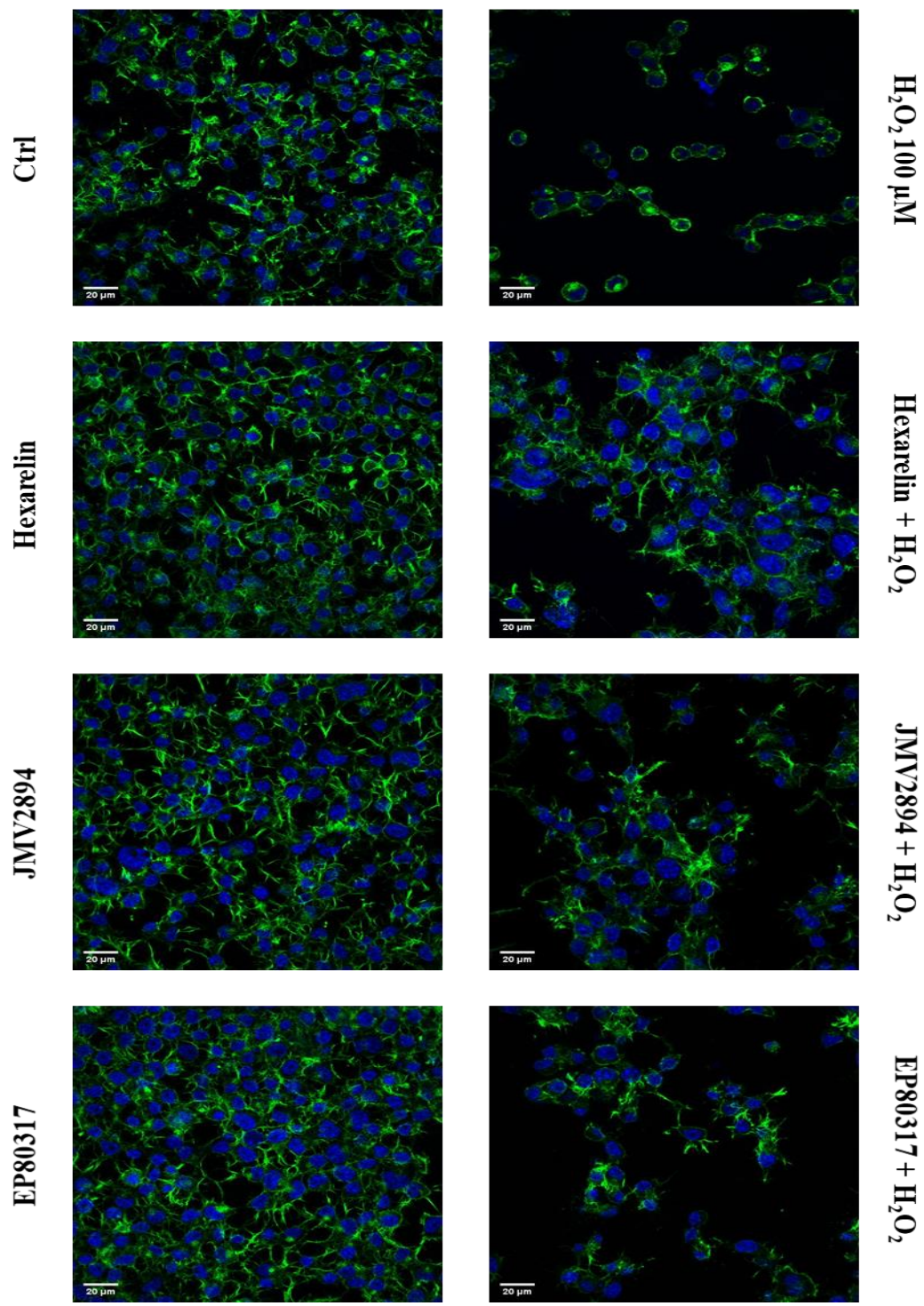
Ctrl
Hexarelin
JMV2894
EP80317
H_2O_2 100 µM
Hexarelin + H_2O_2
JMV2894 + H_2O_2
EP80317 + H_2O_2
20 µm

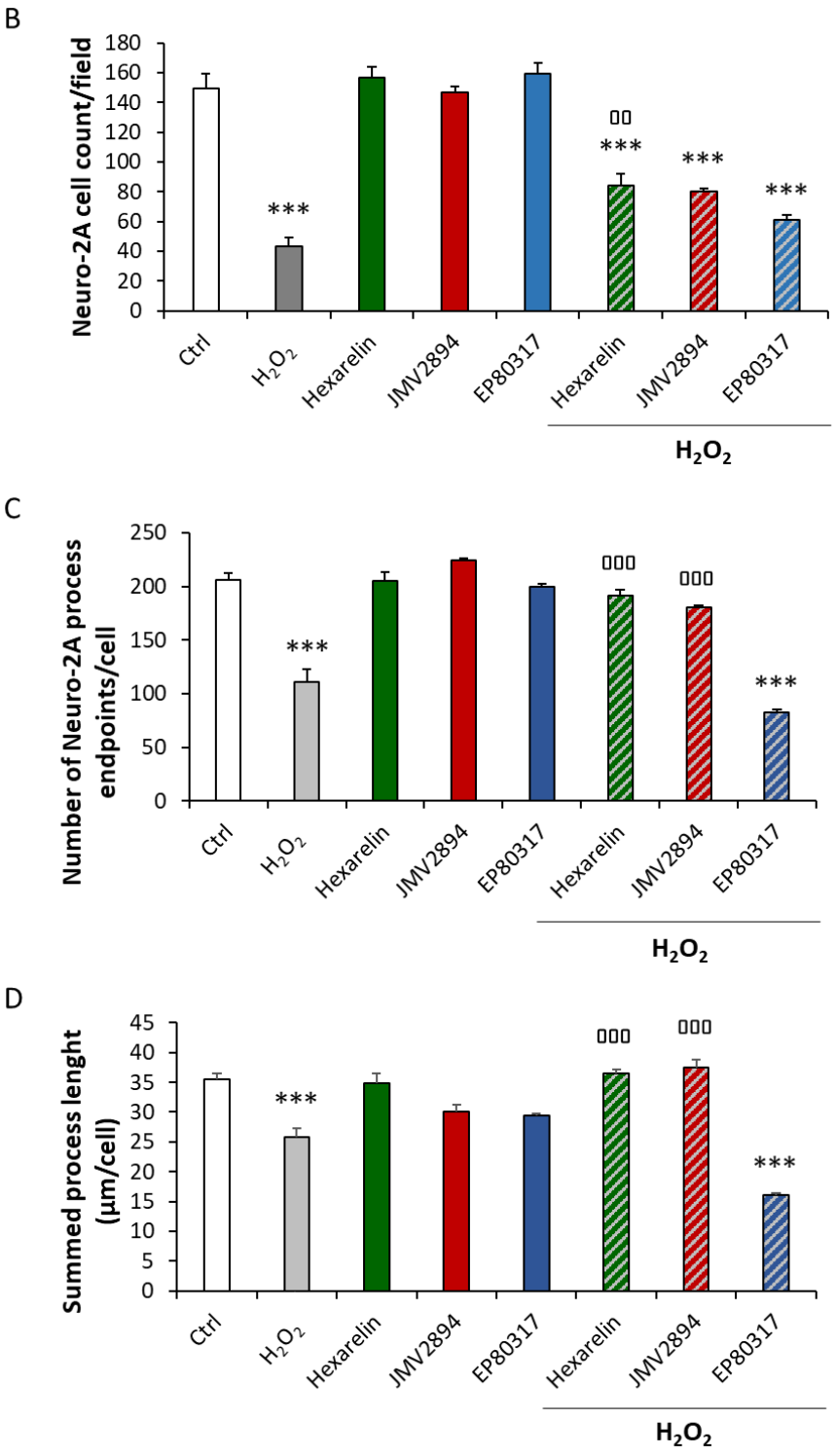

Figure 15. *GHSs inhibit Neuro-2A cells de-ramification induced by H_2O_2.*
(A) Neuro-2A cells were seeded on poly-D-lysine pre-treated coverslips and incubated for 24 h with or without GHSs and 100 µM H_2O_2. At the end of the treatment, cells were fixed and stained for phalloidin and DAPI. Images were captured with confocal laser scan microscope. Scale bar: 20 µm. Graphical representation of the number of: (B) cells in the same areas for each treatment; (C) process endpoints/cells; and (D) process length/cells. Data are expressed as mean ± SEM of replicates obtained in 3 independent experiments (total number of cells analyzed = 160). Statistical significance: *** $p < 0.001$ vs. Ctrl; °° $p < 0.01$, and °°° $p < 0.001$ vs. H_2O_2.

A

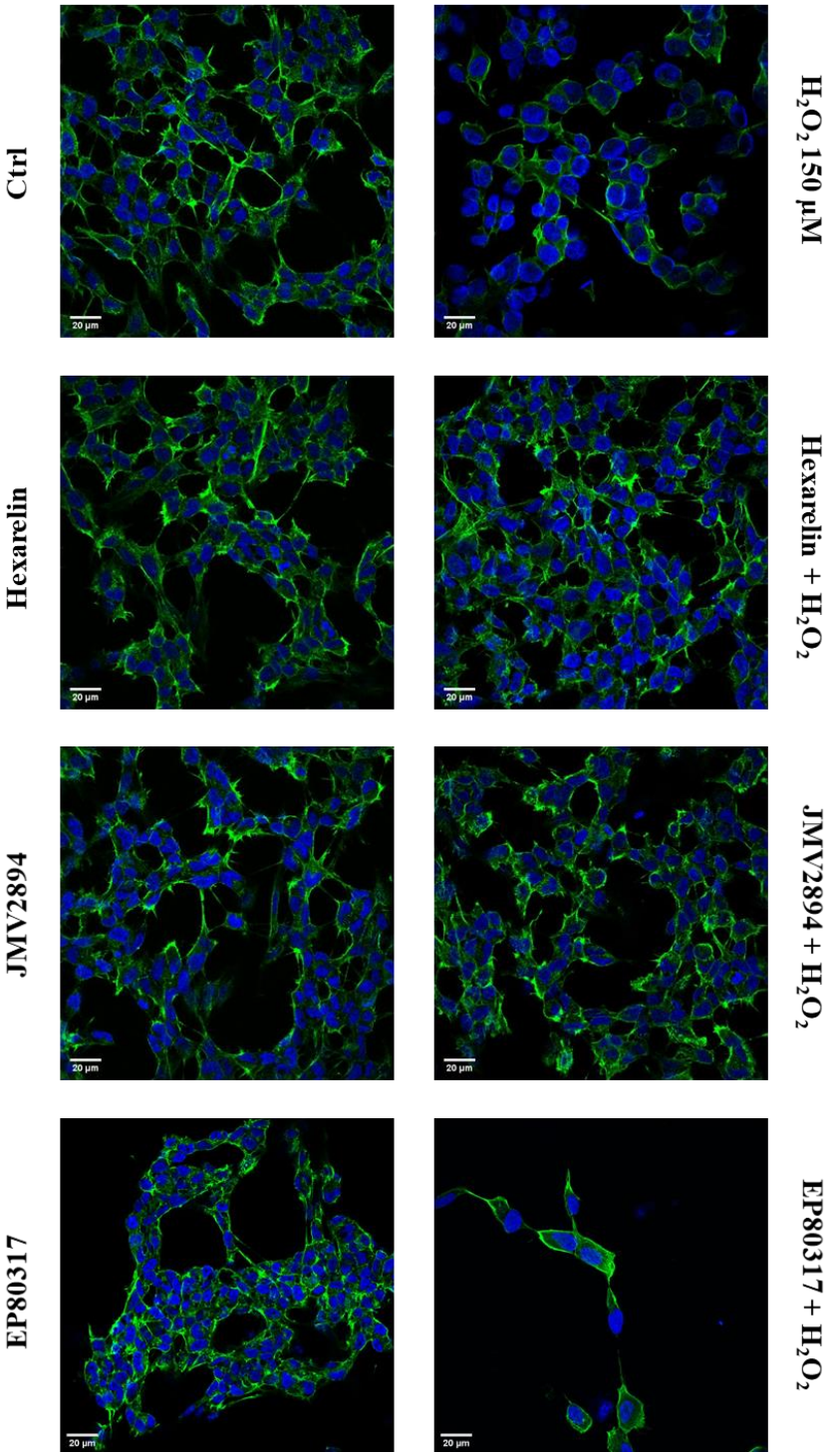
Ctrl
Hexarelin
JMV2894
EP80317
H_2O_2 150 µM
Hexarelin + H_2O_2
JMV2894 + H_2O_2
EP80317 + H_2O_2
20 µm

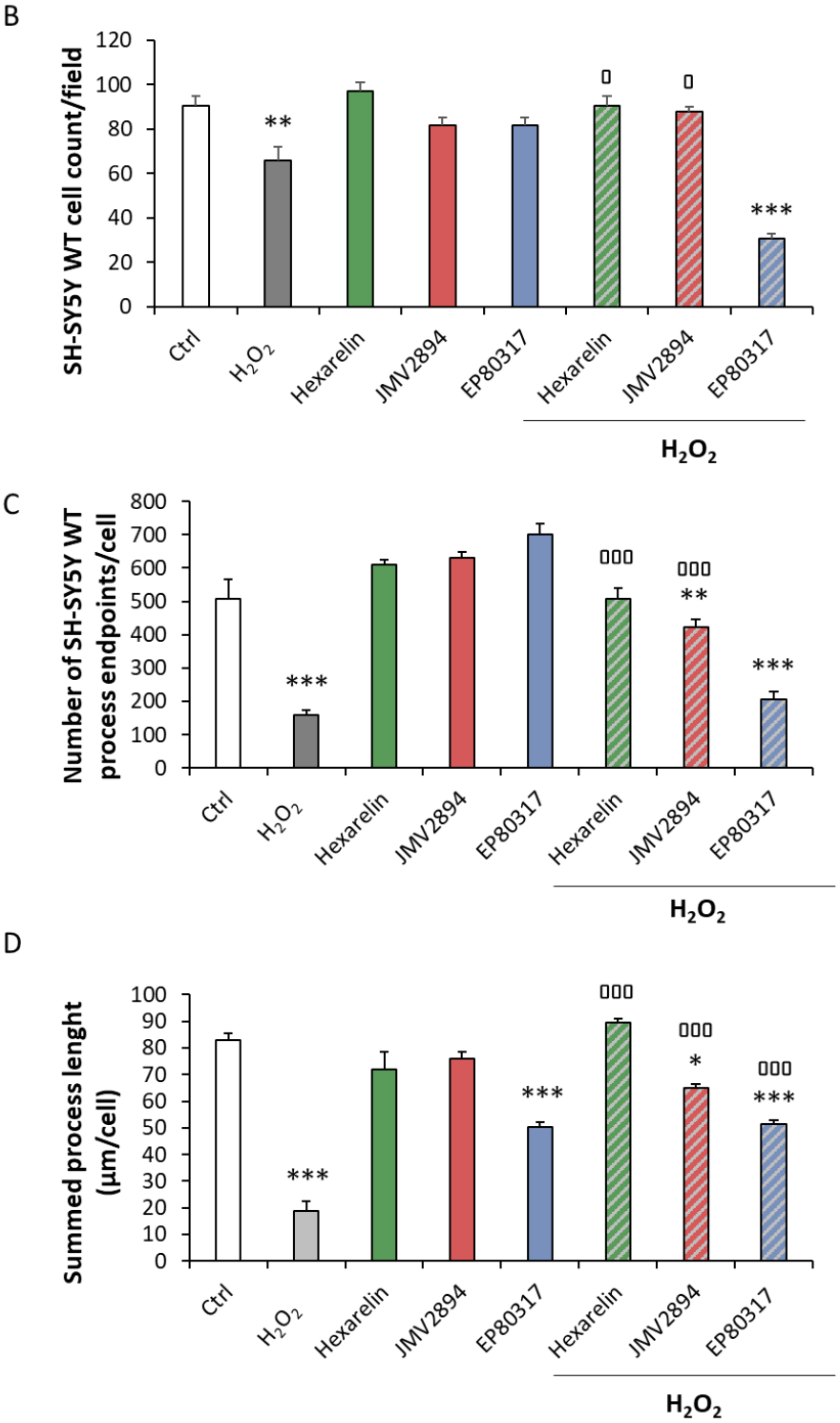

Figure 16. *GHSs modulate SH-SY5Y WT cells de-ramification induced by H_2O_2.*
(A) SH-SY5Y WT cells were seeded on poly-D-lysine pre-treated coverslips and incubated for 24 h with or without GHSs and 150 µM H_2O_2. At the end of the treatment, cells were fixed and stained for phalloidin and DAPI. Images were captured with confocal laser scan microscope. Scale bar: 20 µm. Graphical representation of: (B) the number of cells in the same areas per each treatment; (C) process endpoints/cells; and (D) process length/cells. Data are expressed as mean ± SEM of replicates obtained in 3 independent experiments (total number of cells analyzed = 100). Statistical significance: * $p < 0.05$, ** $p < 0.01$, and *** $p < 0.001$ vs. Ctrl; ° $p < 0.05$, and °°° $p < 0.001$ vs. H_2O_2.

A

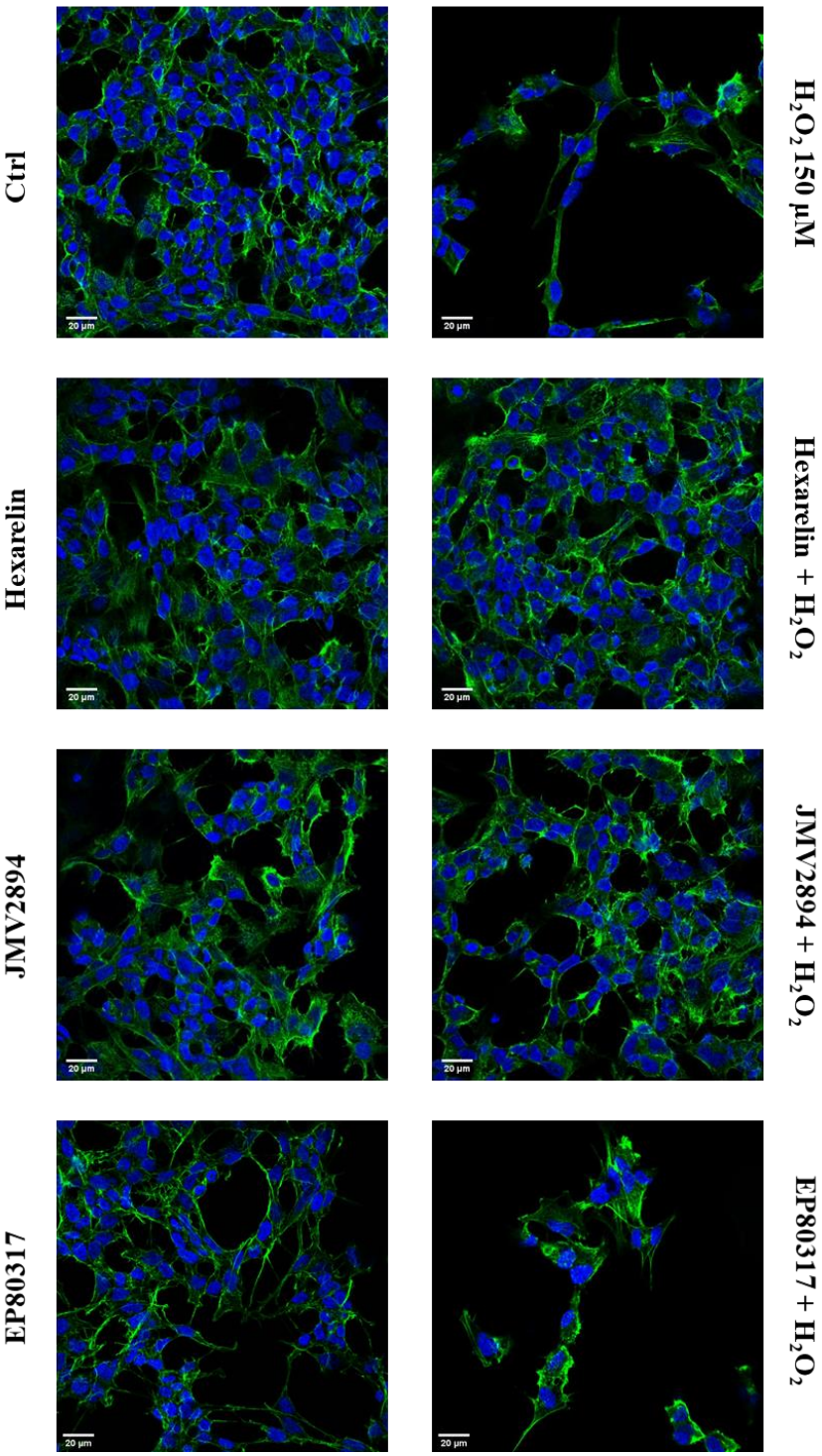
Ctrl
H_2O_2 150 µM
Hexarelin
Hexarelin + H_2O_2
JMV2894
JMV2894 + H_2O_2
EP80317
EP80317 + H_2O_2
20 µm

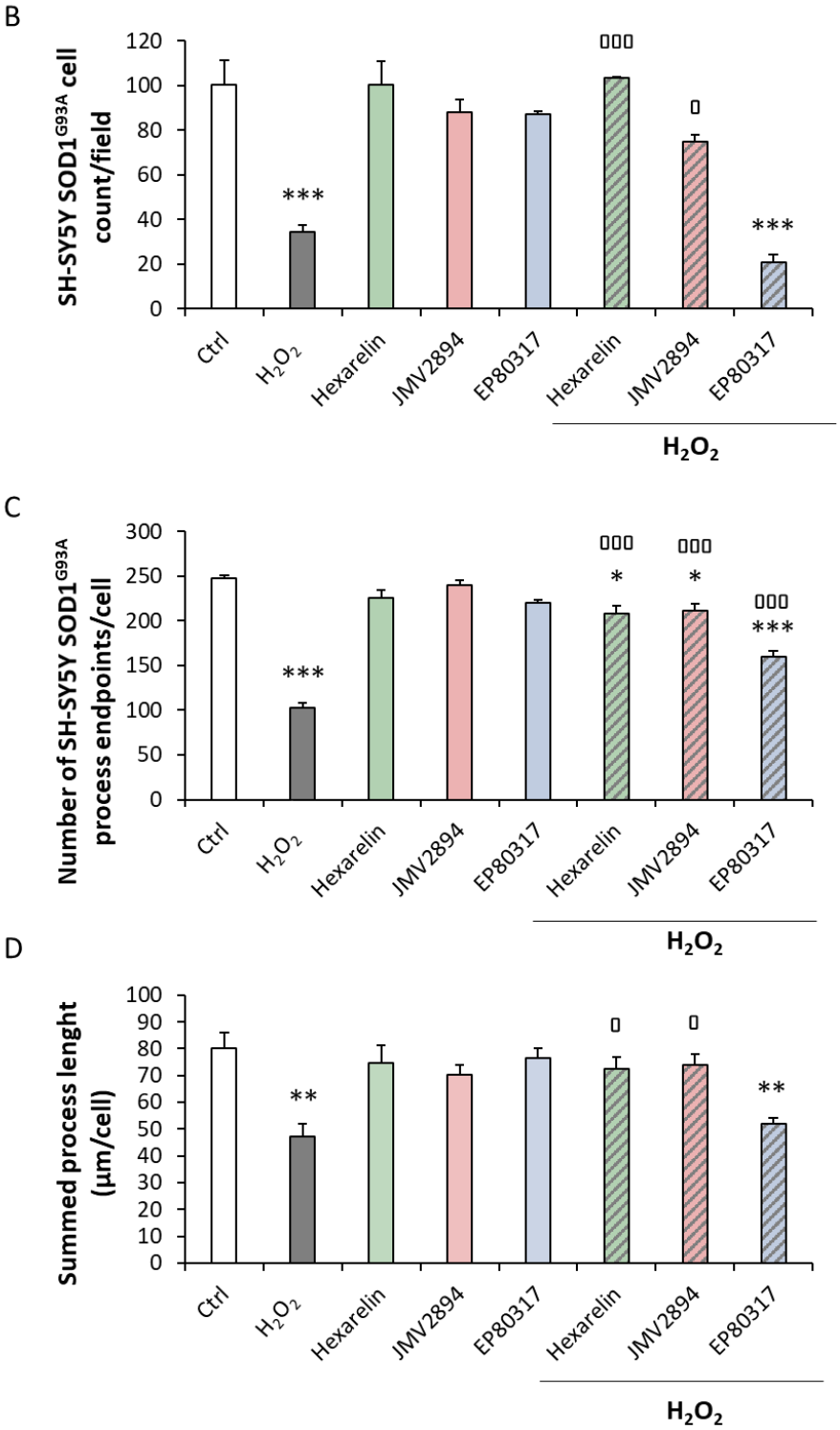

Figure 17. *GHSs modulate SH-SY5Y SOD1^{G93A} cells de-ramification induced by H_2O_2.*
(A) SH-SY5Y SOD1^{G93A} cells were seeded on poly-D-lysine pre-treated coverslips and incubated for 24 h with or without GHSs and 150 µM H_2O_2. At the end of the treatment, cells were fixed and stained for phalloidin and DAPI. Images were captured with confocal laser scan microscope. Scale bar: 20 µm. Graphical representation of: (B) the number of cells in the same areas per each treatment; (C) the process endpoints/cells; and (D) process length/cells. Data are expressed as mean ± SEM replicates obtained in 3 independent experiments (total number of cells analyzed = 100). Statistical significance: * $p < 0.05$, ** $p < 0.01$, and *** $p < 0.001$ vs. Ctrl; ° $p < 0.05$, and °°° $p < 0.001$ vs. H_2O_2.

A

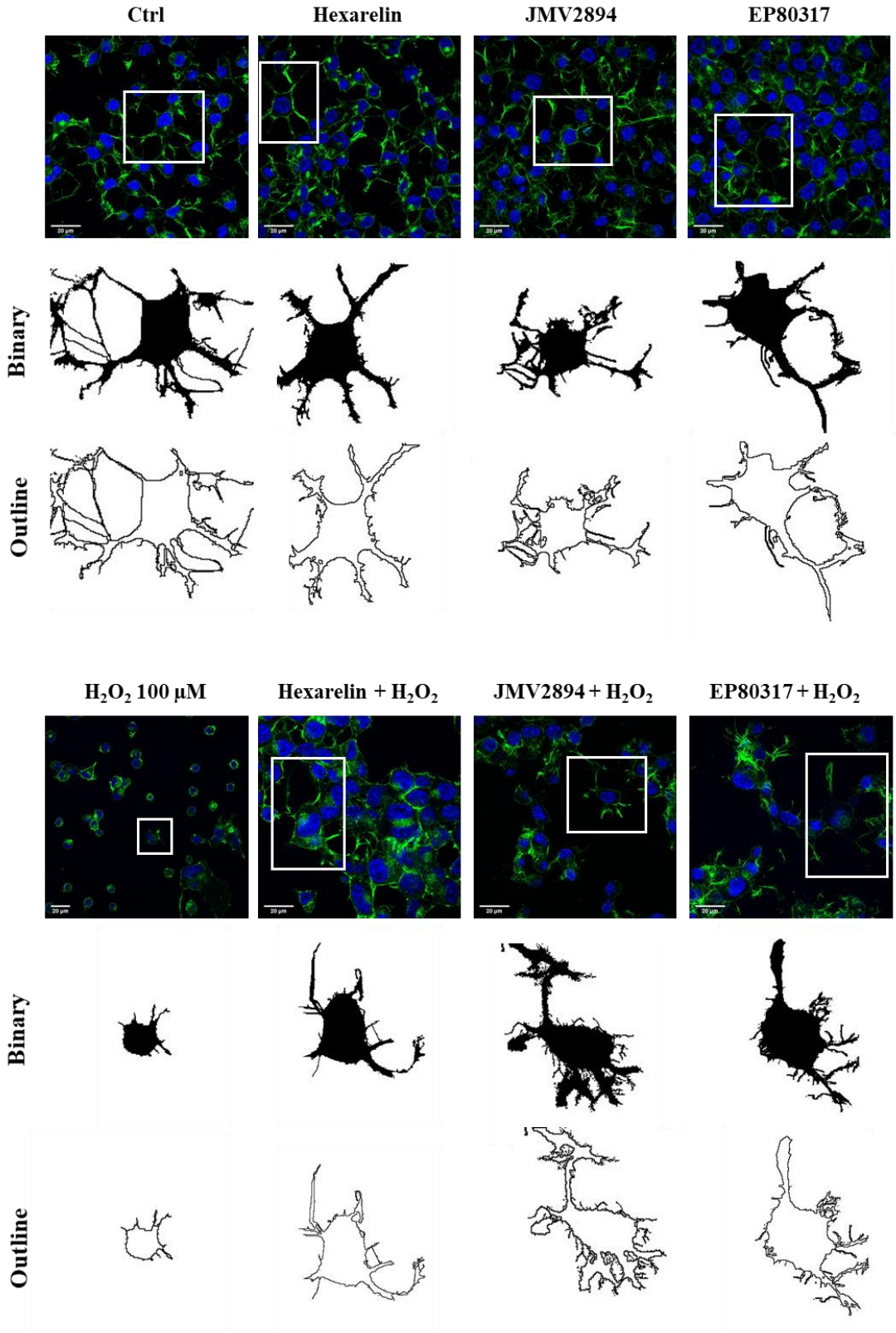
Ctrl
Hexarelin
JMV2894
EP80317
Binary
Outline
H_2O_2 100 µM
Hexarelin + H_2O_2
JMV2894 + H_2O_2
EP80317 + H_2O_2
Binary
Outline

B

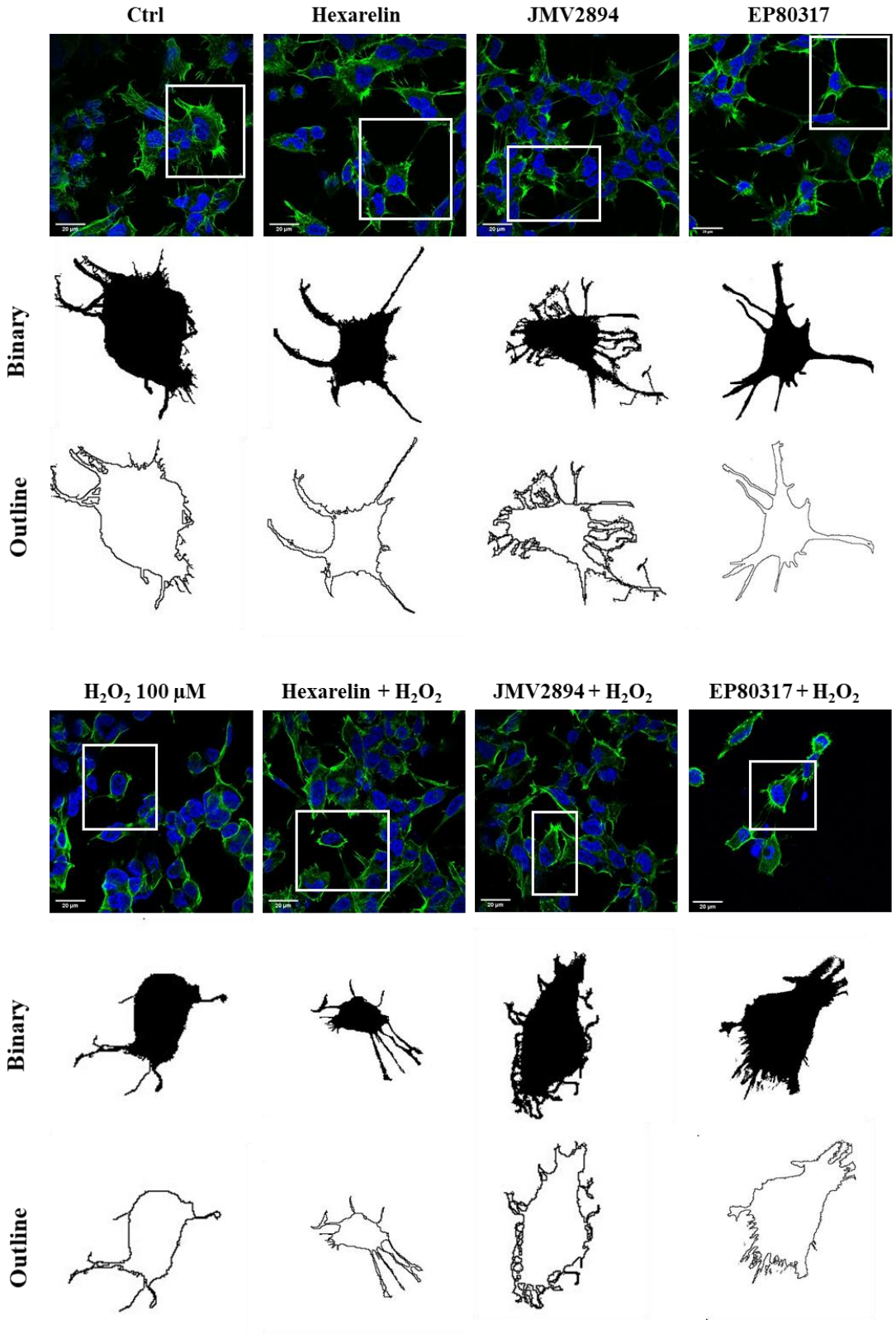
Ctrl
Hexarelin
JMV2894
EP80317
Binary
Outline
H_2O_2 100 µM
Hexarelin + H_2O_2
JMV2894 + H_2O_2
EP80317 + H_2O_2
Binary
Outline

C

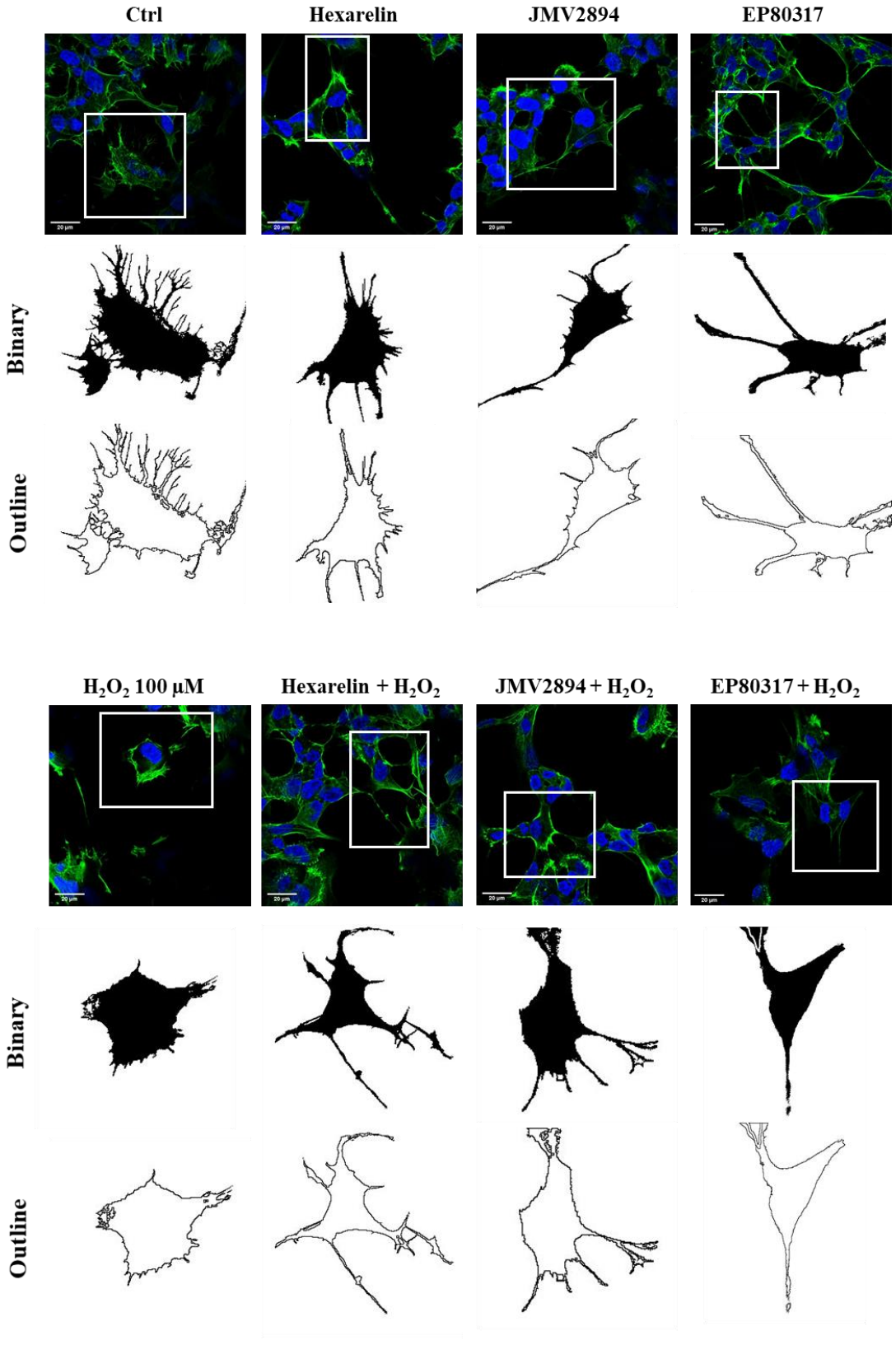
Ctrl
Hexarelin
JMV2894
EP80317
Binary
Outline
H_2O_2 100 µM
Hexarelin + H_2O_2
JMV2894 + H_2O_2
EP80317 + H_2O_2
Binary
Outline

Figure 18. *Effects of GHSs on morphology of Neuro-2A, SH-SY5Y WT and SH-SY5Y SOD1^{G93A} cells stimulated with H_2O_2.*
Representative photomicrographs of (A) Neuro-2A, (B) SH-SY5Y WT and (C) SH-SY5Y SOD1^{G93A} cells incubated for 24 h with or without GHSs and the selected concentration of H_2O_2, and examples of cell binarized and outlined. Cells were seeded on poly-D-lysine pre-treated coverslips and, at the end of the treatments, were fixed and stained with phalloidin and DAPI. Images were captured with a confocal laser scan microscope. Scale bar: 20 µm.

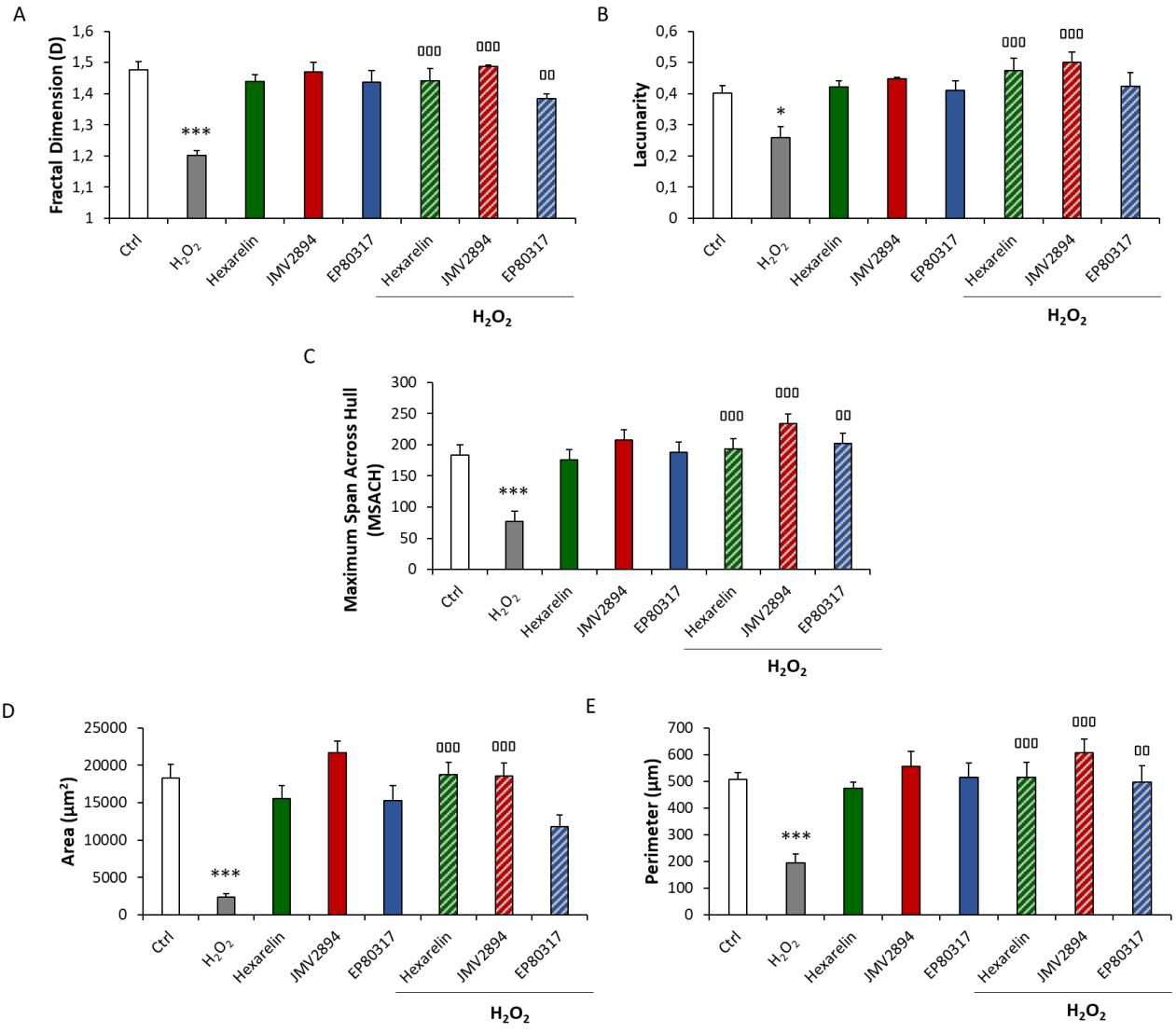

Figure 19. *GHSs modulate morphological changes of Neuro-2A cells induced by H_2O_2 treatment.* Numeric representation of: (A) Fractal dimension, (B) lacunarity, (C) maximum span across the convex hull, (D) area, and (E) perimeter of Neuro-2A cells treated for 24 h with 100 µM H_2O_2 alone or in combination with GHSs. Total number of cells analyzed for each condition = 10. Data are expressed as mean ± SEM. Statistical significance: * $p < 0.05$, and *** $p < 0.001$ vs. Ctrl; °° $p < 0.01$, and °°° $p < 0.001$ vs. H_2O_2.

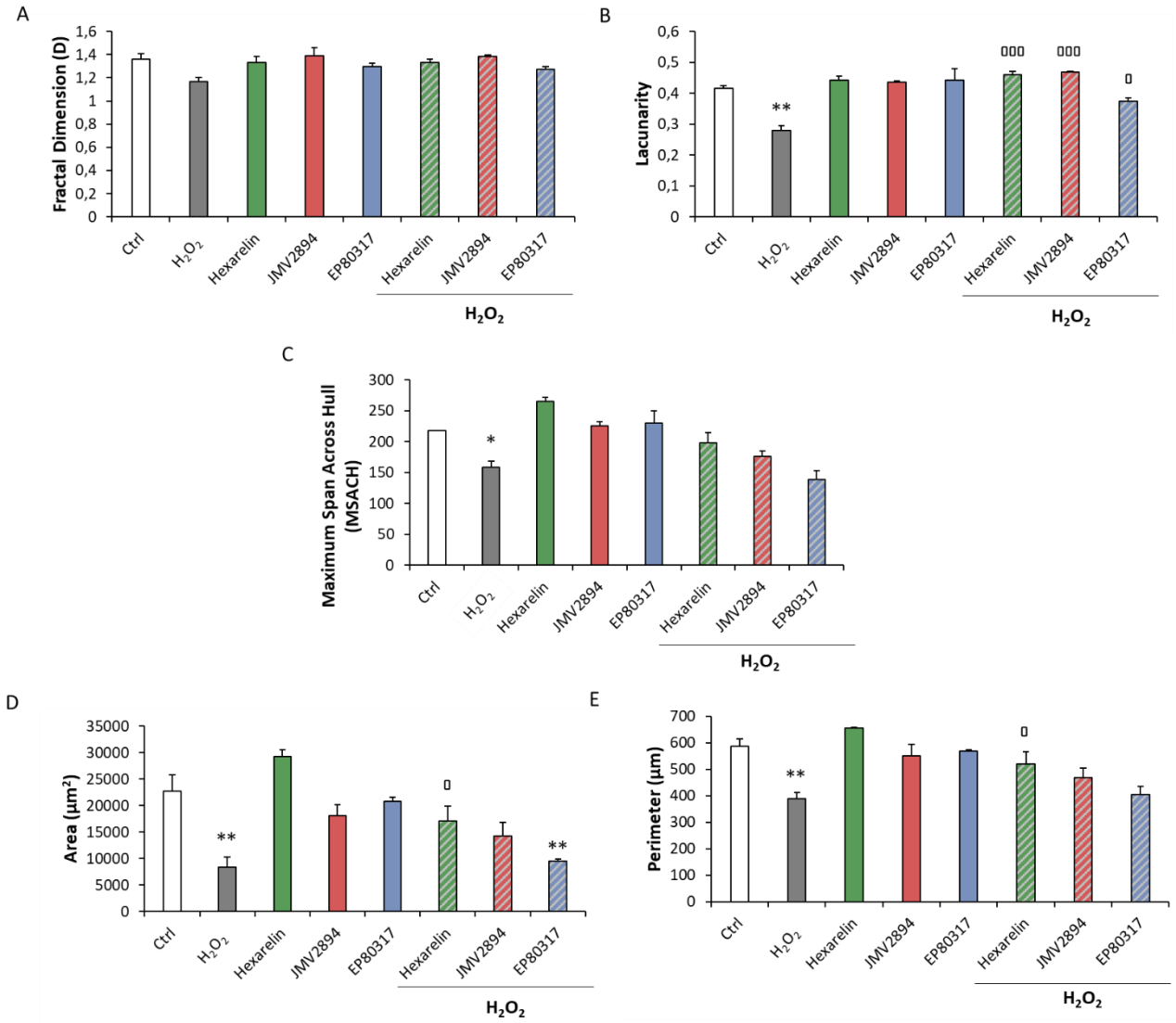

Figure 20. *GHSs modulation of morphological changes in SH-SY5Y WT cells induced by H_2O_2 treatment.*

Numeric representation of: (A) Fractal dimension, (B) lacunarity, (C) maximum span across the convex hull, (D) area, and (E) perimeter in SH-SY5Y WT cells treated for 24 h with 150 µM H_2O_2 alone or in combination with GHSs. Total number of cells analyzed for each condition = 10. Data are expressed as mean ± SEM. Statistical significance: * $p < 0.05$, and ** $p < 0.01$ vs. Ctrl; ° $p < 0.05$, and °°° $p < 0.001$ vs. H_2O_2.

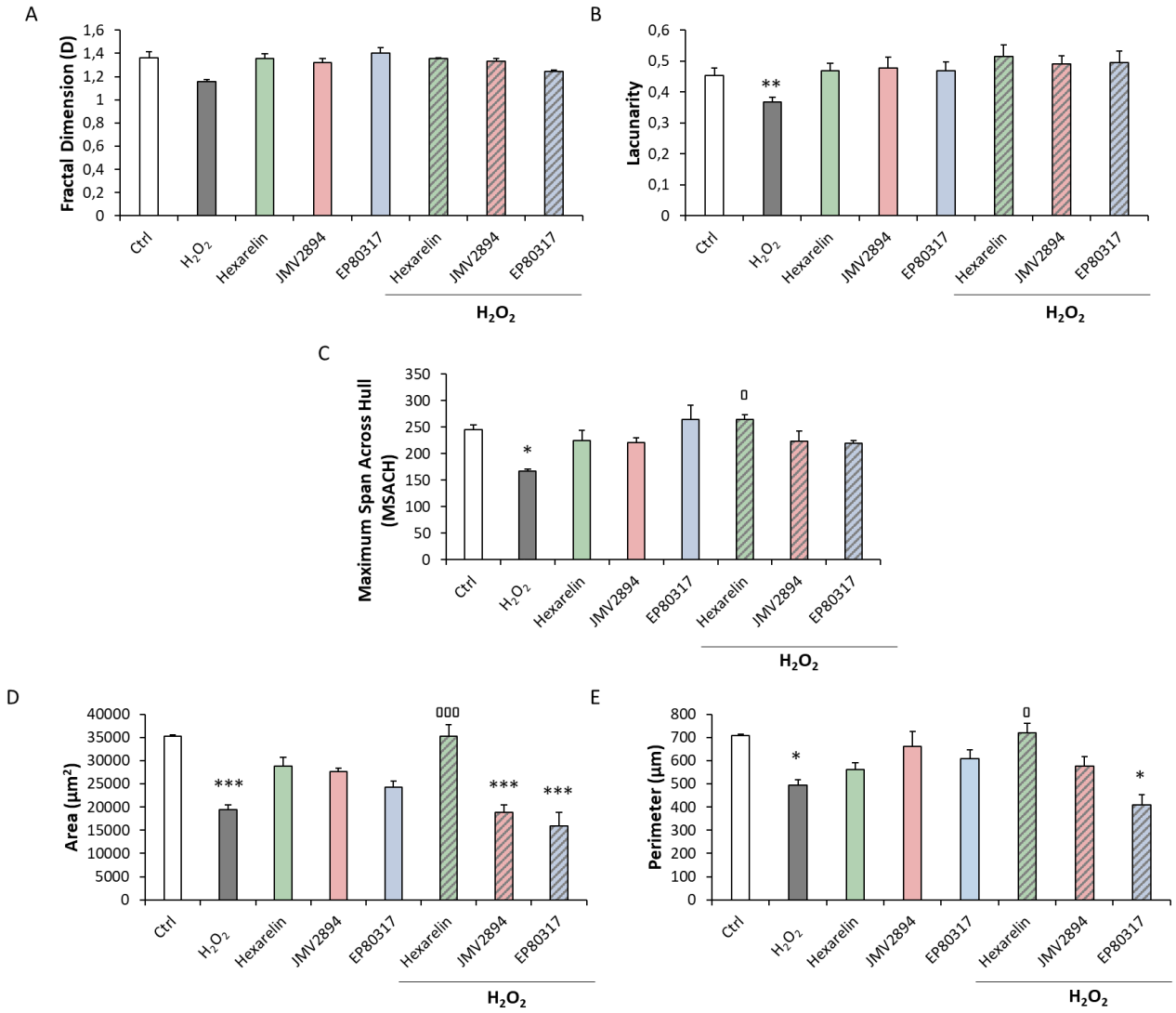

Figure 21. *GHSs modulation of morphological changes in SH-SY5Y SOD1^{G93A} cells induced by H_2O_2 treatment.*

Numeric representation of: (A) Fractal dimension, (B) lacunarity, (C) maximum span across the convex hull, (D) area, and (E) perimeter in SH-SY5Y SOD1^{G93A} cells treated for 24 h with 150 µM H_2O_2 alone or in combination with GHSs. Total number of cells analyzed for each condition = 10. Data are expressed as mean ± SEM. Statistical significance: * $p < 0.05$, ** $p < 0.01$, *** $p < 0.001$ vs. Ctrl; ° $p < 0.05$, °°° $p < 0.001$ vs. H_2O_2.

A

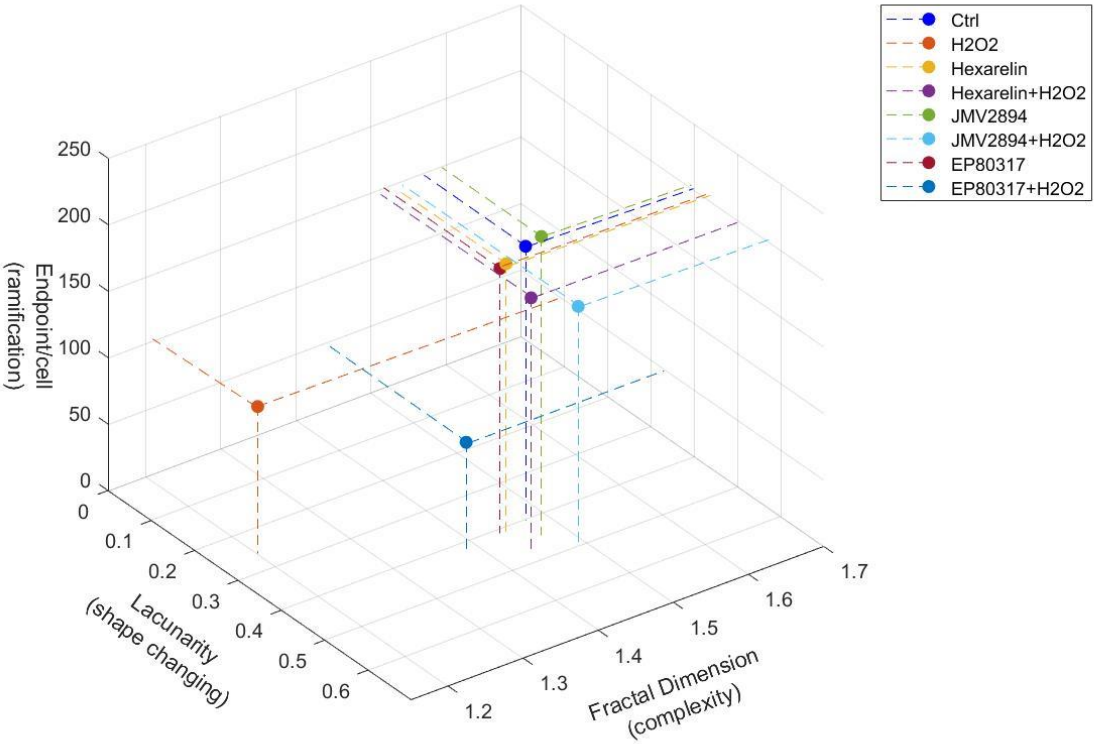
Ctrl
H2O2
Hexarelin
Hexarelin+H2O2
JMV2894
JMV2894+H2O2
EP80317
EP80317+H2O2
Endpoint/cell (ramification)
250
200
150
100
50
0
0
0.1
0.2
0.3
0.4
0.5
0.6
Lacunarity (shape changing)
1.2
1.3
1.4
1.5
1.6
1.7
Fractal Dimension (complexity)

B

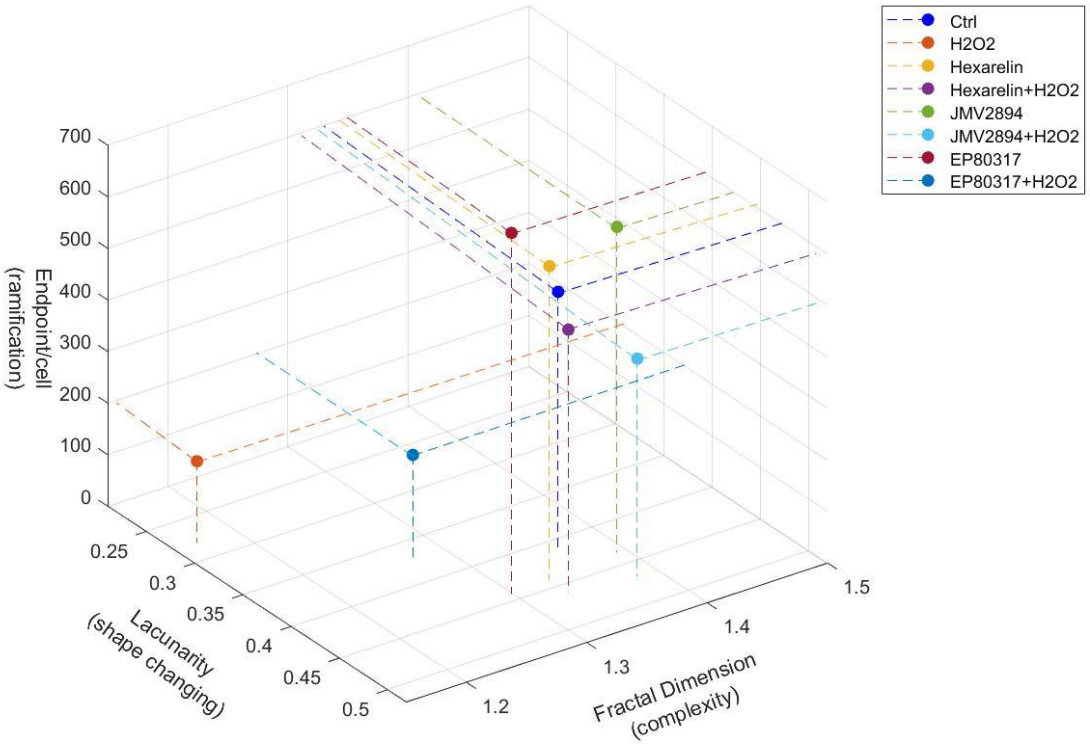
Ctrl
H2O2
Hexarelin
Hexarelin+H2O2
JMV2894
JMV2894+H2O2
EP80317
EP80317+H2O2
Endpoint/cell (ramification)
700
600
500
400
300
200
100
0
0.25
0.3
0.35
0.4
0.45
0.5
Lacunarity (shape changing)
1.2
1.3
1.4
1.5
Fractal Dimension (complexity)

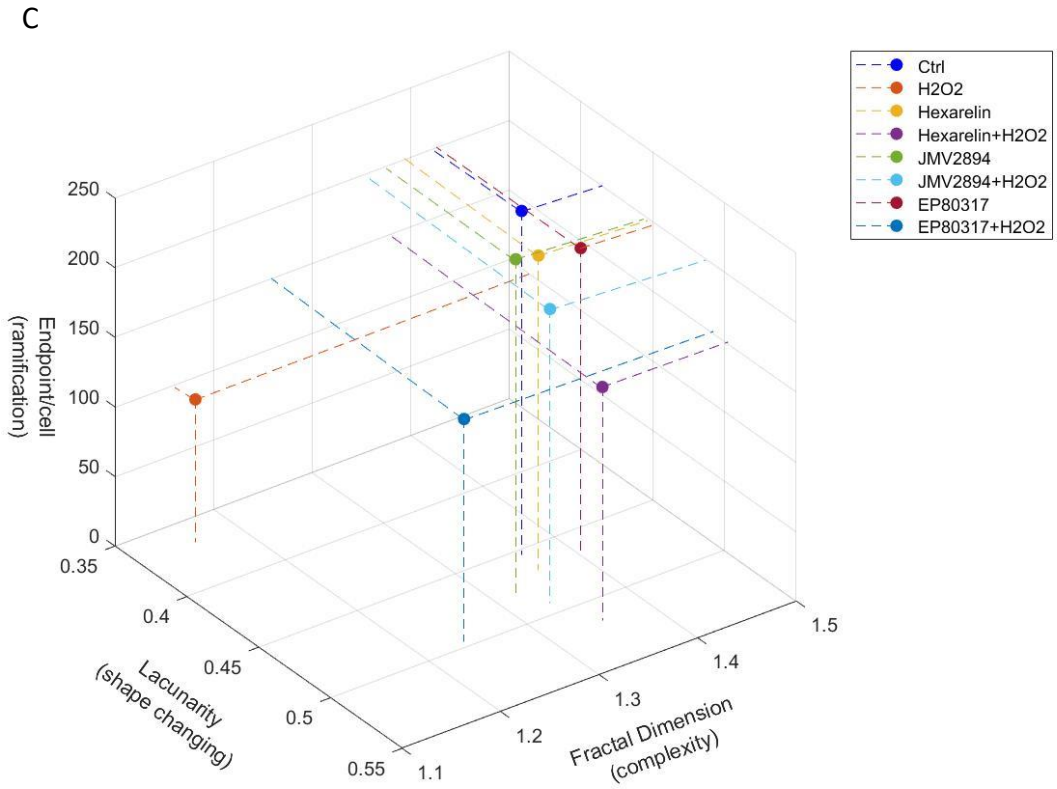

Figure 22. *Summary representation of Skeleton and FracLac analysis by 3D scatter plot.*
Figures summarize the relationship between ramifications (endpoints/cell), shape changing (lacunarity) and complexity (fractal dimension) in (A) Neuro-2A, (B) SH-SY5Y WT and (C) SH-SY5Y SOD1^{G93A}.

6. Effects of GHSs on caspases-3 and -7 mRNA expressions and protein levels

Caspase-3 and caspase-7 activations after damage induced by H_2O_2 occur at an early stage of apoptotic cell death; therefore, we hypothesized that GHSs could inhibit caspase-3 and caspase-7 mRNA levels. First, our results demonstrated that mRNA levels of both caspases were increased by H_2O_2 in a dose-dependent manner and that the selected concentration induced a significant increase in caspase-3 and caspase-7 mRNA levels in our experimental models (Figure 23, 24 and 25, panels A and B).

Figure 23C and D shows that in Neuro-2A cells 100 µM H_2O_2 increased caspase-3 ($p < 0.001$) and caspase-7 ($p < 0.001$) mRNA levels, while GHSs alone did not affect mRNA levels of both caspases. Notably, 1 µM hexarelin and JMV2894 antagonized the increase in caspase-3 mRNA levels induced by 100 µM H_2O_2 (hexarelin: 25.63 ± 0.09%, $p < 0.01$; JMV2894: 33.21 ± 0.06%, $p < 0.01$), whereas GHSs did not inhibit the effects of 100 µM H_2O_2 on caspase-7 mRNA levels.

H_2O_2 stimulated a significant increase of mRNA levels for caspase-3 and caspase-7 ($p < 0.001$) in SH-SY5Y WT cells. The co-incubation with GHSs 1 µM antagonized H_2O_2 stimulation of caspases mRNA levels: hexarelin and JMV2894 blunted H_2O_2 effects (36.56 ± 0.12% and 39.88 ± 0.17% respectively ($p < 0.01$)), while EP80317 induced only a trend toward to the reduction of caspase-3 (Figure 24C). Interestingly, all GHSs significantly antagonized the increase in the expression of caspase-7 induced by H_2O_2 ($p < 0.001$ for hexarelin and JMV2894, $p < 0.01$ for EP80317) (Figure 24D).

As shown in Figure 25C, in SH-SY5Y $SOD1^{G93A}$ cells H_2O_2 induced an over expression of caspase-3 mRNA level ($p < 0.001$) which was significantly antagonized only by hexarelin (26.06 ± 0.14%, $p < 0.05$), while JMV2894 and EP80317 induced a trend toward its reduction. Additionally, GHSs did not reduce the effects of 150 µM H_2O_2 on caspase-7 mRNA levels (Figure 25D).

We also quantified the cellular content of activated caspase-3 and -7 proteins; both species are effector caspases, which are activated through proteolytic processing by upstream caspases to produce the mature subunit.

In Neuro-2A cells, western blot analysis showed that H_2O_2 treatment significantly increased the levels of cleaved caspase-3 and cleaved caspase-7 ($p < 0.001$) (Figure 26A,B). Hexarelin and JMV2894 blunted only caspase-3 activation ($p < 0.05$), while 1 µM EP80317 did not antagonize H_2O_2 effects (Figure 26A). GHSs induced also a trend toward a reduction of cleaved caspase-7 protein levels (Figure 26B).

Interestingly, in SH-SY5Y WT cells the significant increase ($p < 0.001$) of caspase-3 and caspase-7 protein levels caused by H_2O_2 were blunted by the treatment with GHSs (Figure 27A,B). In detail, hexarelin reduced protein level of caspase-3 by 32.94 ± 0.07% ($p < 0.01$), and that of caspase-7 by 27.44 ± 0.08% ($p < 0.05$); JMV2894 decreased levels of both proteins by 43.57 ± 0.20% ($p < 0.01$) and 29.28 ± 0.04 ($p < 0.05$); EP80317 reduced only the activation of caspase-7 (28.60 ± 0.06%, $p < 0.05$) compared to H_2O_2-treated cells.

Also in SH-SY5Y $SOD1^{G93A}$ the protein levels of caspase-3 and caspase-7 measured by western blot were consistent with their mRNA levels: in this cellular model, hexarelin was the only GHS that antagonized the apoptotic mechanism induced by H_2O_2 reducing the protein expression of both cleaved caspases ($p < 0.001$, Figure 28A,B).

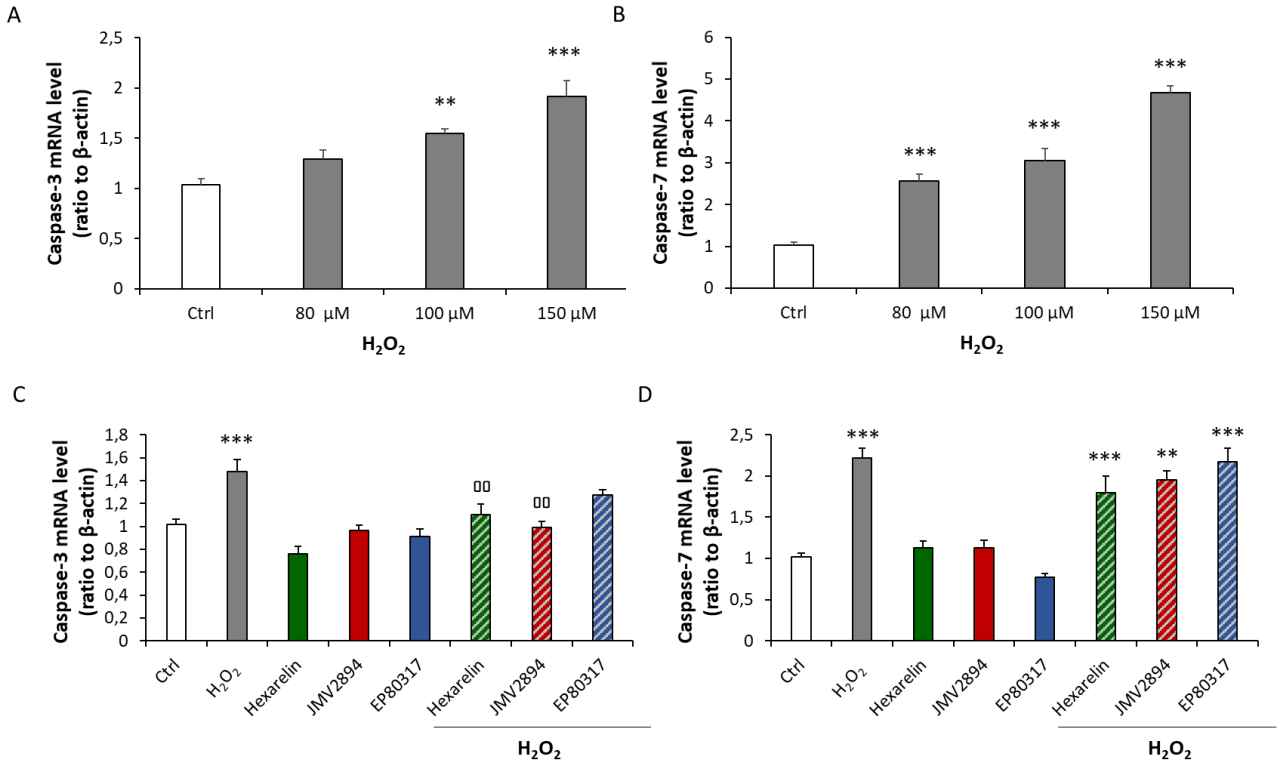

Figure 23. *Caspase-3 and caspase-7 mRNA levels following incubation with H_2O_2 and GHSs.* Neuro-2A cells were incubated with different concentrations of H_2O_2 (0, 80, 100, 150 µM) or co-incubated with 1 µM GHSs and 100 µM H_2O_2 for 24 h. (A,C) Caspase-3 and (B,D) caspase-7 mRNA levels were measured by RT-PCR and normalized for the respective β-actin mRNA levels. Data are expressed as mean ± SEM of replicates obtained in 3 independent experiments (n = 18). ** $p < 0.01$, and *** $p < 0.001$ vs. Ctrl; °° $p < 0.01$ vs. H_2O_2.

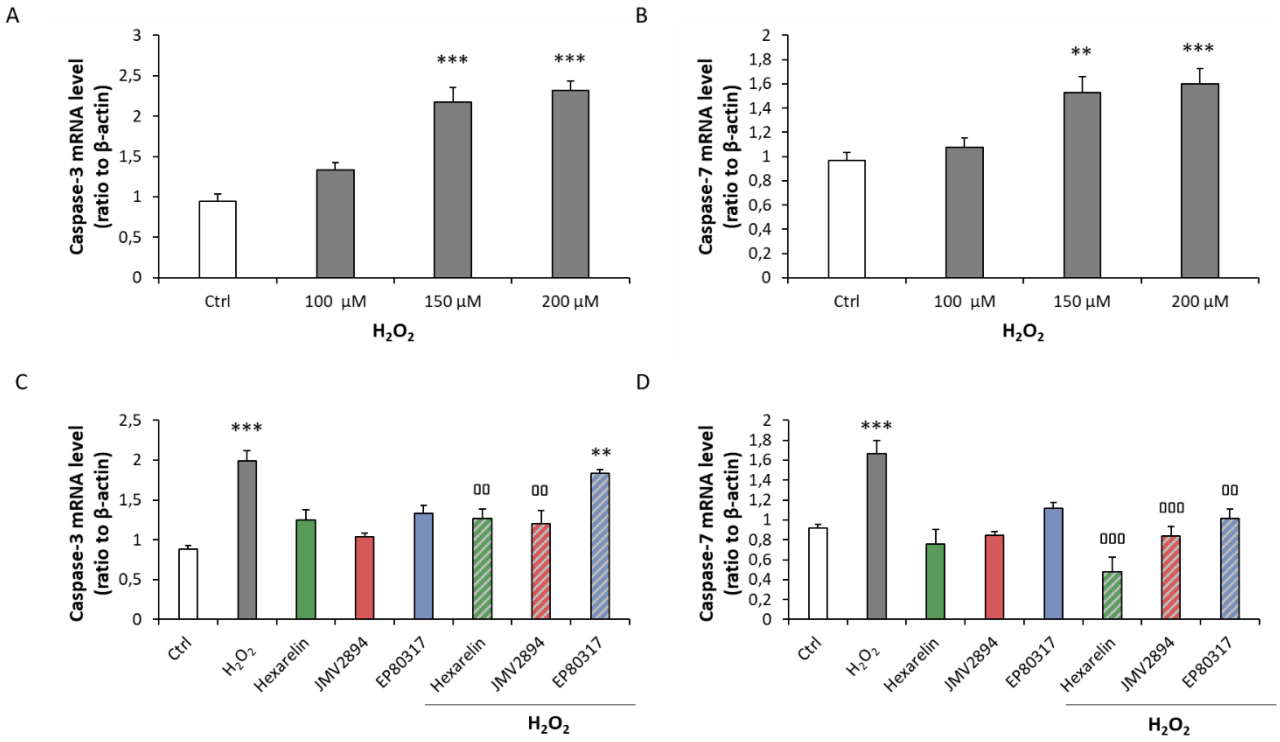

Figure 24. *Caspase-3 and caspase-7 mRNA levels following incubation with H_2O_2 and GHSs.* SH-SY5Y WT cells were incubated with different concentrations of H_2O_2 (0, 100, 150, 200 µM) or co-incubated with 1 µM GHSs and 150 µM H_2O_2 for 24 h. (A,C) Caspase-3 and (B,D) caspase-7 mRNA levels were measured by RT-PCR and normalized for the respective β-actin mRNA levels. Data are expressed as mean ± SEM of replicates obtained in 3 independent experiments (n = 18). ** $p < 0.01$, *** $p < 0.001$ vs. Ctrl; °° $p < 0.01$, °°° $p < 0.001$ vs. H_2O_2.

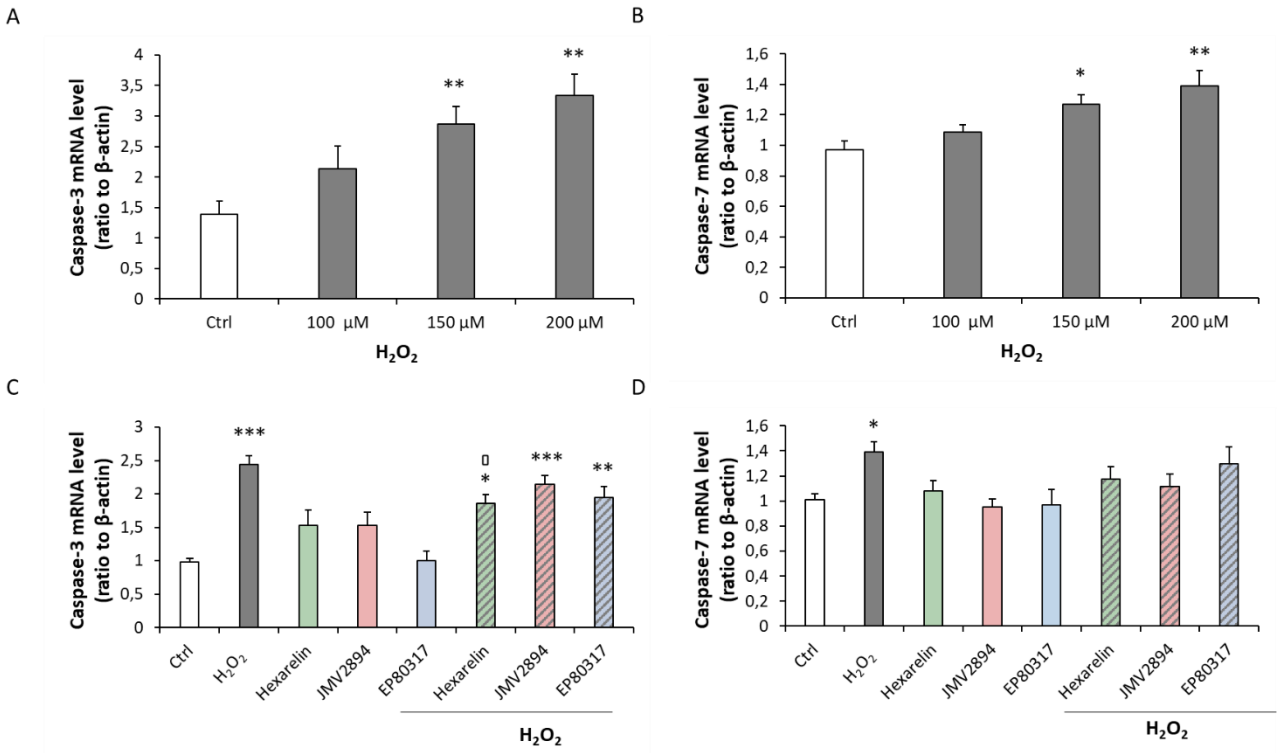

Figure 25. *Caspase-3 and caspase-7 mRNA levels following incubation with H_2O_2 and GHSs.* SH-SY5Y SOD1^{G93A} cells were incubated with different concentrations of H_2O_2 alone (0, 100, 150, 200 µM) or co-incubated with 1 µM GHSs and 150 µM H_2O_2 for 24 h. (A,C) Caspase-3 and (B,D) caspase-7 mRNA levels were measured by RT-PCR and normalized for the respective β-actin mRNA levels. Data are expressed as mean ± SEM of replicates obtained in 3 independent experiments (n = 18). * $p < 0.05$, ** $p < 0.01$, and *** $p < 0.001$ vs. Ctrl; ° $p < 0.05$ vs. H_2O_2.

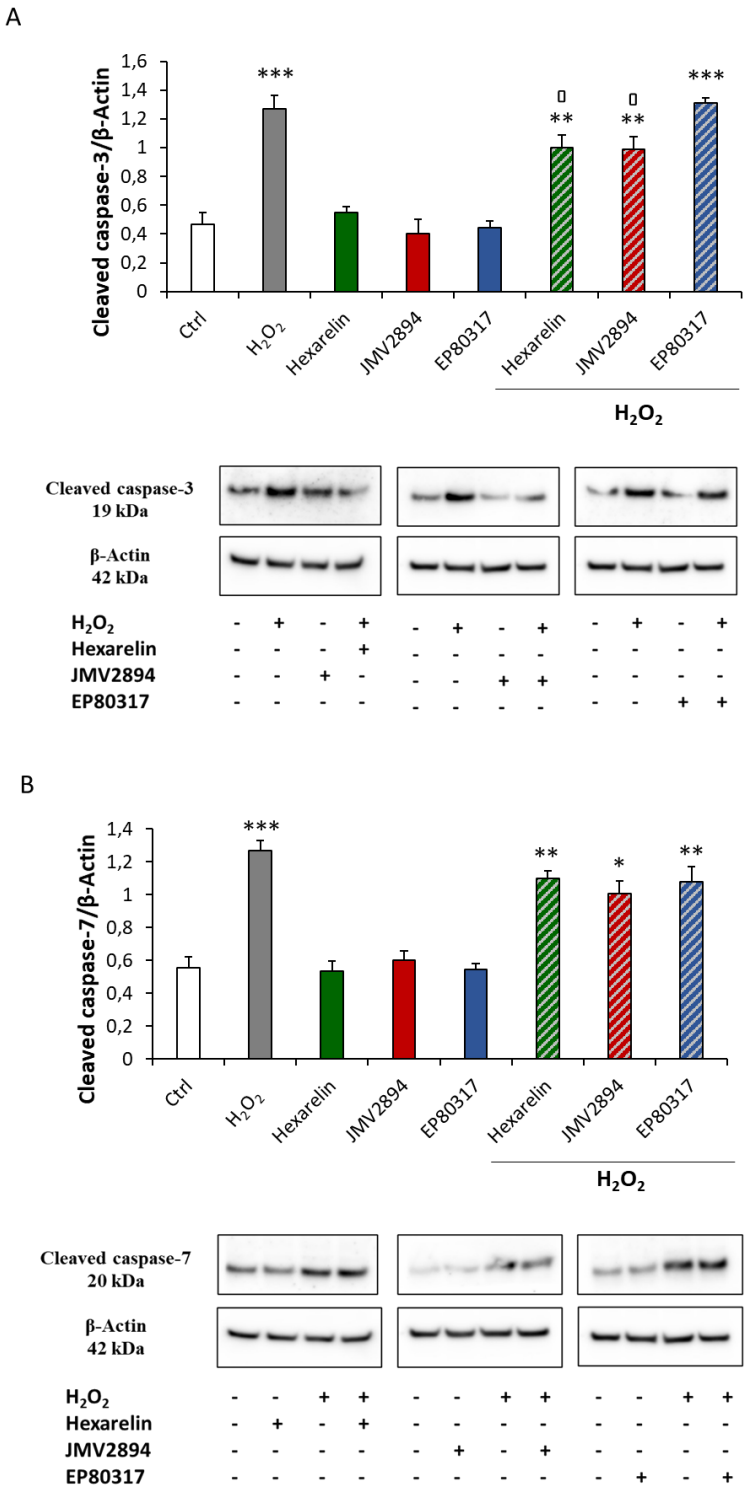

Figure 26. *GHSs inhibits apoptotic pathway through caspase-3 inactivation.*
Neuro-2A cells were incubated with H_2O_2 alone, GHSs alone, or with a combination of GHSs and H_2O_2 for 24 h. Western blot assays were used to measure levels of (A) cleaved caspase-3/β-actin, and (B) cleaved caspase-7/β-actin. All assays were performed in at least 3 independent experiments (n = 3). Statistical significance: * $p < 0.05$, ** $p < 0.01$, and *** $p < 0.001$ vs. Ctrl; ° $p < 0.05$ vs. H_2O_2.

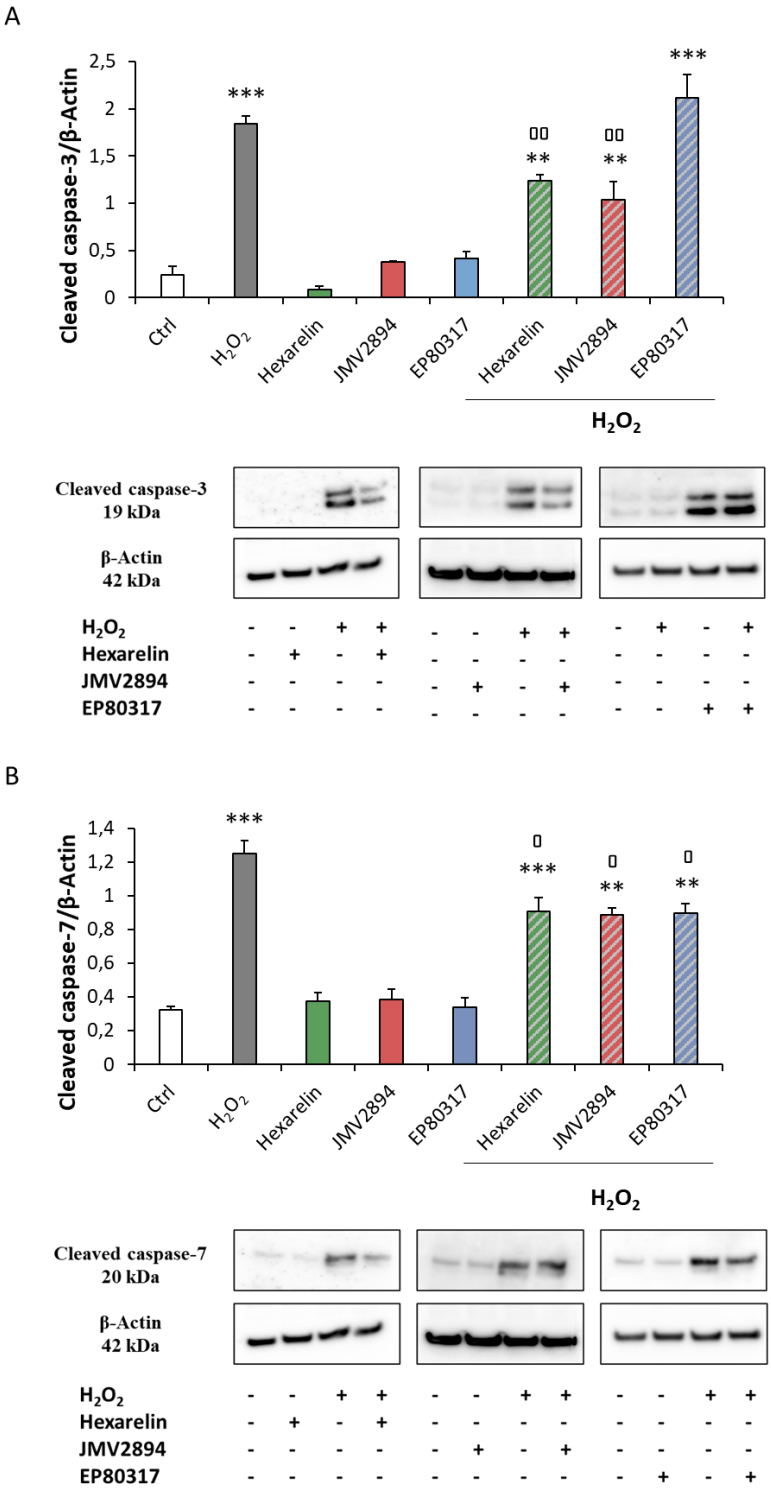

Figure 27. *GHSs inhibits apoptotic pathway through caspases inactivation.*
SH-SY5Y WT cells were treated with H_2O_2 alone, GHSs alone, or with a combination of GHSs and H_2O_2 for 24 h. Western blot assays were used to measure levels of (A) cleaved caspase-3/β-actin, and (B) cleaved caspase-7/β-actin. All assays were performed in at least 3 independent experiments (n = 3). Statistical significance: ** $p < 0.01$, and *** $p < 0.001$ vs. Ctrl; ° $p < 0.05$, and °° $p < 0.01$ vs. H_2O_2.

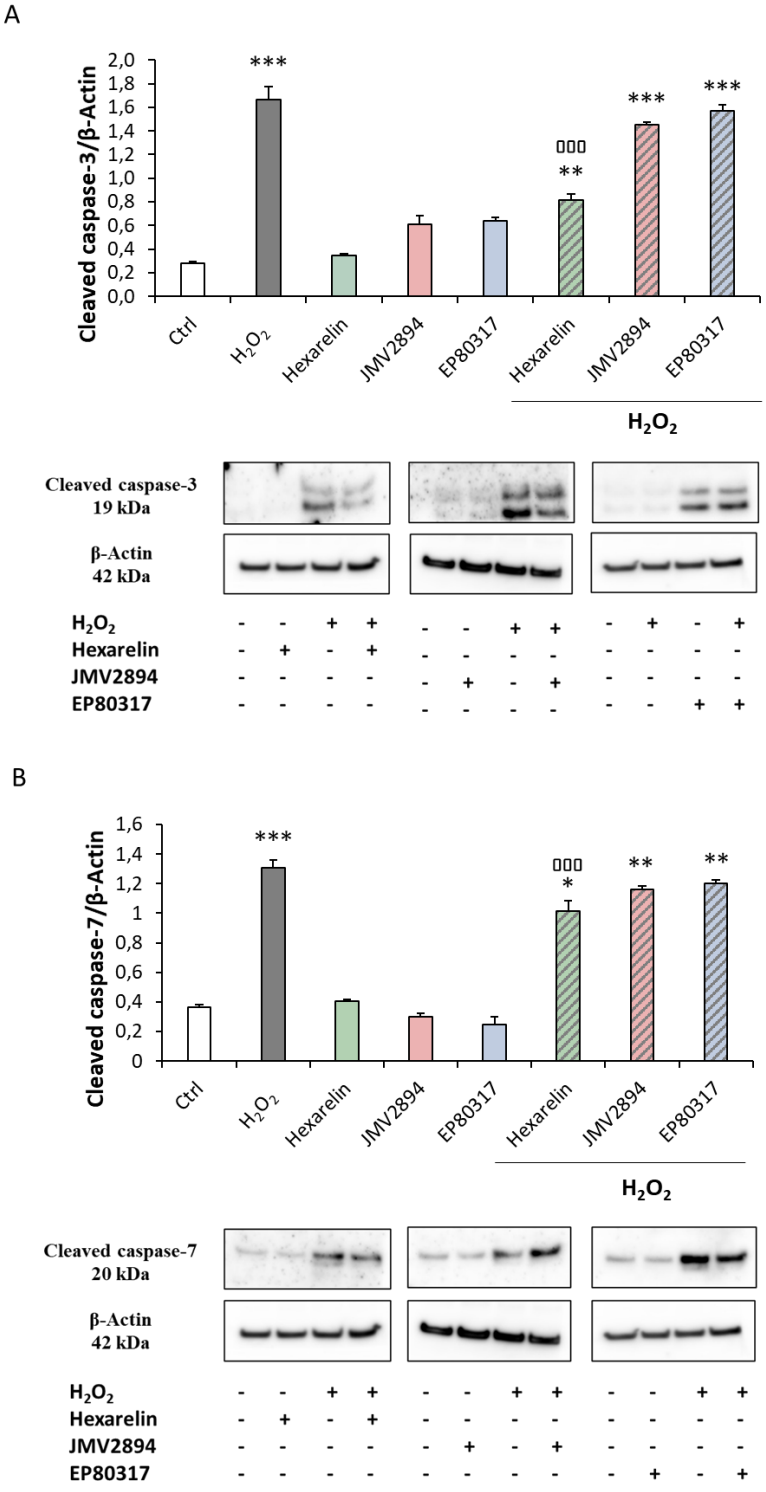

Figure 28. *GHSs inhibits apoptotic pathway through caspases inactivation.*
SH-SY5Y SOD1^{G93A} cells were treated with H_2O_2 alone, GHSs alone, or with a combination of GHSs and H_2O_2 for 24 h. Western blot assays were used to measure levels of (A) cleaved caspase-3/β-actin, and (B) cleaved caspase-7/β-actin. All assays were performed in at least 3 independent experiments (n = 3). Statistical significance: * $p < 0.05$, ** $p < 0.01$, and *** $p < 0.001$ vs. Ctrl; °°° $p < 0.001$ vs. H_2O_2.

7. Effects of GHSs on BCL-2 family mRNA levels

Mitochondria play a crucial role in the process of cell apoptosis with the activation of the BCL-2 protein family.

Figure 29A shows that in Neuro-2A cells H_2O_2 stimulated in a concentration-dependent manner a significant increase of the pro-apoptotic Bax mRNA levels and trend toward an increase of the anti-apoptotic Bcl-2 mRNA levels (Figure 29B). Co-incubation for 24 h with 100 µM H_2O_2 and 1 µM GHSs revealed the anti-apoptotic effects of GHSs, especially of hexarelin. The mRNA levels of Bax, increased by H_2O_2 ($p<0.001$) were significantly ($p < 0.05$) reduced by hexarelin or JMV2894, but not by EP80317; moreover, only hexarelin significantly ($p < 0.05$) increased Bcl-2 mRNA levels (Figure 29C,D).

In SH-SY5Y WT cells, H_2O_2 treatment induced a significant and dose-dependent increase in Bax mRNA levels (Figure 30A), whereas the expression of Bcl-2 mRNA did not undergo any variation compared to control group (Figure 30B). As shown in Figure 30C, both hexarelin and JMV2894 co-incubation with H_2O_2 induced a significant reduction in Bax expression (hexarelin: 34.60 ± 0.15%, $p < 0.001$; JMV2894: 26.80 ± 0.14%, $p < 0.05$), whereas there was any variation to Bcl-2 mRNA levels (Figure 30D).

In SH-SY5Y $SOD1^{G93A}$ cells, H_2O_2 induced overran increase in the expression of pro-apoptotic Bax mRNA levels, and a trend toward an increase of the anti-apoptotic Bcl-2 mRNA levels in a concentration dependent-manner (Figure 31A and B). In this cell line only hexarelin exerted protective effects against 150 µM H_2O_2, blunting Bax expression (30.04 ± 0.25%, $p < 0.01$) and with a significant stimulation of Bcl-2 mRNA levels (34.50 ± 0.13, $p < 0.01$) (Figure 31C,D).

Altogether, these results demonstrate that among the three GHSs tested, hexarelin is the most promising due to its capability to disrupt the apoptotic process, followed by JMV2894.

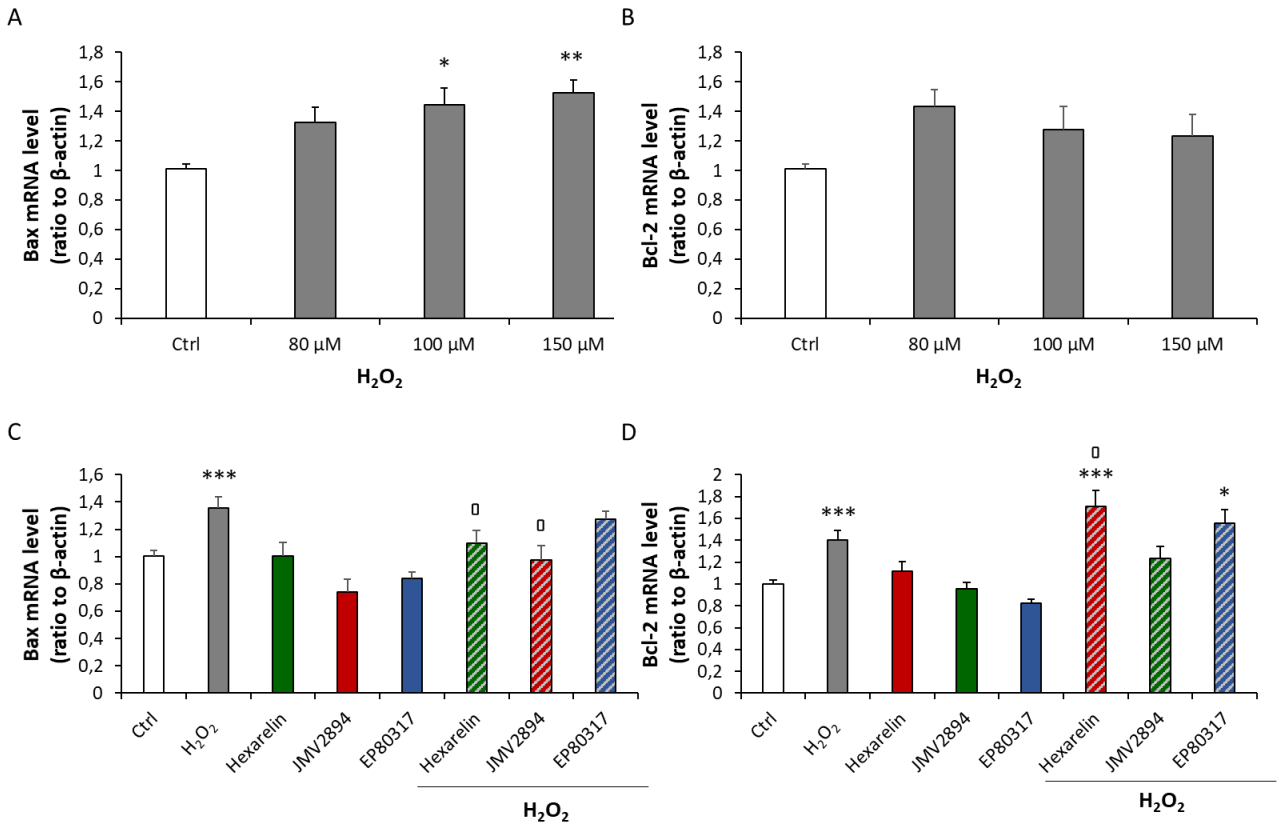

Figure 29. *Quantification of mRNA levels of apoptosis markers following H_2O_2 exposure and their modulation induced by GHSs.*
Panels A and B: Neuro-2A cells were treated with different concentrations (0, 80, 100, 150 µM) of H_2O_2 alone. Panels C and D: Neuro-2A cells were treated with H_2O_2, GHSs alone, or co-incubated with GHSs 1 µM and H_2O_2 100 µM for 24 h. (A,C) Bax and (B,D) Bcl-2 mRNA levels were normalized for the respective β-actin mRNA levels. Data are expressed as mean ± SEM of of replicates obtained in 3 independent experiments (n = 18). * $p < 0.05$, ** $p < 0.01$, and *** $p < 0.001$ vs. Ctrl; ° $p < 0.05$ vs. H_2O_2.

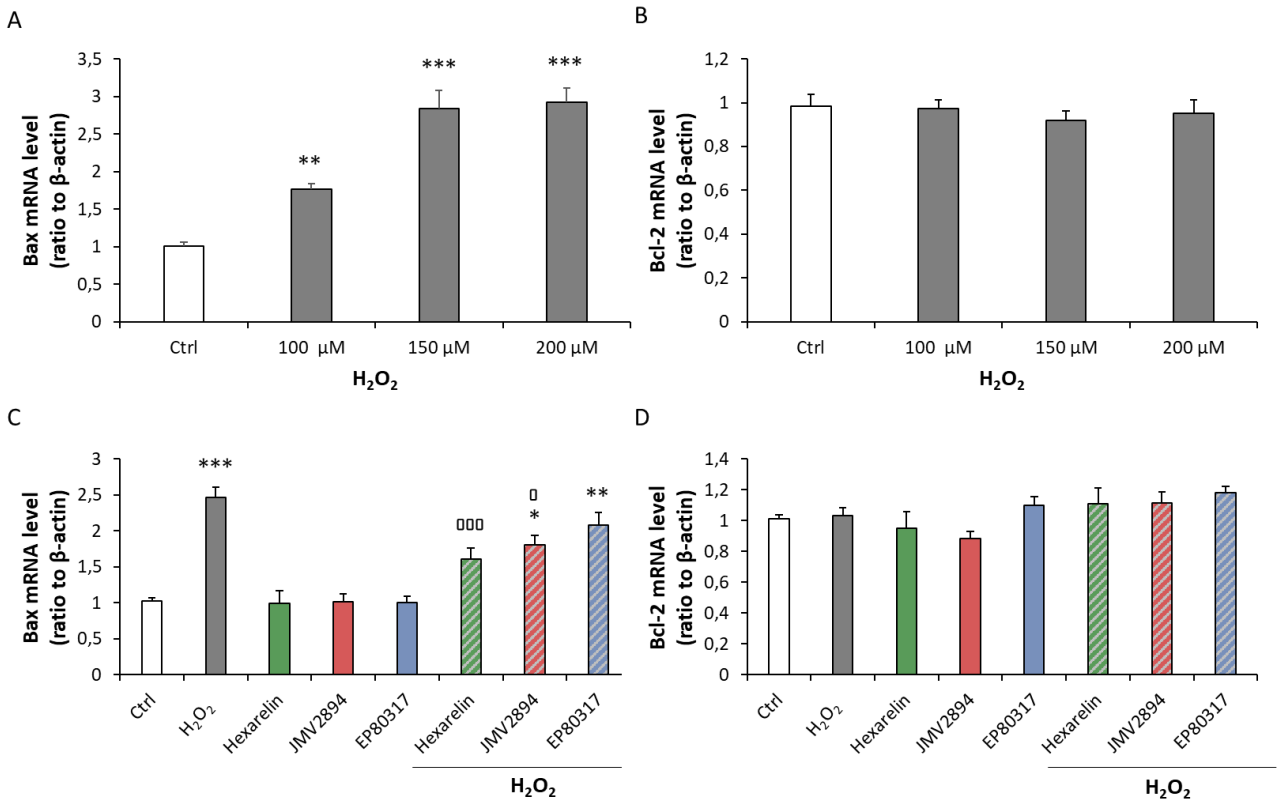

Figure 30. *Quantification of mRNA levels of apoptosis markers following H_2O_2 exposure and their modulation induced by GHSs.*

Panels A and B: SH-SY5Y WT cells were treated with different concentrations (0, 80, 100, 150 µM) of H_2O_2 alone. Panels C and D: SH-SY5Y WT cells were treated with H_2O_2, GHSs alone, or co-incubated with GHSs 1 µM and H_2O_2 100 µM for 24 h. Bax (A,C) and Bcl-2 (B,D) mRNA levels were normalized for the respective β-actin mRNA levels. Data are expressed as mean ± SEM of of replicates obtained in 3 independent experiments (n = 18). * $p < 0.05$, ** $p < 0.01$, and *** $p < 0.001$ vs. Ctrl; ° $p < 0.05$, and °°° $p < 0.001$ vs. H_2O_2.

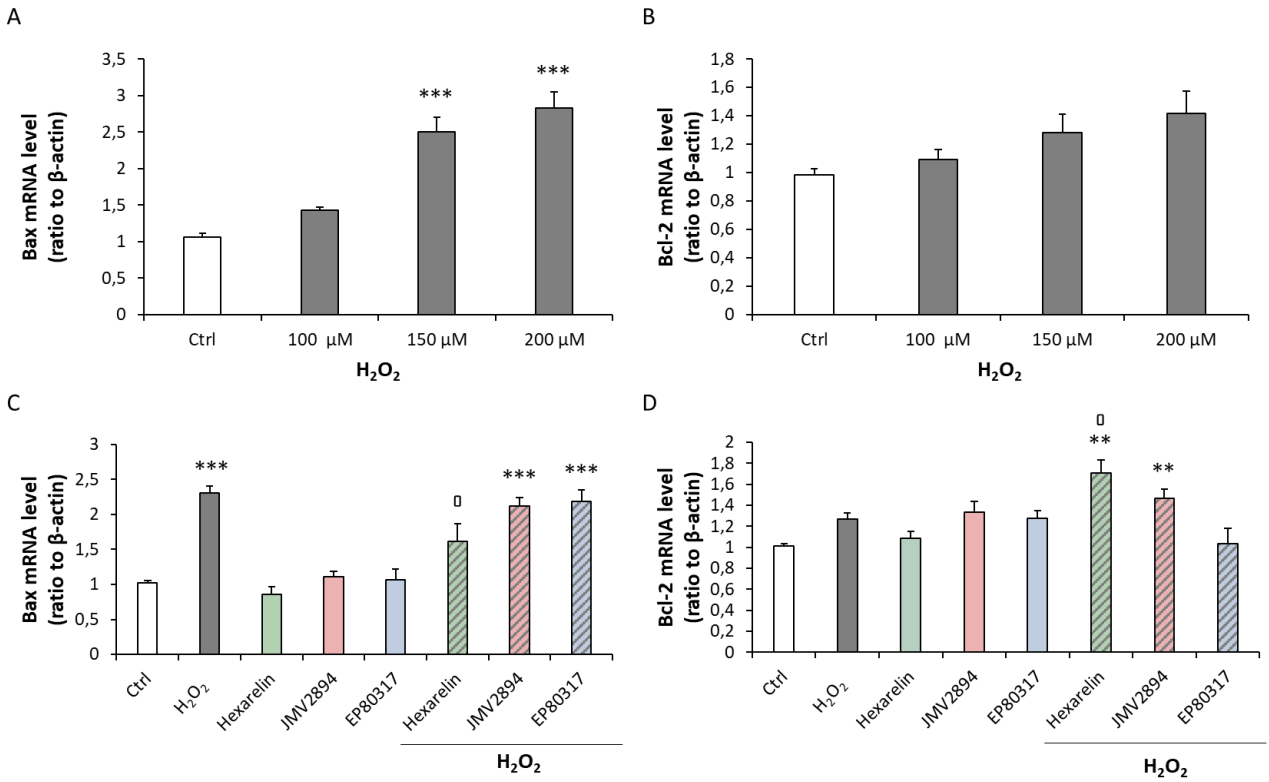

Figure 31. *Quantification of mRNA levels of apoptosis markers following H_2O_2 exposure and their modulation induced by GHSs.*

Panels A and B: SH-SY5Y SOD1^{G93A} cells were treated with different concentrations (0, 80, 100, 150 µM) of H_2O_2 alone. Panels C and D: SH-SY5Y SOD1^{G93A} cells were treated with H_2O_2, GHSs alone, or co-incubated with GHSs 1 µM and H_2O_2 100 µM for 24 h. Bax (A,C) and Bcl-2 (B,D) mRNA levels were normalized for the respective β-actin mRNA levels. Data are expressed as mean ± SEM of of replicates obtained in 3 independent experiments (n = 18). ** $p < 0.01$, and *** $p < 0.001$ vs. Ctrl; ° $p < 0.05$ vs. H_2O_2.

8. Effects of GHSs on ERK 1/2, p38 and Akt protein levels in H_2O_2-treated cells

We hypothesized that GHSs could modulate also MAPK signalling. Among members of the MAPK family, ERK and p38 are known to be associated with cell death or survival, respectively (204).

Compared to the control group, exposure to 100 µM H_2O_2 alone significantly increased the p-ERK/t-ERK ratio ($p < 0.05$), whereas 1 µM GHSs alone did not affect ERK protein levels in Neuro-2A cells. Notably, co-incubation with hexarelin, JMV2894, or EP80317 and H_2O_2 induced a trend toward a reduction of p-ERK protein levels compared to the H_2O_2 alone group (Figure 32A).

As shown in the second panel of Figure 32B, incubation with 100 µM H_2O_2 alone significantly increased the p-p38/t-p38 ratio compared to controls, and this effect was significantly antagonized by co-incubation with GHSs ($p < 0.001$). Furthermore, levels of p-Akt, associated with cell survival after oxidative stress (257), were significantly reduced by H_2O_2 treatment ($p < 0.05$). Notably, p-Akt levels in cells co-incubated with GHSs and H_2O_2 were significantly ($p < 0.05$) higher than those in cells treated with H_2O_2 alone (Figure 32C).

In SH-SY5Y WT cells, the treatment with 150 µM H_2O_2 alone significantly increased the phosphorylation of ERK, p38 and Akt to 49.27 ± 0.05%, 73.40 ± 0.04% and 54.43 ± 0.06% of the control values, respectively ($p < 0.001$, Figure 33). Among the GHSs, only hexarelin significantly antagonized the activation of all these proteins compared to the H_2O_2 alone group; in fact, p-ERK/t-ERK ratio was reduced to 27.93 ± 0.03% ($p < 0.05$, Figure 33A), p-p38/t-p38 ratio to 36.02 ± 0.01% ($p < 0.001$, Figure 33B) and p-Akt/t-Akt ratio to 32.60 ± 0.01% ($p < 0.05$, Figure 33C). Moreover, p-38 levels were also significantly lower than those in cells treated with H_2O_2 alone when co-incubated with JMV2894 ($p < 0.01$, Figure 33B).

Notably, also in SH-SY5Y $SOD1^{G93A}$ cells H_2O_2 induced an increase in p-ERK/t-ERK, p-p38/t-p38 and p-Akt/t-Akt ratios ($p < 0.001$), whereas 1 µM GHSs alone did not affect any protein compared to control groups (Figure 34). The co-incubation with GHSs and H_2O_2 induced a non-significant trend toward a reduction for ERK and Akt phosphorylation compared to the H_2O_2 alone group (Figure 34A,C), while p-p38 levels in cells co-incubated with hexarelin or JMV2894 and H_2O_2 were significantly ($p < 0.01$) lower than those in cells treated with H_2O_2 alone (Figure 34B).

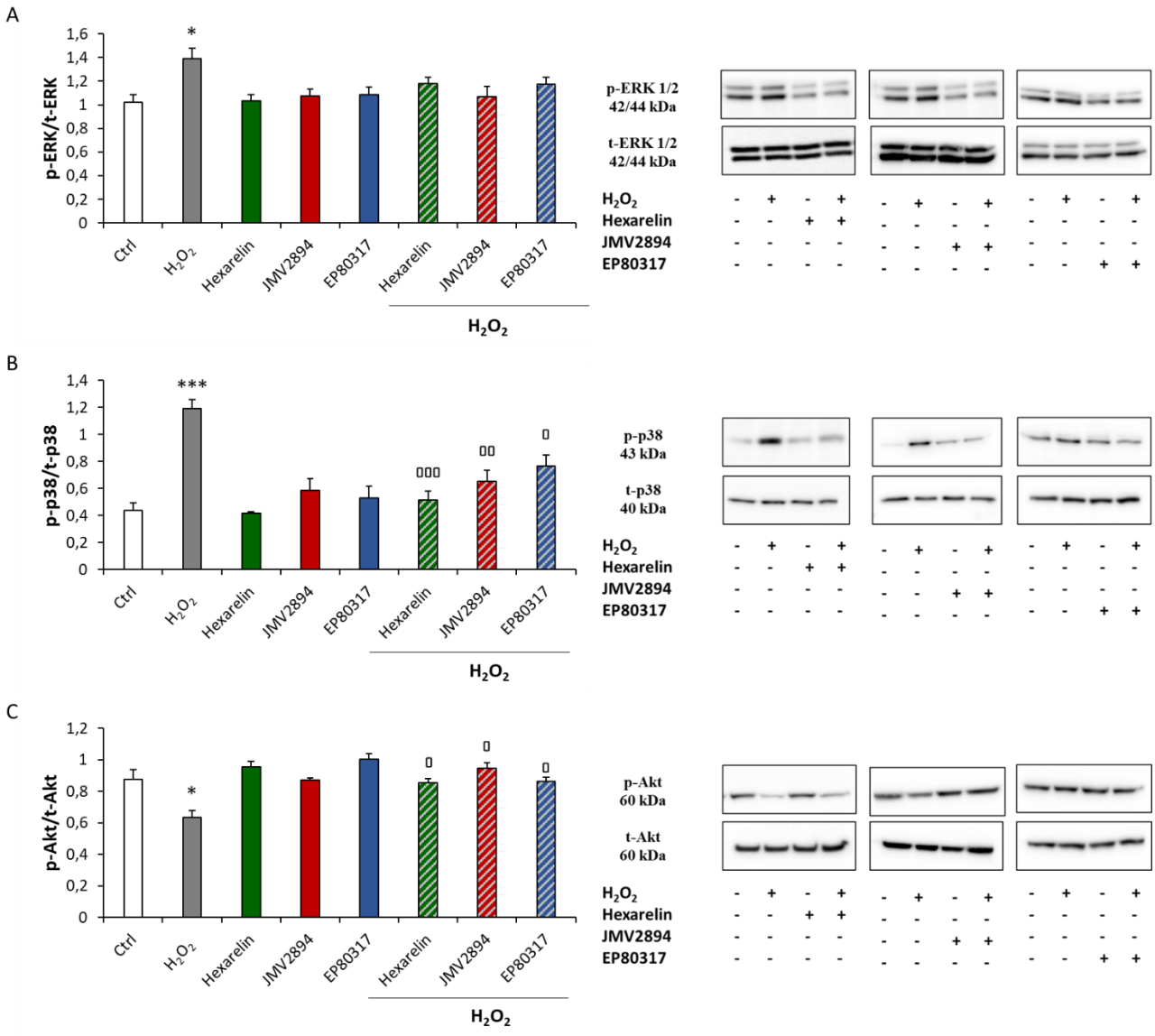

Figure 32. *GHSs modulate ERK, p38 and Akt activation.*
Neuro-2A cells were treated with or without GHSs and H_2O_2 for 24 h and Western blot assay was used to measure (A) p-ERK/t-ERK, (B) p-p38/t-p38, and (C) p-Akt/t-Akt levels. All assays were performed for at least 3 independent experiments. Statistical significance: * $p < 0.05$, and *** $p < 0.001$ vs. Ctrl; ° $p > 0.05$, °° $p < 0.01$, and °°° $p < 0.001$ vs. H_2O_2.

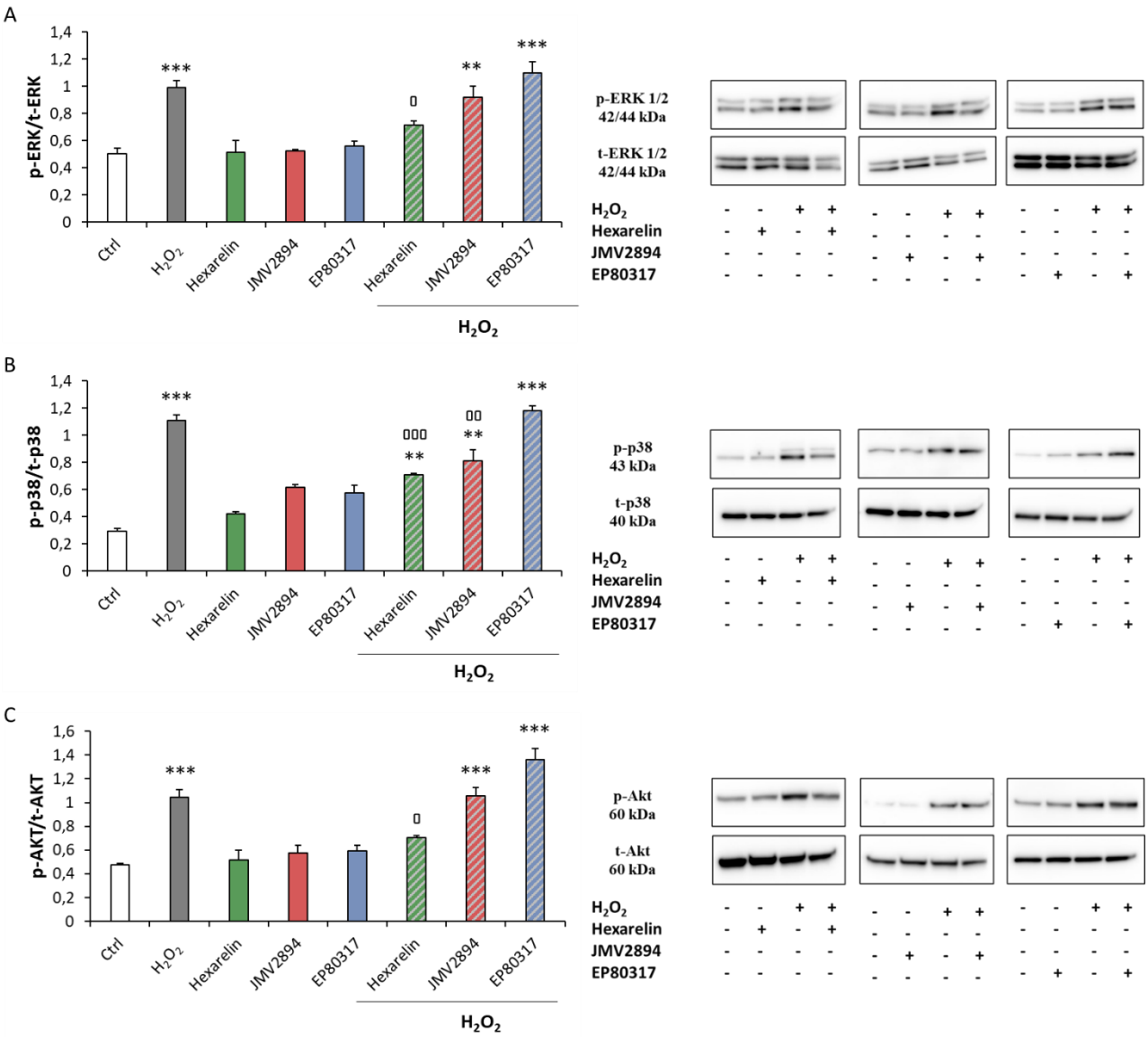

Figure 33. *GHSs modulates ERK, p38 and Akt activation.*
SH-SY5Y WT cells were treated with or without GHSs and H_2O_2 for 24 h and Western blot was used to measure (A) p-ERK/t-ERK, p-(B) p38/t-p38, and (C) p-Akt/t-Akt ratios. All assays were performed for at least 3 independent experiments. Statistical significance: ** $p < 0.01$, and *** $p < 0.001$ vs. Ctrl; ° $p > 0.05$, °° $p < 0.01$, and °°° $p < 0.001$ vs. H_2O_2.

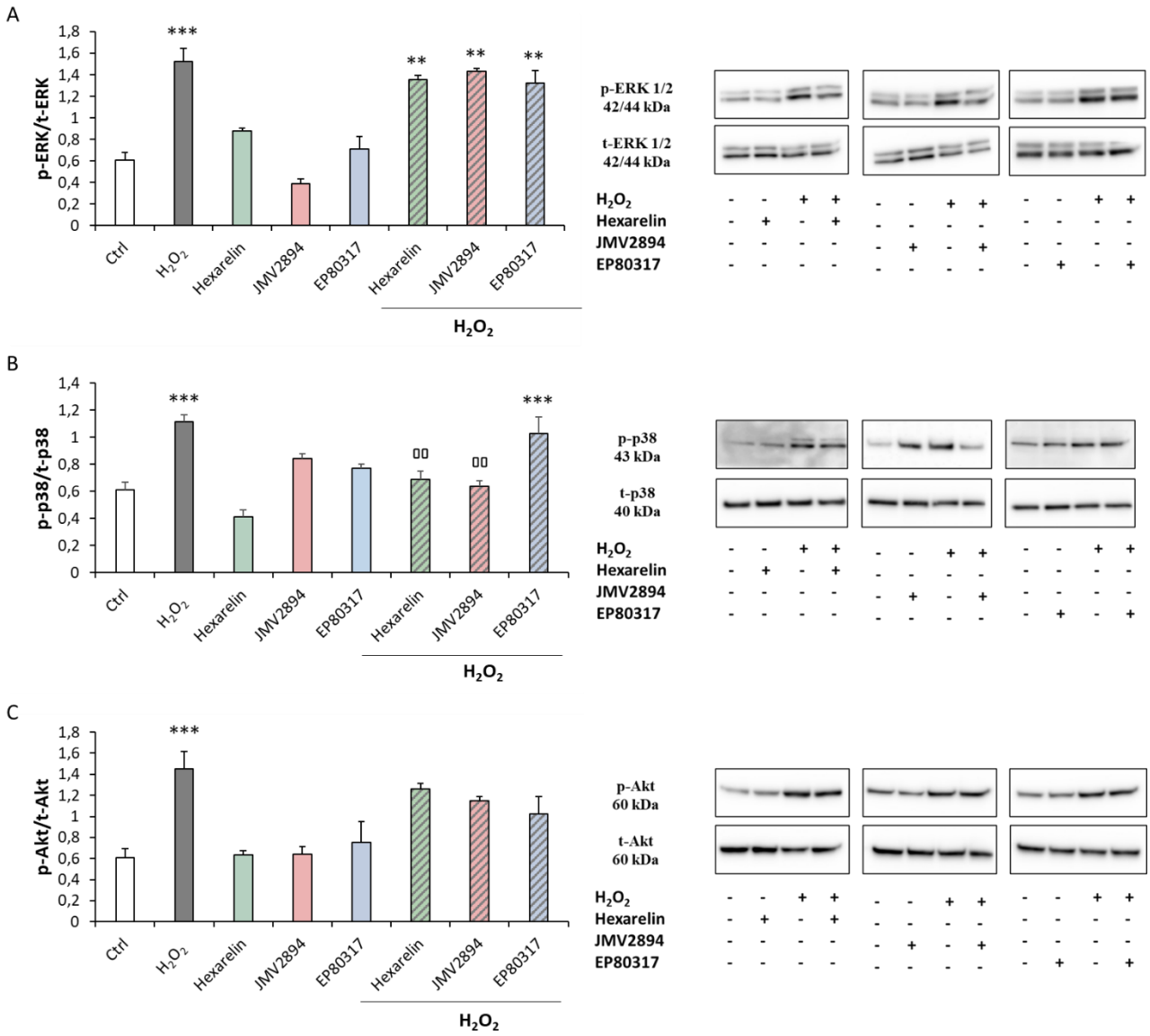

Figure 34. *GHSs modulates ERK, p38 and Akt activation.*
SH-SY5Y SOD1^{G93A} cells were treated with or without GHSs and H_2O_2 for 24 h and Western blot assay was used to measure (A) p-ERK/t-ERK, (B) p-p38/t-p38, and (C) p-Akt/t-Akt ratios. All assays were performed for at least 3 independent experiments. Statistical significance: ** $p < 0.01$, and *** $p < 0.001$ vs. Ctrl; °° $p < 0.01$ vs. H_2O_2.

9. Isolation and characterization of N9-derived EVs

The involvement of microglia in ALS exacerbation and propagation is still under debate. In fact, there were conflicting observations suggesting that activated microglia may be a double-edged sword with the abilities to promote either neuronal protection or injury.

Moreover, increasing evidences have demonstrated an interplay between glial cells and the extracellular environment mediated by the secretion of EVs, which are involved in many physiological and pathological processes, and have the role to deliver their cargo to adjacent or distant recipient cells.

Starting from these observations, we have treated N9 microglia cells with 1 µM GHSs (hexarelin or JMV2894) for 48 h, and EVs were isolated from conditioned media, as previously described.

Figure 35 shown the characterization of EVs in terms of (i) size distribution, (ii) particle and (iii) protein concentrations.

Nanoparticle tracking analysis (NTA) allowed to demonstrate that in GHSs treated groups there were differences in terms of both size distribution and particles concentration compared to control: although the mean size of isolated EVs was 152.01 ± 103.4 nm for the control group, 158.2 ± 52.1 and 155.8 ± 50.8 for hexarelin and JMV2894, respectively (values expressed as mean ± SD), the EVs derived from the control N9 cells showed a greater heterogeneity in size distribution (Figure 35A,B and C). Moreover, significant variations ($p < 0.001$; Figure 35D) were found in particles concentration of GHSs-derived EVs compared to control. These data suggested (i) the presence of a complex population of EVs derived from control N9 cells, and (ii) the capability of GHSs treatment to induce a higher release of EVs, which are mainly EXOs without contaminants of different nature.

It is important to note that similar total protein concentrations were found also in EVs derived from N9 cells treated with GHSs, which ranged between 30 and 50 µg/mL.

Finally, we labelled EVs with the fluorescent PKH-26 lipophilic dye to monitor their internalization by SH-SY5Y WT and $SOD1^{G93A}$ cells. As shown in Figure 36, no differences were found in EVs distribution. Moreover, the incubation of labelled-EVs for 24 h with SH-SY5Y WT and $SOD1^{G93A}$ cells showed a preferential localization of EVs proximally to the nucleus, as shown in Figure 37.

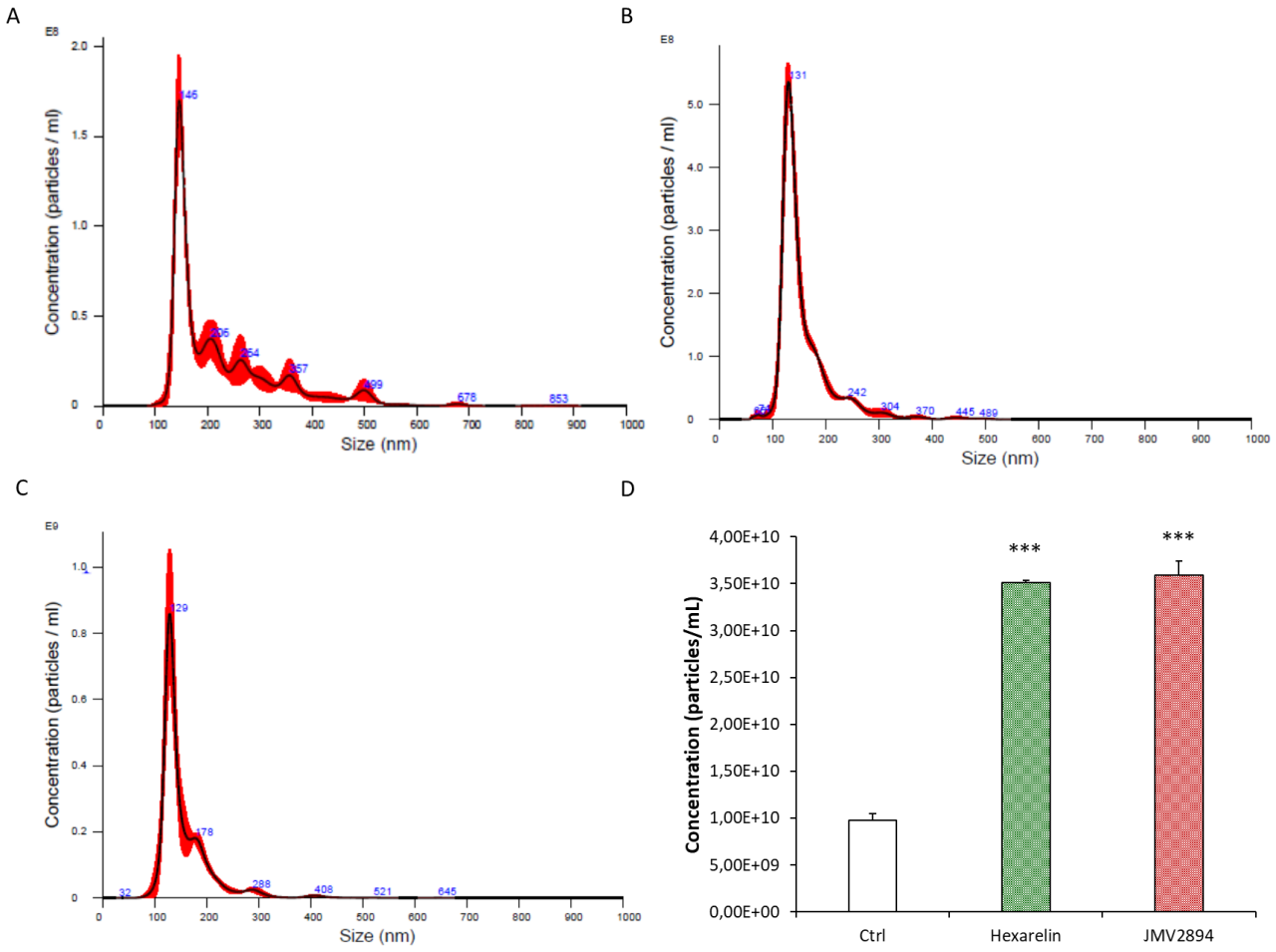

Figure 35. *Characterization of EVs derived from N9 cells treated with hexarelin and JMV2894.* N9 cells were treated with hexarelin or JMV2894 for 48 h and conditioned media were used to isolate EVs. NTA size/concentration curve of N9 cells in: (A) control group; (B) cells treated with hexarelin; and (C) cells treated with JMV2894. Data were obtained by mean of three tracking video files. (D) Quantification of EVs density comparing treatments. Statistical significance: *** $p < 0.001$ vs. Ctrl.

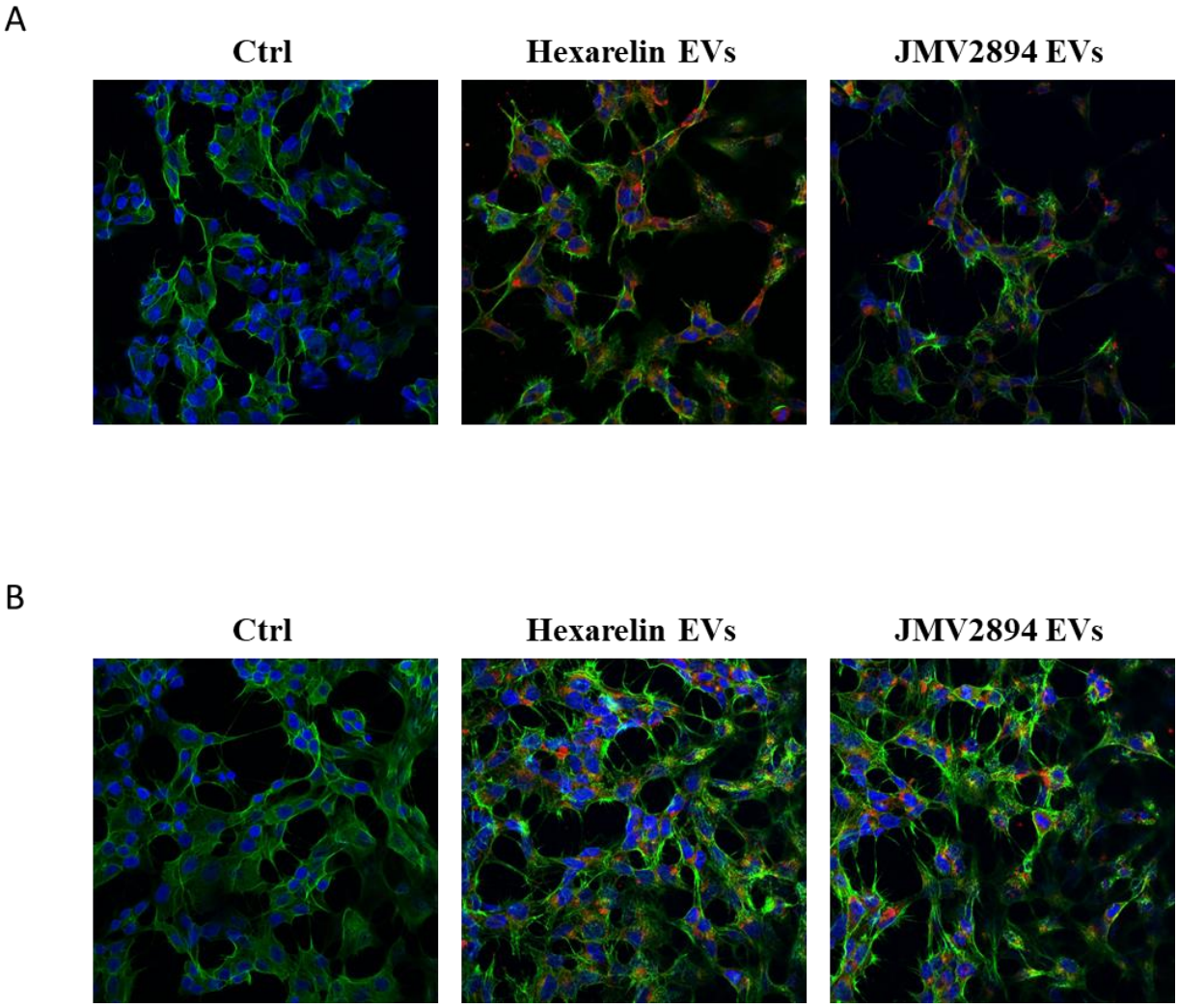

Figure 36. *Distribution of EVs from N9 cells treated with hexarelin and JMV2894 in SH-SY5Y WT and SOD1^{G93A} cell lines.*
Representative photomicrographs of (A) SH-SY5Y WT and (B) SH-SY5Y SOD1^{G93A} cells incubated for 24 h with or without N9-derived EVs. EVs were isolated from conditioned media of N9 microglial cells treated with hexarelin or JMV2894 for 48 h, stained with PKH-26 fluorescent cell linker kit (in red) and incubated with SH-SY5Y WT and SOD1^{G93A} cells for 24 h.

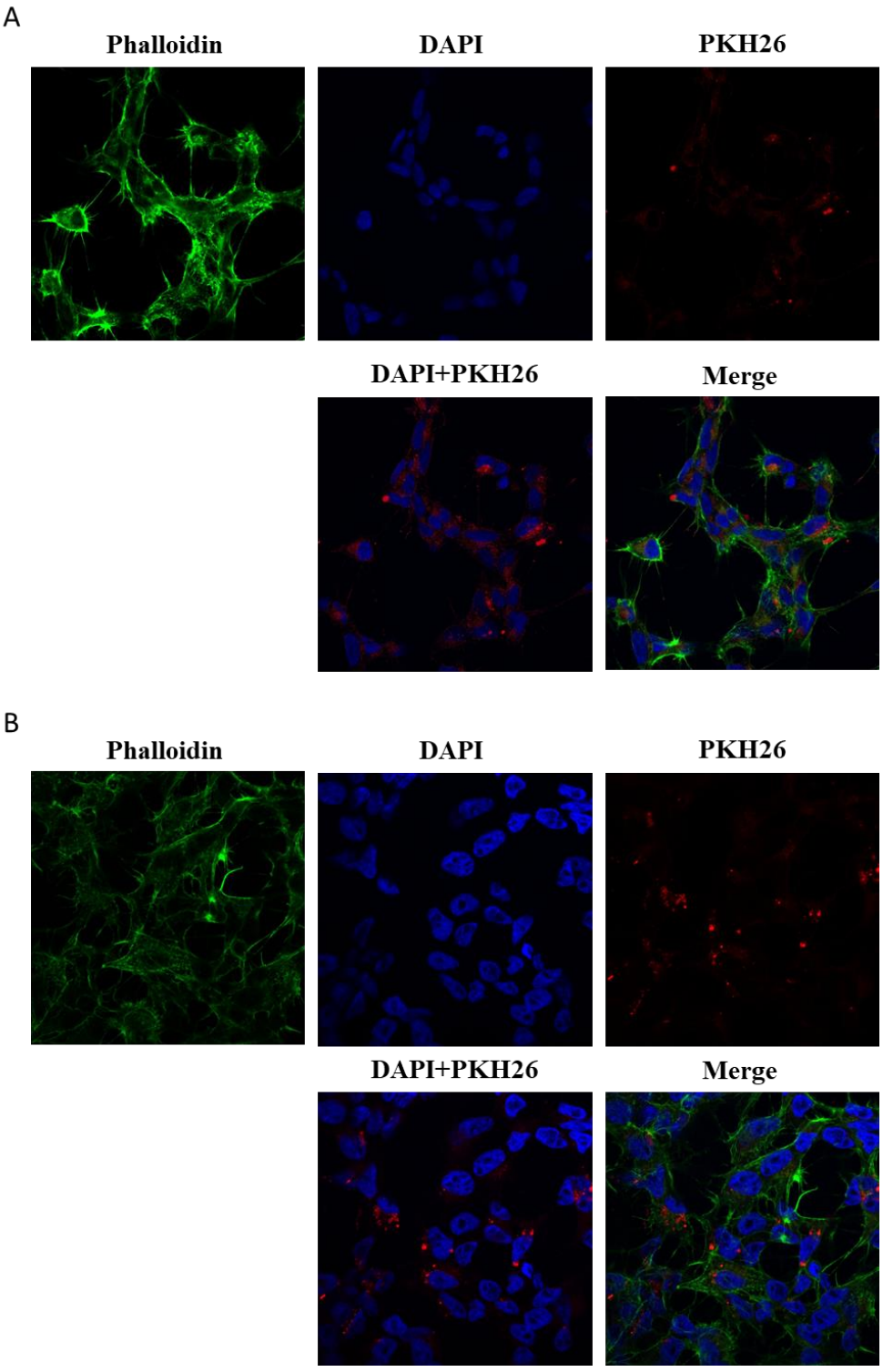

Figure 37. *Localization of EVs from N9 cells treated with hexarelin and JMV2894 in SH-SY5Y WT and SOD1^{G93A} cell lines.*

Representative photomicrographs of (A) SH-SY5Y WT and (B) SH-SY5Y SOD1^{G93A} cells incubated for 24 h with or without N9-derived EVs. EVs were isolated from conditioned media of N9 microglial cells treated with hexarelin or JMV2894 for 48 h, stained with PKH-26 fluorescent cell linker kit (in red) and incubated with SH-SY5Y WT and SOD1^{G93A} cells for 24 h. As shown in photomicrographs, EVs preferentially localized proximal to the nucleus.

10. Effects of EVs derived from GHSs-conditioned N9 media on apoptotic markers mRNA expressions

To evaluate whether EVs derived from the conditioned media of N9 cells treated with the two most promising GHSs were capable to antagonize the apoptotic effect of H_2O_2 in human neuroblastoma cell lines, we have treated SH-SY5Y WT and SOD1^{G93A} with 150 µM H_2O_2, 1.5*10^9 particles/mL (corresponding to 1 µg of total protein) EVs or the combination of H_2O_2 and EVs for 24 h.

The significant increase observed in SH-SY5Y WT of caspase-3, caspase-7 and Bax mRNA levels induced by H_2O_2 ($p < 0.001$ for caspase-3; $p < 0.01$ for caspase-7 and Bax) were antagonized by EVs. In particular, EVs-derived from hexarelin-treatment significantly decreased the level of caspase-7 and Bax ($p < 0.05$), while for caspase-3 the reduction was not significant. EVs-derived from JMV2894-treated N9 cells significantly counteracted caspase-3 ($p < 0.001$) and caspase-7 ($p < 0.01$), and induced a tendency toward a reduction of Bax (Figure 38).

As shown in Figure 39, in SH-SY5Y SOD1^{G93A} cells, EVs derived from hexarelin- and JMV2894-treatments significantly reduced the mRNA levels of pro-apoptotic Bax compared to H_2O_2 treated cells ($p < 0.01$ and $p < 0.001$, respectively), but did not exert any beneficial effects on other apoptosis markers.

In both SH-SY5Y WT and SOD1^{G93A} cells, EVs did not modulate the mRNA levels of the anti-apoptotic molecule Bcl2 (Figure 38D and 39D).

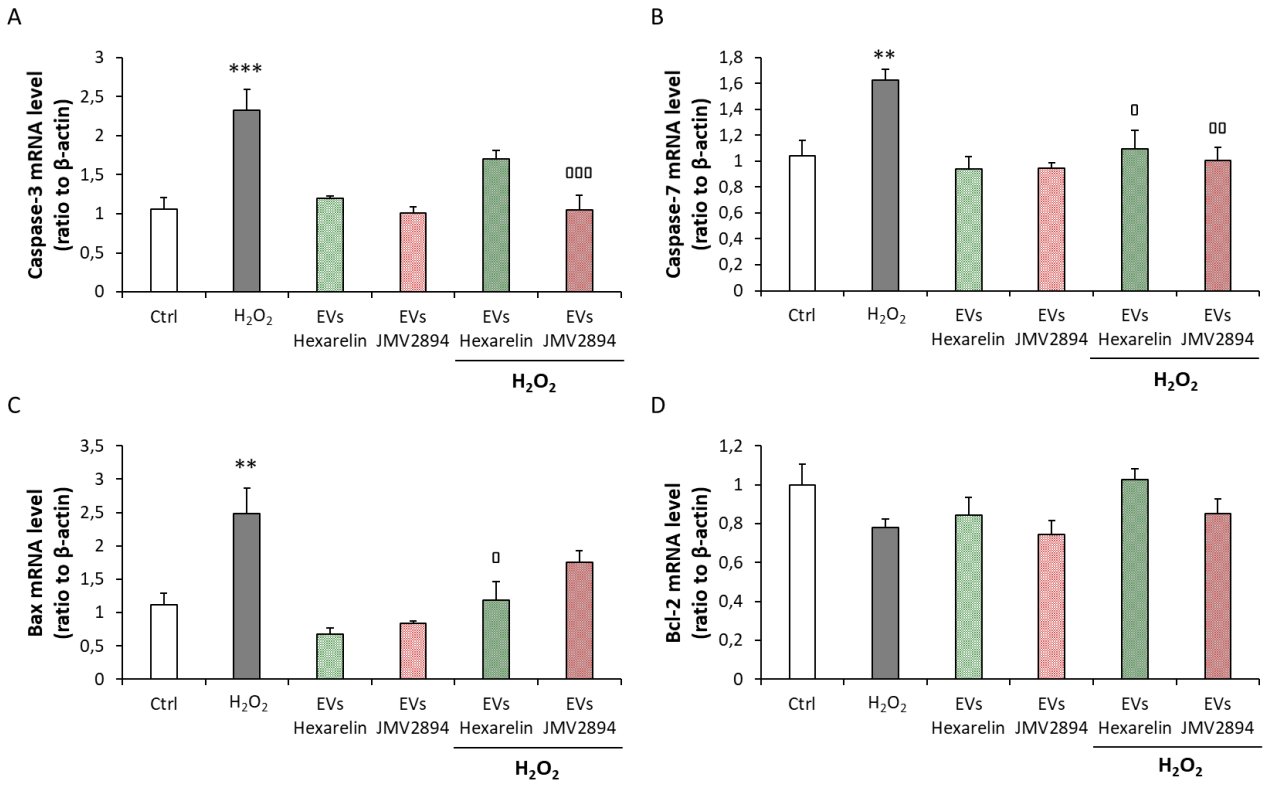

Figure 38. *Analysis of mRNA levels of apoptosis markers following H_2O_2 exposure and their modulation induced by EVs.*

SH-SY5Y WT cells were treated with 150 µM H_2O_2, EVs or their co-incubation for 24 h. (A) Caspase-3, (B) caspase-7, (C) Bax and (D) Bcl-2 mRNA levels were normalized for the respective β-actin mRNA levels. ** $p < 0.01$, and *** $p < 0.001$ vs. Ctrl; ° $p < 0.05$, °° $p < 0.01$, and °°° $p < 0.001$ vs. H_2O_2.

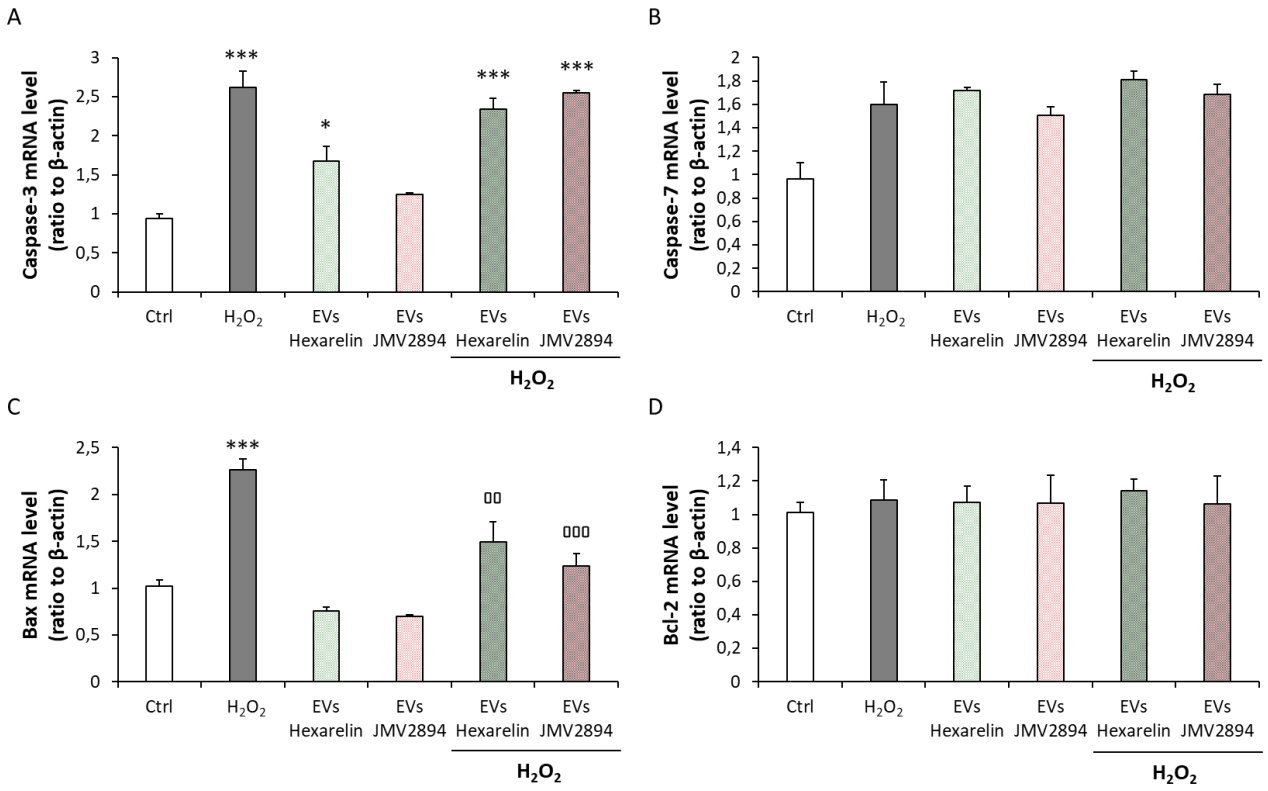

Figure 39. *Analysis of mRNA levels of apoptosis markers following H_2O_2 exposure and their modulation induced by EVs.*
SH-SY5Y SOD1^{G93A} cells were treated with 150 µM H_2O_2, EVs or their co-incubation for 24 h. (A) Caspase-3, (B) caspase-7, (C) Bax and (D) Bcl-2 mRNA levels were normalized for the respective β-actin mRNA levels. * $p < 0.05$, and *** $p < 0.001$ vs. Ctrl; °° $p < 0.01$, and °°° $p < 0.001$ vs. H_2O_2.

DISCUSSION

Reactive oxygen and nitrogen species (ROS/RNS) are chemically active molecules arising as by-products of aerobic metabolism, mostly due to leakage of electrons from the mitochondrial respiratory chain. This results in incomplete reduction of molecular oxygen and nitrogen during oxidative phosphorylation, to produce superoxide radical anion (O_2^-), hydrogen peroxide (H_2O_2), nitric oxide (NO), and peroxynitrite anions ($ONOO^-$) (44). In physiological conditions, ROS/RNS are short-lived and can act as signalling molecules in different cellular pathways, but when the balance between oxidants and antioxidants is disrupted in favour of the former, biochemical defences are overwhelmed and oxidative stress (OS) prevails (258,259).

Mitochondria are important generators of OS, as they use oxygen for energy production via oxidative phosphorylation. They often become the target of elevated ROS exposure, resulting in depletion of ATP, inhibition of enzymes of the electron transport chain, impaired calcium buffering capacity, defective mitochondrial dynamics and mutations in mitochondrial DNA (mtDNA).

As well, mitochondrial dysfunction and OS are implicated in cellular damage to DNA, proteins and lipids, which results in inflammation, excitotoxicity, protein aggregation, and ultimately to neuronal death, playing a major role in the development of many disorders, including aging and neurodegenerative diseases (260).

Although each neurodegenerative disease (NDD) has its own specific aetiology and differentially affects brain regions, NDDs share several elements in common, such as OS, free radical generation and mitochondrial changes, all contributing to apoptosis (261).

Among NDDs, amyotrophic lateral sclerosis (ALS) is an adult-onset, progressive neurodegenerative disease caused by the deterioration of motor neurons within motor cortex, brain stem, and spinal cord, in which OS appears intimately linked to several cellular events in motor neurons that contribute to neuronal degeneration and death (262). Biopsies samples from spinal cord, nerves and muscles, from ALS patients show abnormalities in mitochondrial structure, number and localization, and alterations in activities of respiratory-chain complexes (263). The identification of mutations in genes implicated in mitochondrial functions revealed a clear association between OS and ALS onset, even if they are not the only cause of the pathology.

Superoxide dismutase 1 (SOD1) is an enzyme involved in the scavenging of O_2^- to H_2O_2 and O_2, and in the modulation of cellular respiration, energy metabolism, and post-translational modifications (263,264). It is known that SOD1-related ALS accounts for about 20% of fALS and 5% of sALS, and more than 170 mutations in this gene have been identified (63). Among all, G93A (glycine 93 substituted for alanine) mutation is the best studied, and it is characterized by the loss of antioxidant capability due to a gain-of-function, which determined (i) enzyme's change in affinity to the natural and abnormal substrates, and (ii) the increase of enzyme's aggregation in neurons (61).

Therefore, the coexistence of OS, defective mitochondrial function, and $SOD1^{G93A}$ mutation seem to be determinants of neuronal degeneration in ALS, and are strictly linked to apoptosis mechanisms (265,266).

Apoptosis is known to be one of the most sensitive biological markers for evaluating oxidative stress caused by imbalance between ROS generation and efficient activity of antioxidant systems (267,268). Apoptotic cell death is an active process initiated by genetic programs and culminating in DNA fragmentation, characterized by morphological changes, including cell shrinkage, formation of membrane-packaged inclusions called apoptotic bodies (269), activation of caspases, nucleases, inactivation of nuclear repair polymerases (270), and finally condensation of nuclei (271).

There are several inducers of OS that are capable of causing cytotoxicity and apoptosis, and which permits to obtain a simplified in vitro model of NDDs. To this aim, we have chosen the murine neuroblastoma Neuro-2A cell line, which can be used to study OS in neurodegeneration (209,272). We have also used and two different lines of human neuroblastoma SH-SY5Y cells, which constitutively express (i) wild-type SOD1 or (ii) the mutant $SOD1^{G93A}$, that are a well-established and representative in vitro model of ALS (68,273).

The three cell lines were treated with H_2O_2 as OS inducer, because it is (i) an established method to study putative neuroprotective agents and (ii) the natural by-products of SOD1 activity (274,275).

H_2O_2 induced neuronal cytotoxicity in both Neuro-2A and SH-SY5Y (WT and $SOD1^{G93A}$) cells in a dose-dependent manner, as demonstrated by MTT assays, while increasing concentrations of GHSs (hexarelin, JMV2894 and EP80317) did not affect cell viability. In order to determine the protective effects of GHSs against H_2O_2-induced cytotoxicity, all cell lines were treated with 1 μM hexarelin, JMV2894 or EP80317. As expected, cell viabilities of the GHSs treated group were superimposable to those of control cells. Interestingly,

hexarelin and JMV2894 blunted H_2O_2-induced cell death in Neuro-2A cells. In SH-SY5Y WT only hexarelin increased cell survival, confirming its ability to exert protective effects against H_2O_2. However, in SH-SY5Y SOD1^{G93A} all GHS treatments failed to protect cell viability, probably due to the excessive ROS production induced by both SOD1 mutation and H_2O_2 treatment. EP80317 did not antagonize the reduction of cell viability caused by H_2O_2-treatment in any cellular line.

The protective effects of GHSs, in particular hexarelin and JMV2894, were further confirmed by Griess assay. Excessive levels of NO, an important mediator of cellular communication implicated in the pathogenesis of NDDs (276) and in caspase-dependent cellular death (277), could be quantified by the measurement of extracellular NO_2^-, a primary stable product of NO breakdown. Previous studies reported that H_2O_2incubation resulted in increased production of NO in neuronal and glial cells (278,279), through the stimulation of inducible nitric oxide synthase. In this study, we demonstrated that in Neuro-2A and SH-SY5Y (WT and SOD1^{G93A}) cells H_2O_2 increased extracellular NO_2^- release, an effect that was blunted by the coincubation with hexarelin and JMV2894. In fact, although hexarelin is apparently more effective than JMV2894, both GHS significantly inhibited NO_2^- synthesis in Neuro-2A and SH-SY5Y WT cells, and induced a trend toward reduction in SH-SY5Y SOD1^{G93A}. Also in this case, EP80317 did not exert any significant effect against OS induced by H_2O_2 in both Neuro-2A and SH-SY5Y cells. The ability of these GHSs to reduce NO_2^- release suggests that their protective effects against H_2O_2 oxidative stress could be mediated through the modulation of apoptosis and downstream pathways.

Moreover, H_2O_2-stimulation induced cellular morphological changes that are characteristic of an apoptotic phenotype, including a drastic loss of cell/field, de-ramification and reduction of process length, loss of cellular complexity and shape, as well as reduction of cell size. In Neuro-2A cells, both skeleton and fractal analysis suggested that hexarelin and JMV2894 maintained the cellular complexity, ramification, dimension, heterogeneity and shape comparable to values observed in the control group; on the contrary, EP80317 exert such a protective effect only for cellular dimension, but not restoring cellular morphology to the complexity of control cells. These observations led to the hypothesis that EP80317 could maintain cellular morphology but did not exert an effective protective effect against H_2O_2-induced cellular loss.

SH-SY5Y WT cells, both hexarelin and JMV2894 restored cellular morphological characteristics, maintaining cellular ramification and process length, even though only

hexarelin maintained normal cellular complexity and shape, demonstrating again to be the most effective GHS.

Among GHSs, we have selected hexarelin, JMV2894 and EP80317 for their potential neuroprotective activities demonstrated in our previous studies (229,234,242,247,248,280,281).

Hexarelin is a synthetic hexapeptide ligand of the GHS-R1a, which has been shown to stimulate cell proliferation of adult hippocampal progenitors (AHP) and to protect against growth factor deprivation-induced apoptosis and necrosis (282), principally through the activation of PI3K/Akt pathway (283,284). Interestingly, hexarelin also blunts the inflammatory processes activated by neurodegenerative diseases, stroke, and tumor invasion (285), by modulating the release of pro-inflammatory mediators such as cytokines, reactive oxygen species, free radical species and nitric oxide, which could contribute to both neuronal dysfunction and cell death (280,286). Hexarelin also exert cardioprotective effects, attenuating cardiomyocyte hypertrophy and apoptosis (287), and attenuating mitochondrial abnormalities reported in cancer cachexia (234,288), stimulating biogenesis, mitochondrial mass and dynamics restoration, reducing expression of autophagy-related genes and ROS production.

JMV2894 is a synthetic agonist of GHS-R1a, as demonstrated by its ability to stimulate (i) Ca^{2+} mobilization in vitro and (ii) growth hormone release in neonatal rats (229). Similar to hexarelin, JMV2894 antagonizes cisplatin induced weight loss in rats, restoring body weight to levels similar to controls, without stimulating perirenal and epididymal fat accumulation, but directly acting on skeletal muscle (234,288). Interestingly, JMV2894 acts through the modulation of mitochondria (i) biogenesis, (ii) mass, and (iii) fusion index, in addition to changes in the expression of autophagy-related genes (Akt/FoxO pathway) and reduction of ROS production (234).

EP80317 is a hexapeptide agonist of CD36, a secondary receptor of GHS, without GH-releasing properties. Interestingly, EP80317 did not exert anti-apoptotic effects like hexarelin and JMV2894. EP80317 is mainly involved in the modulation of the production of inflammatory cytokines (289) in (i) in vitro model of Alzheimer's disease and epilepsy, and (ii) in vivo model of atherosclerosis and vascular inflammation (248,280,290).

Different studies reported that EP80317 effectively counteracted the production of inflammatory cytokines stimulated by β-amyloid fibrils in mouse microglia cells (280), primarily through the activation of peroxisome proliferator-activated receptor-γ (PPAR-γ) and changes in levels of phosphorylated MAPK (247). Moreover, EP80317 is also endowed

with anti-atherosclerotic and hypocholesterolemic effects through reverse cholesterol transport activity, and consequent cardioprotective function (291).

This study demonstrates that have GHSs anti-apoptotic effects via the inhibition of caspases activation. Neuro-2A and SH-SY5Y cells treated for 24 h with increasing concentrations of H_2O_2 showed a significant activation of caspase-3 and -7. In Neuro-2A cells, treatment with 1 µM hexarelin and JMV2894 attenuated the activation of caspase-3, both in terms of mRNA levels and protein activation. In SH-SY5Y WT cells, hexarelin, JMV2894, and also EP80317 significantly reduced both caspase-3 and caspase-7 mRNA and protein levels, while in SH-SY5Y $SOD1^{G93A}$ only hexarelin exerted anti-apoptotic effects. Our hypothesis was that the modulation of caspase mRNA levels induced by GHSs, in particular by hexarelin and JMV2894, was dependent on the intracellular pro-apoptotic signalling molecules belonging to the BCL-2 family.

The BCL-2 family consist of two groups of mediators including (i) the anti-apoptotic group, mainly represented by Bcl-2, and (ii) a pro-apoptotic group, represented primarily by Bax. Both groups play important roles in mitochondrial related apoptosis pathways (292).

Therefore, we quantified by RT-PCR, the effects of GHSs on Bcl-2 and Bax mRNA levels in our experimental in vitro models. As expected, H_2O_2 treatment induced a concentration-dependent activation of pro-apoptotic Bax, and the inhibition of anti-apoptotic Bcl-2, in both Neuro-2A and SH-SY5Y cells. GHSs treatment alone did not affect mRNA levels of apoptotic signalling molecules compared to the control group, demonstrating that these compounds do not stimulate the apoptosis pathway. At the same time, the reduction in Bax mRNA levels, and the increase in Bcl-2 mRNA levels in the group incubated with the combination of hexarelin or JMV2894 and H_2O_2 confirmed the anti-apoptotic effect of GHSs. Taken together, these results demonstrated the potential anti-oxidant, anti-apoptotic and neuroprotective effect of hexarelin in in vitro models of neurodegeneration and ALS.

To investigate the molecular pathways involved in GHSs neuroprotection, we quantified the expression of MAPKs (ERK and p38) and PI3K/Akt. MAPKs activation contribute to neuronal dysfunction and are involved in NDDs (293,294). Furthermore, ERK has been shown to participate in the regulation of cell growth and differentiation, and responses to cellular stress (295).

In this study, treatment of Neuro-2A cells with H_2O_2 led to cell death by up-regulating p-ERK and p-p38 protein expression. The up-regulation of MAPKs induced by H_2O_2 stimulation were blunted by GHSs treatment. In addition, GHSs alone did not affect the MAPKs proteins compared to control.

In SH-SY5Y WT, hexarelin stimulated the down-regulation of MAPKs protein level induced by H_2O_2-treatment, while JMV2894 blunted only the activation of p38. Also in SH-SY5Y $SOD1^{G93A}$ cells, both hexarelin and JMV2894 significantly down-regulated p38 phosphorylation compared to H_2O_2-stimulated cells.

PI3K/Akt is a key apoptotic modulator in the growth factor signalling pathway (296). In particular, the phosphorylation of Thr-308 and Ser-473 of Akt serves a key role in modulating the actions of growth factors on cells, and plays an important role in neuronal protection (297,298). In this study, H_2O_2 significantly increased the de-phosphorylation of Akt in Neuro-2A cells. GHSs treatment did not alter the p-Akt/t-Akt ratio compared to controls, but in cells treated for 24 h with both GHSs and H_2O_2, Akt protein levels were significantly increased compared with cells treated with H_2O_2 alone.

In SH-SY5Y cells only hexarelin treatment suppressed Akt signalling pathway: the level of p-Akt was significantly increased by H_2O_2, and the treatment with hexarelin decreased the levels of activated Akt. In SH-SY5Y $SOD1^{G93A}$, GHSs induced a trend toward reduction of phosphorylated Akt protein levels.

Our findings demonstrate that H_2O_2 caused the activation of early and late apoptotic pathways in Neuro-2A and SH-SY5Y cells. Results obtained in the first part of this research suggested that hexarelin and JMV2894 are promising compounds, since they inhibit apoptotic mechanisms induced by H_2O_2-treatment in different cell lines, throught the inhibition of apoptosis and potentiation of MAPKs and PI3K/Akt survival pathways.

ALS neurodegeneration is usually accompanied by neuroinflammation, and a key role is played by the complex interplay between motor neurons and glial cells (19,180). In fact, in the last decades, many studies have demonstrated that ALS could be also considered a non-cell autonomous disease, in which glial cells participate in both disease onset and progression by a complex interaction with motor neurons (152). Moreover, the bidirectional neuron-glial cross-talk through EVs provide a new type of inter-cellular communication, which permits to preserve brain homeostasis or contributes to neurodegeneration and diseases spread, depending on their cargo (19).

Given the results described above, we have treated N9 microglia cells with hexarelin and JMV2894 and isolated EVs from conditioned culture media to test the potential neuroprotective effect of EVs in SH-SY5Y WT and $SOD1^{G93A}$ cells.

EVs derived from N9 cells treated for 48 h with hexarelin or JMV2894 were significantly more concentrated and homogeneous in size distribution compared to those of controls, suggesting that GHSs treatment enhanced the release of EVs, in particular of exosomes, from

N9 cells. Moreover, images of EVs-internalization showed a preferential localization of EVs proximally to the nucleus.

Since EVs can transfer biological information and are capable to cross the BBB, increasing attention has been paid to EVs as promoter of suppressors of pathological processes. For example, recent studies have demonstrated that EVs exert neuroprotective effect in an in vitro model of ALS (19), probably counteracting the apoptosis pathway, reducing mutant SOD1 aggregation and restoring mitochondrial protein functions.

Starting from the knowledge that EVs could inhibit apoptosis (299), we have demonstrated that the incubation of SH-SY5Y WT and $SOD1^{G93A}$ cells with EVs derived from N9 cells treated with hexarelin or JMV2894 significantly reduced the apoptotic mechanism through the reduction of Bax mRNA level. Moreover, in SH-SY5Y WT cells, EVs exert an inhibitory effect on caspases activation. Therefore, treatment with EVs stimulated by GHSs may become a promising strategy for the modulation of OS.

In conclusion, this study demonstrated that, among GHS, hexarelin and JMV2894 are capable of protecting cells from H_2O_2-caused cytotoxicity, suggesting the possibility of developing new anti-oxidant and neuroprotective drugs with improved therapeutic potential. However, further investigations are required to (i) clarify GHSs molecular mechanisms of action, and (ii) whether their effects are mediated by the ghrelin receptor (GHS-R1a).

Future steps will be to (i) investigate EVs-derived from SH-SY5Y $SOD1^{G93A}$ cells effects in terms of microglial activation and polarization, and (ii) evaluate the effects of GHSs in the modulation of inflammation.

REFERENCES

1. Rowland LP, Shneider NA. Amyotrophic Lateral Sclerosis [Internet]. http://dx.doi.org/10.1056/NEJM200105313442207. Massachusetts Medical Society; 2009 [citato 13 settembre 2021]. Disponibile su: https://www.nejm.org/doi/10.1056/NEJM200105313442207

2. Carrera-Juliá S, Moreno ML, Barrios C, de la Rubia Ortí JE, Drehmer E. Antioxidant Alternatives in the Treatment of Amyotrophic Lateral Sclerosis: A Comprehensive Review. Front Physiol [Internet]. 6 febbraio 2020 [citato 24 maggio 2021];11. Disponibile su: https://www.ncbi.nlm.nih.gov/pmc/articles/PMC7016185/

3. Masrori P, Van Damme P. Amyotrophic lateral sclerosis: a clinical review. Eur J Neurol. ottobre 2020;27(10):1918–29.

4. Chiò A, Logroscino G, Traynor B, Collins J, Simeone J, Goldstein L, et al. Global Epidemiology of Amyotrophic Lateral Sclerosis: a Systematic Review of the Published Literature. Neuroepidemiology. 2013;41(2):118–30.

5. Brotman RG, Moreno-Escobar MC, Joseph J, Pawar G. Amyotrophic Lateral Sclerosis. In: StatPearls [Internet]. Treasure Island (FL): StatPearls Publishing; 2021 [citato 24 maggio 2021]. Disponibile su: http://www.ncbi.nlm.nih.gov/books/NBK556151/

6. Armon C. Smoking may be considered an established risk factor for sporadic ALS. Neurology. 17 novembre 2009;73(20):1693–8.

7. Kuraszkiewicz B, Goszczyńska H, Podsiadły-Marczykowska T, Piotrkiewicz M, Andersen P, Gromicho M, et al. Potential Preventive Strategies for Amyotrophic Lateral Sclerosis. Front Neurosci [Internet]. 26 maggio 2020 [citato 24 maggio 2021];14. Disponibile su: https://www.ncbi.nlm.nih.gov/pmc/articles/PMC7264408/

8. Zarei S, Carr K, Reiley L, Diaz K, Guerra O, Altamirano PF, et al. A comprehensive review of amyotrophic lateral sclerosis. Surg Neurol Int [Internet]. 16 novembre 2015 [citato 24 maggio 2021];6. Disponibile su: https://www.ncbi.nlm.nih.gov/pmc/articles/PMC4653353/

9. Logroscino G, Traynor BJ, Hardiman O, Chiò A, Mitchell D, Swingler RJ, et al. Incidence of Amyotrophic Lateral Sclerosis in Europe. J Neurol Neurosurg Psychiatry. aprile 2010;81(4):385–90.

10. Byrne S, Walsh C, Lynch C, Bede P, Elamin M, Kenna K, et al. Rate of familial amyotrophic lateral sclerosis: a systematic review and meta-analysis. Journal of Neurology, Neurosurgery & Psychiatry. 1 giugno 2011;82(6):623–7.

11. de Jong S, Huisman M, Sutedja N, van der Kooi A, de Visser M, Schelhaas J, et al. Endogenous female reproductive hormones and the risk of amyotrophic lateral sclerosis. J Neurol. febbraio 2013;260(2):507–12.

12. Marin B, Boumédiene F, Logroscino G, Couratier P, Babron M-C, Leutenegger AL, et al. Variation in worldwide incidence of amyotrophic lateral sclerosis: a meta-analysis. Int J Epidemiol. febbraio 2017;46(1):57–74.

13. Turner MR, Bowser R, Bruijn L, Dupuis L, Ludolph A, McGrath M, et al. Mechanisms, models and biomarkers in amyotrophic lateral sclerosis. Amyotroph Lateral Scler Frontotemporal Degener. maggio 2013;14 Suppl 1:19–32.

14. Blecher R, Elliott MA, Yilmaz E, Dettori JR, Oskouian RJ, Patel A, et al. Contact Sports as a Risk Factor for Amyotrophic Lateral Sclerosis: A Systematic Review. Global Spine J. febbraio 2019;9(1):104–18.

15. Mejzini R, Flynn LL, Pitout IL, Fletcher S, Wilton SD, Akkari PA. ALS Genetics, Mechanisms, and Therapeutics: Where Are We Now? Front Neurosci [Internet]. 6 dicembre 2019 [citato 24 maggio 2021];13. Disponibile su: https://www.ncbi.nlm.nih.gov/pmc/articles/PMC6909825/

16. Ferraiuolo L, Kirby J, Grierson AJ, Sendtner M, Shaw PJ. Molecular pathways of motor neuron injury in amyotrophic lateral sclerosis. Nature Reviews Neurology. novembre 2011;7(11):616–30.

17. Kiernan MC, Vucic S, Cheah BC, Turner MR, Eisen A, Hardiman O, et al. Amyotrophic lateral sclerosis. The Lancet. 12 marzo 2011;377(9769):942–55.

18. Bendotti C, Carrì MT. Lessons from models of SOD1-linked familial ALS. Trends in Molecular Medicine. 1 agosto 2004;10(8):393–400.

19. Bonafede R, Mariotti R. ALS Pathogenesis and Therapeutic Approaches: The Role of Mesenchymal Stem Cells and Extracellular Vesicles. Front Cell Neurosci [Internet]. 21 marzo 2017 [citato 25 maggio 2021];11. Disponibile su: https://www.ncbi.nlm.nih.gov/pmc/articles/PMC5359305/

20. Heath PR, Shaw PJ. Update on the glutamatergic neurotransmitter system and the role of excitotoxicity in amyotrophic lateral sclerosis. Muscle & Nerve. 2002;26(4):438–58.

21. Shigeri Y, Seal RP, Shimamoto K. Molecular pharmacology of glutamate transporters, EAATs and VGLUTs. Brain Research Reviews. 1 luglio 2004;45(3):250–65.

22. Vucic S, Rothstein JD, Kiernan MC. Advances in treating amyotrophic lateral sclerosis: insights from pathophysiological studies. Trends in Neurosciences. 1 agosto 2014;37(8):433–42.

23. Rothstein JD. Excitotoxic mechanisms in the pathogenesis of amyotrophic lateral sclerosis. Adv Neurol. 1995;68:7–20; discussion 21-27.

24. Lin C-LG, Bristol LA, Jin L, Dykes-Hoberg M, Crawford T, Clawson L, et al. Aberrant RNA Processing in a Neurodegenerative Disease: the Cause for Absent EAAT2, a Glutamate Transporter, in Amyotrophic Lateral Sclerosis. Neuron. 1 marzo 1998;20(3):589–602.

25. Goodall EF, Morrison KE. Amyotrophic lateral sclerosis (motor neuron disease): proposed mechanisms and pathways to treatment. Expert Reviews in Molecular Medicine. maggio 2006;8(11):1–22.

26. Matyja E, Taraszewska A, Nagańska E, Rafałowska J, Gębarowska J. Original article
Astroglial alterations in amyotrophic lateral sclerosis (ALS) model of slow glutamate excitotoxicity in vitro. Folia Neuropathol. 2006;44(3):183–90.

27. Guo H, Lai L, Butchbach MER, Stockinger MP, Shan X, Bishop GA, et al. Increased expression of the glial glutamate transporter EAAT2 modulates excitotoxicity and delays the onset but not the outcome of ALS in mice. Human Molecular Genetics. 1 ottobre 2003;12(19):2519–32.

28. Van Den Bosch L, Van Damme P, Vleminckx V, Van Houtte E, Lemmens G, Missiaen L, et al. An α-mercaptoacrylic acid derivative (PD150606) inhibits selective motor neuron death via inhibition of kainate-induced Ca2+ influx and not via calpain inhibition. Neuropharmacology. 1 aprile 2002;42(5):706–13.

29. Kawahara Y, Ito K, Sun H, Aizawa H, Kanazawa I, Kwak S. RNA editing and death of motor neurons. Nature. febbraio 2004;427(6977):801–801.

30. Forsberg K, Andersen PM, Marklund SL, Brännström T. Glial nuclear aggregates of superoxide dismutase-1 are regularly present in patients with amyotrophic lateral sclerosis. Acta Neuropathol. 2011;121(5):623–34.

31. Kiselyov K, Muallem S. ROS and intracellular ion channels. Cell Calcium. agosto 2016;60(2):108–14.

32. Bannwarth S, Ait-El-Mkadem S, Chaussenot A, Genin EC, Lacas-Gervais S, Fragaki K, et al. A mitochondrial origin for frontotemporal dementia and amyotrophic lateral sclerosis through CHCHD10 involvement. Brain. agosto 2014;137(8):2329–45.

33. Granatiero V, Manfredi G. Mitochondrial Transport and Turnover in the Pathogenesis of Amyotrophic Lateral Sclerosis. Biology (Basel) [Internet]. 11 maggio 2019 [citato 25 maggio 2021];8(2). Disponibile su: https://www.ncbi.nlm.nih.gov/pmc/articles/PMC6627920/

34. Lewinski F von, Keller BU. Ca2+, mitochondria and selective motoneuron vulnerability: implications for ALS. Trends in Neurosciences. 1 settembre 2005;28(9):494–500.

35. Cozzolino M, Rossi S, Mirra A, Carrì MT. Mitochondrial dynamism and the pathogenesis of Amyotrophic Lateral Sclerosis. Front Cell Neurosci [Internet]. 10 febbraio 2015 [citato 25 maggio 2021];9. Disponibile su: https://www.ncbi.nlm.nih.gov/pmc/articles/PMC4322717/

36. Echaniz-Laguna A, Zoll J, Ribera F, Tranchant C, Warter J-M, Lonsdorfer J, et al. Mitochondrial respiratory chain function in skeletal muscle of ALS patients. Annals of Neurology. 2002;52(5):623–7.

37. Jaiswal MK. Selective vulnerability of motoneuron and perturbed mitochondrial calcium homeostasis in amyotrophic lateral sclerosis: implications for motoneurons specific calcium dysregulation. Mol Cell Ther [Internet]. 14 agosto 2014 [citato 25 maggio 2021];2. Disponibile su: https://www.ncbi.nlm.nih.gov/pmc/articles/PMC4452055/

38. Pasinelli P, Brown RH. Molecular biology of amyotrophic lateral sclerosis: insights from genetics. Nature Reviews Neuroscience. settembre 2006;7(9):710–23.

39. Boillée S, Vande Velde C, Cleveland DW. ALS: A Disease of Motor Neurons and Their Nonneuronal Neighbors. Neuron. 5 ottobre 2006;52(1):39–59.

40. Chiurchiù V, Orlacchio A, Maccarrone M. Is Modulation of Oxidative Stress an Answer? The State of the Art of Redox Therapeutic Actions in Neurodegenerative Diseases. Oxid Med

Cell Longev [Internet]. 2016 [citato 25 maggio 2021];2016. Disponibile su: https://www.ncbi.nlm.nih.gov/pmc/articles/PMC4736210/

41. Singh AK, Singh S, Tripathi VK, Bissoyi A, Garg G, Rizvi SI. Rapamycin Confers Neuroprotection Against Aging-Induced Oxidative Stress, Mitochondrial Dysfunction, and Neurodegeneration in Old Rats Through Activation of Autophagy. Rejuvenation Res. febbraio 2019;22(1):60–70.

42. Carrì MT, Valle C, Bozzo F, Cozzolino M. Oxidative stress and mitochondrial damage: importance in non-SOD1 ALS. Front Cell Neurosci [Internet]. 17 febbraio 2015 [citato 25 maggio 2021];9. Disponibile su: https://www.ncbi.nlm.nih.gov/pmc/articles/PMC4330888/

43. Bozzo F, Mirra A, Carrì MT. Oxidative stress and mitochondrial damage in the pathogenesis of ALS: New perspectives. Neuroscience Letters. 1 gennaio 2017;636:3–8.

44. D'Amico E, Factor-Litvak P, Santella RM, Mitsumoto H. Clinical Perspective of Oxidative Stress in Sporadic ALS. Free Radic Biol Med [Internet]. dicembre 2013 [citato 25 maggio 2021];65. Disponibile su: https://www.ncbi.nlm.nih.gov/pmc/articles/PMC3859834/

45. Wijesekera LC, Leigh PN. Amyotrophic lateral sclerosis. Orphanet J Rare Dis. 3 febbraio 2009;4:3.

46. Okamoto K, Mizuno Y, Fujita Y. Bunina bodies in amyotrophic lateral sclerosis. Neuropathology. aprile 2008;28(2):109–15.

47. Prudencio M, Hart PJ, Borchelt DR, Andersen PM. Variation in aggregation propensities among ALS-associated variants of SOD1: correlation to human disease. Hum Mol Genet. 1 settembre 2009;18(17):3217–26.

48. Vance C, Rogelj B, Hortobágyi T, De Vos KJ, Nishimura AL, Sreedharan J, et al. Mutations in FUS, an RNA processing protein, cause familial amyotrophic lateral sclerosis type 6. Science. 27 febbraio 2009;323(5918):1208–11.

49. Lagier-Tourenne C, Polymenidou M, Cleveland DW. TDP-43 and FUS/TLS: emerging roles in RNA processing and neurodegeneration. Hum Mol Genet. 15 aprile 2010;19(R1):R46-64.

50. Grad LI, Yerbury JJ, Turner BJ, Guest WC, Pokrishevsky E, O'Neill MA, et al. Intercellular propagated misfolding of wild-type Cu/Zn superoxide dismutase occurs via exosome-dependent and -independent mechanisms. Proc Natl Acad Sci U S A. 4 marzo 2014;111(9):3620–5.

51. De Vos KJ, Hafezparast M. Neurobiology of axonal transport defects in motor neuron diseases: Opportunities for translational research? Neurobiol Dis. settembre 2017;105:283–99.

52. Corbo M, Hays AP. Peripherin and Neurofilament Protein Coexist in Spinal Spheroids of Motor Neuron Disease. Journal of Neuropathology & Experimental Neurology. 1 settembre 1992;51(5):531–7.

53. Ikenaka K, Katsuno M, Kawai K, Ishigaki S, Tanaka F, Sobue G. Disruption of Axonal Transport in Motor Neuron Diseases. Int J Mol Sci. 23 gennaio 2012;13(1):1225–38.

54. Magrané J, Cortez C, Gan W-B, Manfredi G. Abnormal mitochondrial transport and morphology are common pathological denominators in SOD1 and TDP43 ALS mouse models. Hum Mol Genet. 15 marzo 2014;23(6):1413–24.

55. Bozzoni V, Pansarasa O, Diamanti L, Nosari G, Cereda C, Ceroni M. Amyotrophic lateral sclerosis and environmental factors. Funct Neurol. 30 marzo 2016;31(1):7–19.

56. Kamel F, Umbach DM, Munsat TL, Shefner JM, Hu H, Sandler DP. Lead exposure and amyotrophic lateral sclerosis. Epidemiology. maggio 2002;13(3):311–9.

57. Trojsi F, Monsurrò MR, Tedeschi G. Exposure to environmental toxicants and pathogenesis of amyotrophic lateral sclerosis: state of the art and research perspectives. Int J Mol Sci. 24 luglio 2013;14(8):15286–311.

58. Capozzella A, Sacco C, Chighine A, Loreti B, Scala B, Casale T, et al. Work related etiology of amyotrophic lateral sclerosis (ALS): a meta-analysis. Ann Ig. ottobre 2014;26(5):456–72.

59. Boylan K. Familial ALS. Neurol Clin. novembre 2015;33(4):807–30.

60. Pang SY-Y, Hsu JS, Teo K-C, Li Y, Kung MHW, Cheah KSE, et al. Burden of rare variants in ALS genes influences survival in familial and sporadic ALS. Neurobiol Aging. ottobre 2017;58:238.e9-238.e15.

61. Zelko IN, Mariani TJ, Folz RJ. Superoxide dismutase multigene family: a comparison of the CuZn-SOD (SOD1), Mn-SOD (SOD2), and EC-SOD (SOD3) gene structures, evolution, and expression. Free Radical Biology and Medicine. 1 agosto 2002;33(3):337–49.

62. Rosen DR, Siddique T, Patterson D, Figlewicz DA, Sapp P, Hentati A, et al. Mutations in Cu/Zn superoxide dismutase gene are associated with familial amyotrophic lateral sclerosis. Nature. 4 marzo 1993;362(6415):59–62.

63. Kaur SJ, McKeown SR, Rashid S. Mutant SOD1 mediated pathogenesis of Amyotrophic Lateral Sclerosis. Gene. 15 febbraio 2016;577(2):109–18.

64. Hand CK, Rouleau GA. Familial amyotrophic lateral sclerosis. Muscle Nerve. febbraio 2002;25(2):135–59.

65. Al-Chalabi A, Andersen PM, Chioza B, Shaw C, Sham PC, Robberecht W, et al. Recessive amyotrophic lateral sclerosis families with the D90A SOD1 mutation share a common founder: evidence for a linked protective factor. Hum Mol Genet. dicembre 1998;7(13):2045–50.

66. Valentine JS, Hart PJ. Misfolded CuZnSOD and amyotrophic lateral sclerosis. Proc Natl Acad Sci U S A. 1 aprile 2003;100(7):3617–22.

67. Lopate G, Baloh RH, Al-Lozi MT, Miller TM, Fernandes Filho JA, Ni O, et al. Familial ALS with extreme phenotypic variability due to the I113T SOD1 mutation. Amyotroph Lateral Scler. 2010;11(1–2):232–6.

68. Carrì MT, Ferri A, Battistoni A, Famhy L, Gabbianelli R, Poccia F, et al. Expression of a Cu,Zn superoxide dismutase typical of familial amyotrophic lateral sclerosis induces mitochondrial alteration and increase of cytosolic Ca2+ concentration in transfected neuroblastoma SH-SY5Y cells. FEBS Lett. 8 settembre 1997;414(2):365–8.

69. Karch CM, Prudencio M, Winkler DD, Hart PJ, Borchelt DR. Role of mutant SOD1 disulfide oxidation and aggregation in the pathogenesis of familial ALS. Proc Natl Acad Sci U S A. 12 maggio 2009;106(19):7774–9.

70. Martin LJ, Price AC, Kaiser A, Shaikh AY, Liu Z. Mechanisms for neuronal degeneration in amyotrophic lateral sclerosis and in models of motor neuron death (Review). Int J Mol Med. gennaio 2000;5(1):3–13.

71. Polkey MI, Lyall RA, Davidson AC, Leigh PN, Moxham J. Ethical and clinical issues in the use of home non-invasive mechanical ventilation for the palliation of breathlessness in motor neurone disease. Thorax. aprile 1999;54(4):367–71.

72. Vucic S, Kiernan MC. Abnormalities in cortical and peripheral excitability in flail arm variant amyotrophic lateral sclerosis. J Neurol Neurosurg Psychiatry. agosto 2007;78(8):849–52.

73. Rowland LP. Diagnosis of amyotrophic lateral sclerosis. J Neurol Sci. ottobre 1998;160 Suppl 1:S6-24.

74. Borasio GD. Palliative care in ALS: searching for the evidence base. Amyotroph Lateral Scler Other Motor Neuron Disord. marzo 2001;2 Suppl 1:S31-35.

75. Salajegheh M, Bryan WW, Dalakas MC. The challenge of diagnosing ALS in patients with prior poliomyelitis. Neurology. 26 settembre 2006;67(6):1078–9.

76. Chiò A, Logroscino G, Hardiman O, Swingler R, Mitchell D, Beghi E, et al. Prognostic factors in ALS: A critical review. Amyotroph Lateral Scler. dicembre 2009;10(5–6):310–23.

77. Beghi E, Chiò A, Couratier P, Esteban J, Hardiman O, Logroscino G, et al. The epidemiology and treatment of ALS: focus on the heterogeneity of the disease and critical appraisal of therapeutic trials. Amyotroph Lateral Scler. gennaio 2011;12(1):1–10.

78. Dubner R, Gold M. The neurobiology of pain. Proc Natl Acad Sci U S A. 6 luglio 1999;96(14):7627–30.

79. Handy CR, Krudy C, Boulis N, Federici T. Pain in amyotrophic lateral sclerosis: a neglected aspect of disease. Neurol Res Int. 2011;2011:403808.

80. Corcia P, Meininger V. Management of amyotrophic lateral sclerosis. Drugs. 2008;68(8):1037–48.

81. Talbot K. Another gene for ALS: mutations in sporadic cases and the rare variant hypothesis. Neurology. 13 ottobre 2009;73(15):1172–3.

82. EFNS Task Force on Diagnosis and Management of Amyotrophic Lateral Sclerosis:, Andersen PM, Abrahams S, Borasio GD, de Carvalho M, Chio A, et al. EFNS guidelines on the clinical management of amyotrophic lateral sclerosis (MALS)--revised report of an EFNS task force. Eur J Neurol. marzo 2012;19(3):360–75.

83. Al-Sarraj S, King A, Cleveland M, Pradat P-F, Corse A, Rothstein JD, et al. Mitochondrial abnormalities and low grade inflammation are present in the skeletal muscle of a minority of patients with amyotrophic lateral sclerosis; an observational myopathology study. Acta Neuropathol Commun. 14 dicembre 2014;2:165.

84. Brooks BR, Bushara K, Khan A, Hershberger J, Wheat JO, Belden D, et al. Functional magnetic resonance imaging (fMRI) clinical studies in ALS--paradigms, problems and promises. Amyotroph Lateral Scler Other Motor Neuron Disord. giugno 2000;1 Suppl 2:S23-32.

85. Hardiman O, van den Berg LH, Kiernan MC. Clinical diagnosis and management of amyotrophic lateral sclerosis. Nat Rev Neurol. 11 ottobre 2011;7(11):639–49.

86. Agosta F, Al-Chalabi A, Filippi M, Hardiman O, Kaji R, Meininger V, et al. The El Escorial criteria: strengths and weaknesses. Amyotroph Lateral Scler Frontotemporal Degener. marzo 2015;16(1–2):1–7.

87. Costa J, Swash M, de Carvalho M. Awaji criteria for the diagnosis of amyotrophic lateral sclerosis:a systematic review. Arch Neurol. novembre 2012;69(11):1410–6.

88. Rechtman L, Wagner L, Kaye W, Villanacci J. Updated Prevalence and Demographic Characteristics for ALS Cases in Texas, 2009–2011. South Med J. agosto 2015;108(8):483–6.

89. de Carvalho M, Swash M, Pinto S. Diaphragmatic Neurophysiology and Respiratory Markers in ALS. Front Neurol. 2019;10:143.

90. Bensimon G, Lacomblez L, Meininger V. A controlled trial of riluzole in amyotrophic lateral sclerosis. ALS/Riluzole Study Group. N Engl J Med. 3 marzo 1994;330(9):585–91.

91. Lacomblez L, Bensimon G, Leigh PN, Guillet P, Meininger V. Dose-ranging study of riluzole in amyotrophic lateral sclerosis. Amyotrophic Lateral Sclerosis/Riluzole Study Group II. Lancet. 25 maggio 1996;347(9013):1425–31.

92. Distad BJ, Meekins GD, Liou LL, Weiss MD, Carter GT, Miller RG. Drug therapy in amyotrophic lateral sclerosis. Phys Med Rehabil Clin N Am. agosto 2008;19(3):633–51, xi–xii.

93. Bellingham MC. A review of the neural mechanisms of action and clinical efficiency of riluzole in treating amyotrophic lateral sclerosis: what have we learned in the last decade? CNS Neurosci Ther. febbraio 2011;17(1):4–31.

94. Dyer AM, Smith A. Riluzole 5 mg/mL oral suspension: for optimized drug delivery in amyotrophic lateral sclerosis. Drug Des Devel Ther. 2017;11:59–64.

95. Schultz J. Disease-modifying treatment of amyotrophic lateral sclerosis. Am J Manag Care. agosto 2018;24(15 Suppl):S327–35.

96. Writing Group, Edaravone (MCI-186) ALS 19 Study Group. Safety and efficacy of edaravone in well defined patients with amyotrophic lateral sclerosis: a randomised, double-blind, placebo-controlled trial. Lancet Neurol. luglio 2017;16(7):505–12.

97. Ito H, Wate R, Zhang J, Ohnishi S, Kaneko S, Ito H, et al. Treatment with edaravone, initiated at symptom onset, slows motor decline and decreases SOD1 deposition in ALS mice. Exp Neurol. ottobre 2008;213(2):448–55.

98. Ahmadinejad F, Geir Møller S, Hashemzadeh-Chaleshtori M, Bidkhori G, Jami M-S. Molecular Mechanisms behind Free Radical Scavengers Function against Oxidative Stress. Antioxidants (Basel). 10 luglio 2017;6(3).

99. Hardiman O, van den Berg LH. Edaravone: a new treatment for ALS on the horizon? Lancet Neurol. luglio 2017;16(7):490–1.

100. Brooks BR, Jorgenson JA, Newhouse BJ, Shefner JM, Agnese W. Edaravone in the treatment of amyotrophic lateral sclerosis: efficacy and access to therapy - a roundtable discussion. Am J Manag Care. aprile 2018;24(9 Suppl):S175–86.

101. Abe K, Aoki M, Tsuji S, Itoyama Y, Sobue G, Togo M, et al. Safety and efficacy of edaravone in well defined patients with amyotrophic lateral sclerosis: a randomised, double-blind, placebo-controlled trial. The Lancet Neurology. 1 luglio 2017;16(7):505–12.

102. Miller RG, Jackson CE, Kasarskis EJ, England JD, Forshew D, Johnston W, et al. Practice parameter update: the care of the patient with amyotrophic lateral sclerosis: drug, nutritional, and respiratory therapies (an evidence-based review): report of the Quality Standards Subcommittee of the American Academy of Neurology. Neurology. 13 ottobre 2009;73(15):1218–26.

103. Kasarskis EJ, Mendiondo MS, Wells S, Malguizo MS, Thompson M, Healey M, et al. The ALS Nutrition/NIPPV Study: design, feasibility, and initial results. Amyotroph Lateral Scler. gennaio 2011;12(1):17–25.

104. Greenwood DI. Nutrition management of amyotrophic lateral sclerosis. Nutr Clin Pract. giugno 2013;28(3):392–9.

105. Talbot K. Motor neurone disease. Postgrad Med J. settembre 2002;78(923):513–9.

106. Weiss MD, Macklin EA, Simmons Z, Knox AS, Greenblatt DJ, Atassi N, et al. A randomized trial of mexiletine in ALS: Safety and effects on muscle cramps and progression. Neurology. 19 aprile 2016;86(16):1474–81.

107. Rosenfeld J, Strong MJ. Challenges in the Understanding and Treatment of Amyotrophic Lateral Sclerosis/Motor Neuron Disease. Neurotherapeutics. aprile 2015;12(2):317–25.

108. Bourke SC, Gibson GJ. Non-invasive ventilation in ALS: current practice and future role. Amyotroph Lateral Scler Other Motor Neuron Disord. giugno 2004;5(2):67–71.

109. Yamanaka K, Komine O. The multi-dimensional roles of astrocytes in ALS. Neurosci Res. gennaio 2018;126:31–8.

110. Filipi T, Hermanova Z, Tureckova J, Vanatko O, Anderova AM. Glial Cells-The Strategic Targets in Amyotrophic Lateral Sclerosis Treatment. J Clin Med. 18 gennaio 2020;9(1).

111. Lepore AC, Rauck B, Dejea C, Pardo AC, Rao MS, Rothstein JD, et al. Focal transplantation-based astrocyte replacement is neuroprotective in a model of motor neuron disease. Nat Neurosci. novembre 2008;11(11):1294–301.

112. Rizzo F, Riboldi G, Salani S, Nizzardo M, Simone C, Corti S, et al. Cellular therapy to target neuroinflammation in amyotrophic lateral sclerosis. Cell Mol Life Sci. marzo 2014;71(6):999–1015.

113. Baumert B, Sobuś A, Gołąb-Janowska M, Paczkowska E, Łuczkowska K, Rogińska D, et al. Repeated Application of Autologous Bone Marrow-Derived Lineage-Negative Stem/Progenitor Cells-Focus on Immunological Pathways in Patients with ALS. Cells. 1 agosto 2020;9(8).

114. Nayak D, Roth TL, McGavern DB. Microglia Development and function. Annu Rev Immunol. 2014;32:367–402.

115. Tay TL, Savage JC, Hui CW, Bisht K, Tremblay M. Microglia across the lifespan: from origin to function in brain development, plasticity and cognition. J Physiol. 15 marzo 2017;595(6):1929–45.

116. Cuadros MA, Martin C, Coltey P, Almendros A, Navascués J. First appearance, distribution, and origin of macrophages in the early development of the avian central nervous system. J Comp Neurol. 1 aprile 1993;330(1):113–29.

117. Alliot F, Godin I, Pessac B. Microglia derive from progenitors, originating from the yolk sac, and which proliferate in the brain. Brain Res Dev Brain Res. 18 novembre 1999;117(2):145–52.

118. Goldmann T, Prinz M. Role of Microglia in CNS Autoimmunity. Clin Dev Immunol. 2013;2013:208093.

119. Wirenfeldt M, Dissing-Olesen L, Anne Babcock A, Nielsen M, Meldgaard M, Zimmer J, et al. Population control of resident and immigrant microglia by mitosis and apoptosis. Am J Pathol. agosto 2007;171(2):617–31.

120. Walton NM, Sutter BM, Laywell ED, Levkoff LH, Kearns SM, Marshall GP, et al. Microglia instruct subventricular zone neurogenesis. Glia. dicembre 2006;54(8):815–25.

121. Luo X-G, Chen S-D. The changing phenotype of microglia from homeostasis to disease. Transl Neurodegener. 24 aprile 2012;1(1):9.

122. Kettenmann H, Kirchhoff F, Verkhratsky A. Microglia: new roles for the synaptic stripper. Neuron. 9 gennaio 2013;77(1):10–8.

123. Nimmerjahn A, Bergles DE. Large-scale recording of astrocyte activity. Curr Opin Neurobiol. giugno 2015;32:95–106.

124. Du L, Zhang Y, Chen Y, Zhu J, Yang Y, Zhang H-L. Role of Microglia in Neurological Disorders and Their Potentials as a Therapeutic Target. Mol Neurobiol. dicembre 2017;54(10):7567–84.

125. Colton CA. Heterogeneity of microglial activation in the innate immune response in the brain. J Neuroimmune Pharmacol. dicembre 2009;4(4):399–418.

126. Chhor V, Le Charpentier T, Lebon S, Oré M-V, Celador IL, Josserand J, et al. Characterization of phenotype markers and neuronotoxic potential of polarised primary microglia in vitro. Brain Behav Immun. agosto 2013;32:70–85.

127. Kigerl KA, de Rivero Vaccari JP, Dietrich WD, Popovich PG, Keane RW. Pattern recognition receptors and central nervous system repair. Exp Neurol. agosto 2014;258:5–16.

128. Tang Y, Le W. Differential Roles of M1 and M2 Microglia in Neurodegenerative Diseases. Mol Neurobiol. marzo 2016;53(2):1181–94.

129. Mantovani A, Sozzani S, Locati M, Allavena P, Sica A. Macrophage polarization: tumor-associated macrophages as a paradigm for polarized M2 mononuclear phagocytes. Trends Immunol. novembre 2002;23(11):549–55.

130. Hooten KG, Beers DR, Zhao W, Appel SH. Protective and Toxic Neuroinflammation in Amyotrophic Lateral Sclerosis. Neurotherapeutics. aprile 2015;12(2):364–75.

131. Hammond TR, Marsh SE, Stevens B. Immune Signaling in Neurodegeneration. Immunity. 16 aprile 2019;50(4):955–74.

132. Brites D, Fernandes A. Neuroinflammation and Depression: Microglia Activation, Extracellular Microvesicles and microRNA Dysregulation. Front Cell Neurosci. 2015;9:476.

133. Brites D, Vaz AR. Microglia centered pathogenesis in ALS: insights in cell interconnectivity. Front Cell Neurosci. 2014;8:117.

134. Geloso MC, Corvino V, Marchese E, Serrano A, Michetti F, D'Ambrosi N. The Dual Role of Microglia in ALS: Mechanisms and Therapeutic Approaches. Front Aging Neurosci. 25 luglio 2017;9:242.

135. McCombe PA, Lee JD, Woodruff TM, Henderson RD. The Peripheral Immune System and Amyotrophic Lateral Sclerosis. Front Neurol. 2020;11:279.

136. Beers DR, Appel SH. Immune dysregulation in amyotrophic lateral sclerosis: mechanisms and emerging therapies. Lancet Neurol. febbraio 2019;18(2):211–20.

137. Liu Z, Cheng X, Zhong S, Zhang X, Liu C, Liu F, et al. Peripheral and Central Nervous System Immune Response Crosstalk in Amyotrophic Lateral Sclerosis. Front Neurosci. 2020;14:575.

138. Zhao W, Beers DR, Hooten KG, Sieglaff DH, Zhang A, Kalyana-Sundaram S, et al. Characterization of Gene Expression Phenotype in Amyotrophic Lateral Sclerosis Monocytes. JAMA Neurol. 1 giugno 2017;74(6):677–85.

139. Zhao W, Beers DR, Henkel JS, Zhang W, Urushitani M, Julien J-P, et al. Extracellular mutant SOD1 induces microglial-mediated motoneuron injury. Glia. 15 gennaio 2010;58(2):231–43.

140. Gravel M, Béland L-C, Soucy G, Abdelhamid E, Rahimian R, Gravel C, et al. IL-10 Controls Early Microglial Phenotypes and Disease Onset in ALS Caused by Misfolded Superoxide Dismutase 1. J Neurosci. 20 gennaio 2016;36(3):1031–48.

141. D'Ambrosi N, Finocchi P, Apolloni S, Cozzolino M, Ferri A, Padovano V, et al. The proinflammatory action of microglial P2 receptors is enhanced in SOD1 models for amyotrophic lateral sclerosis. J Immunol. 1 ottobre 2009;183(7):4648–56.

142. Chiu IM, Phatnani H, Kuligowski M, Tapia JC, Carrasco MA, Zhang M, et al. Activation of innate and humoral immunity in the peripheral nervous system of ALS transgenic mice. Proc Natl Acad Sci U S A. 8 dicembre 2009;106(49):20960–5.

143. Graber DJ, Hickey WF, Harris BT. Progressive changes in microglia and macrophages in spinal cord and peripheral nerve in the transgenic rat model of amyotrophic lateral sclerosis. J Neuroinflammation. 28 gennaio 2010;7:8.

144. Van Dyke JM, Smit-Oistad IM, Macrander C, Krakora D, Meyer MG, Suzuki M. Macrophage-mediated inflammation and glial response in the skeletal muscle of a rat model of familial amyotrophic lateral sclerosis (ALS). Exp Neurol. marzo 2016;277:275–82.

145. Liao B, Zhao W, Beers DR, Henkel JS, Appel SH. Transformation from a neuroprotective to a neurotoxic microglial phenotype in a mouse model of ALS. Exp Neurol. settembre 2012;237(1):147–52.

146. Chiu IM, Morimoto ETA, Goodarzi H, Liao JT, O'Keeffe S, Phatnani HP, et al. A neurodegeneration-specific gene-expression signature of acutely isolated microglia from an amyotrophic lateral sclerosis mouse model. Cell Rep. 25 luglio 2013;4(2):385–401.

147. Lewis KE, Rasmussen AL, Bennett W, King A, West AK, Chung RS, et al. Microglia and motor neurons during disease progression in the SOD1G93A mouse model of amyotrophic lateral sclerosis: changes in arginase1 and inducible nitric oxide synthase. J Neuroinflammation. 23 marzo 2014;11:55.

148. Chiu IM, Chen A, Zheng Y, Kosaras B, Tsiftsoglou SA, Vartanian TK, et al. T lymphocytes potentiate endogenous neuroprotective inflammation in a mouse model of ALS. Proc Natl Acad Sci U S A. 18 novembre 2008;105(46):17913–8.

149. Kaspar BK, Lladó J, Sherkat N, Rothstein JD, Gage FH. Retrograde viral delivery of IGF-1 prolongs survival in a mouse ALS model. Science. 8 agosto 2003;301(5634):839–42.

150. Dodge JC, Treleaven CM, Fidler JA, Hester M, Haidet A, Handy C, et al. AAV4-mediated expression of IGF-1 and VEGF within cellular components of the ventricular system improves survival outcome in familial ALS mice. Mol Ther. dicembre 2010;18(12):2075–84.

151. Pan BT, Johnstone RM. Fate of the transferrin receptor during maturation of sheep reticulocytes in vitro: selective externalization of the receptor. Cell. luglio 1983;33(3):967–78.

152. Ciregia F, Urbani A, Palmisano G. Extracellular Vesicles in Brain Tumors and Neurodegenerative Diseases. Front Mol Neurosci. 2017;10:276.

153. Croese T, Furlan R. Extracellular vesicles in neurodegenerative diseases. Mol Aspects Med. aprile 2018;60:52–61.

154. Li D, Li Y-P, Li Y-X, Zhu X-H, Du X-G, Zhou M, et al. Effect of Regulatory Network of Exosomes and microRNAs on Neurodegenerative Diseases. Chin Med J (Engl). 20 settembre 2018;131(18):2216–25.

155. Théry C, Zitvogel L, Amigorena S. Exosomes: composition, biogenesis and function. Nat Rev Immunol. agosto 2002;2(8):569–79.

156. Crescitelli R, Lässer C, Szabó TG, Kittel A, Eldh M, Dianzani I, et al. Distinct RNA profiles in subpopulations of extracellular vesicles: apoptotic bodies, microvesicles and exosomes. J Extracell Vesicles. 2013;2.

157. Akers JC, Gonda D, Kim R, Carter BS, Chen CC. Biogenesis of extracellular vesicles (EV): exosomes, microvesicles, retrovirus-like vesicles, and apoptotic bodies. J Neurooncol. maggio 2013;113(1):1–11.

158. Mohan A, Agarwal S, Clauss M, Britt NS, Dhillon NK. Extracellular vesicles: novel communicators in lung diseases. Respir Res. 2020;21:175.

159. Biancone L, Bruno S, Deregibus MC, Tetta C, Camussi G. Therapeutic potential of mesenchymal stem cell-derived microvesicles. Nephrol Dial Transplant. agosto 2012;27(8):3037–42.

160. György B, Szabó TG, Pásztói M, Pál Z, Misják P, Aradi B, et al. Membrane vesicles, current state-of-the-art: emerging role of extracellular vesicles. Cell Mol Life Sci. agosto 2011;68(16):2667–88.

161. Abels ER, Breakefield XO. Introduction to Extracellular Vesicles: Biogenesis, RNA Cargo Selection, Content, Release, and Uptake. Cell Mol Neurobiol. aprile 2016;36(3):301–12.

162. Bucki R, Bachelot-Loza C, Zachowski A, Giraud F, Sulpice JC. Calcium induces phospholipid redistribution and microvesicle release in human erythrocyte membranes by independent pathways. Biochemistry. 3 novembre 1998;37(44):15383–91.

163. Raposo G, Stoorvogel W. Extracellular vesicles: exosomes, microvesicles, and friends. J Cell Biol. 18 febbraio 2013;200(4):373–83.

164. Yáñez-Mó M, Siljander PR-M, Andreu Z, Zavec AB, Borràs FE, Buzas EI, et al. Biological properties of extracellular vesicles and their physiological functions. J Extracell Vesicles. 2015;4:27066.

165. Ban LA, Shackel NA, McLennan SV. Extracellular Vesicles: A New Frontier in Biomarker Discovery for Non-Alcoholic Fatty Liver Disease. Int J Mol Sci. 14 marzo 2016;17(3):376.

166. Colombo M, Raposo G, Théry C. Biogenesis, Secretion, and Intercellular Interactions of Exosomes and Other Extracellular Vesicles. Annual Review of Cell and Developmental Biology. 2014;30(1):255–89.

167. Tauro BJ, Greening DW, Mathias RA, Ji H, Mathivanan S, Scott AM, et al. Comparison of ultracentrifugation, density gradient separation, and immunoaffinity capture methods for isolating human colon cancer cell line LIM1863-derived exosomes. Methods. febbraio 2012;56(2):293–304.

168. Wubbolts R, Leckie RS, Veenhuizen PTM, Schwarzmann G, Möbius W, Hoernschemeyer J, et al. Proteomic and biochemical analyses of human B cell-derived exosomes. Potential implications for their function and multivesicular body formation. J Biol Chem. 28 marzo 2003;278(13):10963–72.

169. Laulagnier K, Motta C, Hamdi S, Roy S, Fauvelle F, Pageaux J-F, et al. Mast cell- and dendritic cell-derived exosomes display a specific lipid composition and an unusual membrane organization. Biochem J. 15 maggio 2004;380(Pt 1):161–71.

170. Trajkovic K, Hsu C, Chiantia S, Rajendran L, Wenzel D, Wieland F, et al. Ceramide triggers budding of exosome vesicles into multivesicular endosomes. Science. 29 febbraio 2008;319(5867):1244–7.

171. Llorente A, Skotland T, Sylvänne T, Kauhanen D, Róg T, Orłowski A, et al. Molecular lipidomics of exosomes released by PC-3 prostate cancer cells. Biochim Biophys Acta. luglio 2013;1831(7):1302–9.

172. Ikonen E. Roles of lipid rafts in membrane transport. Curr Opin Cell Biol. agosto 2001;13(4):470–7.

173. Valadi H, Ekström K, Bossios A, Sjöstrand M, Lee JJ, Lötvall JO. Exosome-mediated transfer of mRNAs and microRNAs is a novel mechanism of genetic exchange between cells. Nat Cell Biol. giugno 2007;9(6):654–9.

174. Sung BH, Ketova T, Hoshino D, Zijlstra A, Weaver AM. Directional cell movement through tissues is controlled by exosome secretion. Nat Commun. 13 maggio 2015;6:7164.

175. Lai FW, Lichty BD, Bowdish DME. Microvesicles: ubiquitous contributors to infection and immunity. J Leukoc Biol. febbraio 2015;97(2):237–45.

176. Antonucci F, Turola E, Riganti L, Caleo M, Gabrielli M, Perrotta C, et al. Microvesicles released from microglia stimulate synaptic activity via enhanced sphingolipid metabolism. EMBO J. 7 marzo 2012;31(5):1231–40.

177. Frohlich KM, Hua Z, Quayle AJ, Wang J, Lewis ME, Chou C, et al. Membrane vesicle production by Chlamydia trachomatis as an adaptive response. Front Cell Infect Microbiol. 2014;4:73.

178. Basso M, Pozzi S, Tortarolo M, Fiordaliso F, Bisighini C, Pasetto L, et al. Mutant copper-zinc superoxide dismutase (SOD1) induces protein secretion pathway alterations and exosome release in astrocytes: implications for disease spreading and motor neuron pathology in amyotrophic lateral sclerosis. J Biol Chem. 31 maggio 2013;288(22):15699–711.

179. Gomes C, Keller S, Altevogt P, Costa J. Evidence for secretion of Cu,Zn superoxide dismutase via exosomes from a cell model of amyotrophic lateral sclerosis. Neurosci Lett. 20 novembre 2007;428(1):43–6.

180. Pinto S, Cunha C, Barbosa M, Vaz AR, Brites D. Exosomes from NSC-34 Cells Transfected with hSOD1-G93A Are Enriched in miR-124 and Drive Alterations in Microglia Phenotype. Front Neurosci. 2017;11:273.

181. Zhuang X, Xiang X, Grizzle W, Sun D, Zhang S, Axtell RC, et al. Treatment of brain inflammatory diseases by delivering exosome encapsulated anti-inflammatory drugs from the nasal region to the brain. Mol Ther. ottobre 2011;19(10):1769–79.

182. Pusic AD, Pusic KM, Kraig RP. What are exosomes and how can they be used in multiple sclerosis therapy? Expert Rev Neurother. aprile 2014;14(4):353–5.

183. Gao Z-S, Zhang C-J, Xia N, Tian H, Li D-Y, Lin J-Q, et al. Berberine-loaded M2 macrophage-derived exosomes for spinal cord injury therapy. Acta Biomater. maggio 2021;126:211–23.

184. Zhang B, Lin F, Dong J, Liu J, Ding Z, Xu J. Peripheral Macrophage-derived Exosomes promote repair after Spinal Cord Injury by inducing Local Anti-inflammatory type Microglial Polarization via Increasing Autophagy. Int J Biol Sci. 30 marzo 2021;17(5):1339–52.

185. Ngo ST, Wang H, Henderson RD, Bowers C, Steyn FJ. Ghrelin as a treatment for amyotrophic lateral sclerosis. J Neuroendocrinol [Internet]. 29 gennaio 2021 [citato 14 luglio 2021]; Disponibile su: https://onlinelibrary.wiley.com/doi/10.1111/jne.12938

186. Bowers CY, Momany F, Reynolods GA. In vitro and in vivo activity of a small synthetic peptide with potent GH releasing activity. 1982;P. 205.

187. Howard AD, Feighner SD, Cully DF, Arena JP, Liberator PA, Rosenblum CI, et al. A Receptor in Pituitary and Hypothalamus That Functions in Growth Hormone Release. Science. 16 agosto 1996;273(5277):974–7.

188. Lengyel AMJ. From growth hormone-releasing peptides to ghrelin: discovery of new modulators of GH secretion. Arq Bras Endocrinol Metabol. febbraio 2006;50(1):17–24.

189. Reich N, Hölscher C. Acylated Ghrelin as a Multi-Targeted Therapy for Alzheimer's and Parkinson's Disease. Front Neurosci [Internet]. 2020 [citato 30 luglio 2021];0. Disponibile su: https://www.frontiersin.org/articles/10.3389/fnins.2020.614828/full

190. Bresciani E, Rizzi L, Coco S, Molteni L, Meanti R, Locatelli V, et al. Growth Hormone Secretagogues and the Regulation of Calcium Signaling in Muscle. Int J Mol Sci. 5 settembre 2019;20(18).

191. Frago LM, Pañeda C, Dickson SL, Hewson AK, Argente J, Chowen JA. Growth hormone (GH) and GH-releasing peptide-6 increase brain insulin-like growth factor-I expression and activate intracellular signaling pathways involved in neuroprotection. Endocrinology. ottobre 2002;143(10):4113–22.

192. Savine R, Sönksen P. Growth hormone - hormone replacement for the somatopause? Horm Res. 2000;53 Suppl 3:37–41.

193. Morselli LL, Bongioanni P, Genovesi M, Licitra R, Rossi B, Murri L, et al. Growth hormone secretion is impaired in amyotrophic lateral sclerosis. Clin Endocrinol (Oxf). settembre 2006;65(3):385–8.

194. Tollet-Egnell P, Flores-Morales A, Ståhlberg N, Malek RL, Lee N, Norstedt G. Gene expression profile of the aging process in rat liver: normalizing effects of growth hormone replacement. Mol Endocrinol. febbraio 2001;15(2):308–18.

195. Tresguerres JAF, Kireev R, Tresguerres AF, Borras C, Vara E, Ariznavarreta C. Molecular mechanisms involved in the hormonal prevention of aging in the rat. J Steroid Biochem Mol Biol. febbraio 2008;108(3–5):318–26.

196. Pradhan G, Samson SL, Sun Y. Ghrelin: much more than a hunger hormone. Curr Opin Clin Nutr Metab Care. novembre 2013;16(6):619–24.

197. Steinman J, DeBoer MD. Treatment of cachexia: melanocortin and ghrelin interventions. Vitam Horm. 2013;92:197–242.

198. Vestergaard ET, Krag MB, Poulsen MM, Pedersen SB, Moller N, Jorgensen JOL, et al. Ghrelin- and GH-induced insulin resistance: no association with retinol-binding protein-4. Endocr Connect. 1 giugno 2013;2(2):96–103.

199. Torres Aleman I. Role of insulin-like growth factors in neuronal plasticity and neuroprotection. Adv Exp Med Biol. 2005;567:243–58.

200. Pellecchia MT, Pivonello R, Longo K, Manfredi M, Tessitore A, Amboni M, et al. Multiple system atrophy is associated with changes in peripheral insulin-like growth factor system. Mov Disord. 15 novembre 2010;25(15):2621–6.

201. Callaghan B, Furness JB. Novel and conventional receptors for ghrelin, desacyl-ghrelin, and pharmacologically related compounds. Pharmacol Rev. ottobre 2014;66(4):984–1001.

202. Gnanapavan S, Kola B, Bustin SA, Morris DG, McGee P, Fairclough P, et al. The tissue distribution of the mRNA of ghrelin and subtypes of its receptor, GHS-R, in humans. J Clin Endocrinol Metab. giugno 2002;87(6):2988.

203. Burdyga G, Varro A, Dimaline R, Thompson DG, Dockray GJ. Ghrelin receptors in rat and human nodose ganglia: putative role in regulating CB-1 and MCH receptor abundance. Am J Physiol Gastrointest Liver Physiol. giugno 2006;290(6):G1289-1297.

204. Lee J, Lim E, Kim Y, Li E, Park S. Ghrelin attenuates kainic acid-induced neuronal cell death in the mouse hippocampus. J Endocrinol. giugno 2010;205(3):263–70.

205. Lee S, Kim Y, Li E, Park S. Ghrelin protects spinal cord motoneurons against chronic glutamate excitotoxicity by inhibiting microglial activation. Korean J Physiol Pharmacol. febbraio 2012;16(1):43–8.

206. Jiao Q, Du X, Li Y, Gong B, Shi L, Tang T, et al. The neurological effects of ghrelin in brain diseases: Beyond metabolic functions. Neurosci Biobehav Rev. febbraio 2017;73:98–111.

207. Ahmed RM, Phan K, Highton-Williamson E, Strikwerda-Brown C, Caga J, Ramsey E, et al. Eating peptides: biomarkers of neurodegeneration in amyotrophic lateral sclerosis and frontotemporal dementia. Ann Clin Transl Neurol. 31 gennaio 2019;6(3):486–95.

208. Rhea EM, Salameh TS, Gray S, Niu J, Banks WA, Tong J. Ghrelin transport across the blood-brain barrier can occur independently of the growth hormone secretagogue receptor. Mol Metab. dicembre 2018;18:88–96.

209. Meanti R, Rizzi L, Bresciani E, Molteni L, Locatelli V, Coco S, et al. Hexarelin Modulation of MAPK and PI3K/Akt Pathways in Neuro-2A Cells Inhibits Hydrogen Peroxide-Induced Apoptotic Toxicity. Pharmaceuticals (Basel). 8 maggio 2021;14(5):444.

210. Chung H, Kim E, Lee DH, Seo S, Ju S, Lee D, et al. Ghrelin Inhibits Apoptosis in Hypothalamic Neuronal Cells during Oxygen-Glucose Deprivation. Endocrinology. 1 gennaio 2007;148(1):148–59.

211. Hwang S, Moon M, Kim S, Hwang L, Ahn KJ, Park S. Neuroprotective Effect of Ghrelin Is Associated with Decreased Expression of Prostate Apoptosis Response-4. Endocr J. 2009;56(4):609–17.

212. Morgan AH, Rees DJ, Andrews ZB, Davies JS. Ghrelin mediated neuroprotection - A possible therapy for Parkinson's disease? Neuropharmacology. 1 luglio 2018;136(Pt B):317–26.

213. Moon M, Kim HG, Hwang L, Seo J-H, Kim S, Hwang S, et al. Neuroprotective Effect of Ghrelin in the 1-Methyl-4-Phenyl-1,2,3,6-Tetrahydropyridine Mouse Model of Parkinson's Disease by Blocking Microglial Activation. Neurotox Res. maggio 2009;15(4):332–47.

214. Gahete MD, Córdoba-Chacón J, Kineman RD, Luque RM, Castaño JP. Role of ghrelin system in neuroprotection and cognitive functions: implications in Alzheimer's disease. Peptides. novembre 2011;32(11):2225–8.

215. Lim E, Lee S, Li E, Kim Y, Park S. Ghrelin protects spinal cord motoneurons against chronic glutamate-induced excitotoxicity via ERK1/2 and phosphatidylinositol-3-kinase/Akt/glycogen synthase kinase-3β pathways. Experimental Neurology. 1 luglio 2011;230(1):114–22.

216. Liu F, Li Z, He X, Yu H, Feng J. Ghrelin Attenuates Neuroinflammation and Demyelination in Experimental Autoimmune Encephalomyelitis Involving NLRP3 Inflammasome Signaling Pathway and Pyroptosis. Front Pharmacol. 6 novembre 2019;10:1320.

217. Chung H, Chung H-Y, Bae CW, Kim C-J, Park S. Ghrelin suppresses tunicamycin- or thapsigargin-triggered endoplasmic reticulum stress-mediated apoptosis in primary cultured rat cortical neuronal cells. Endocr J. 2011;58(5):409–20.

218. Vincent AM, Mobley BC, Hiller A, Feldman EL. IGF-I prevents glutamate-induced motor neuron programmed cell death. Neurobiology of Disease. luglio 2004;16(2):407–16.

219. Chung H, Seo S, Moon M, Park S. Phosphatidylinositol-3-kinase/Akt/glycogen synthase kinase-3β and ERK1/2 pathways mediate protective effects of acylated and unacylated ghrelin against oxygen–glucose deprivation-induced apoptosis in primary rat cortical neuronal cells. Journal of Endocrinology. 1 settembre 2008;198(3):511–21.

220. Philips T, Robberecht W. Neuroinflammation in amyotrophic lateral sclerosis: role of glial activation in motor neuron disease. Lancet Neurol. marzo 2011;10(3):253–63.

221. Liu J, Wang F. Role of Neuroinflammation in Amyotrophic Lateral Sclerosis: Cellular Mechanisms and Therapeutic Implications. Front Immunol. 2017;8:1005.

222. Frago LM, Chowen JA. Involvement of Astrocytes in Mediating the Central Effects of Ghrelin. Int J Mol Sci. 2 marzo 2017;18(3):536.

223. Dobrowolny G, Giacinti C, Pelosi L, Nicoletti C, Winn N, Barberi L, et al. Muscle expression of a local Igf-1 isoform protects motor neurons in an ALS mouse model. J Cell Biol. 17 gennaio 2005;168(2):193–9.

224. Dobrowolny G, Aucello M, Molinaro M, Musarò A. Local expression of mIgf-1 modulates ubiquitin, caspase and CDK5 expression in skeletal muscle of an ALS mouse model. Neurol Res. marzo 2008;30(2):131–6.

225. Riddoch-Contreras J, Yang S-Y, Dick JRT, Goldspink G, Orrell RW, Greensmith L. Mechano-growth factor, an IGF-I splice variant, rescues motoneurons and improves muscle function in SOD1(G93A) mice. Exp Neurol. febbraio 2009;215(2):281–9.

226. Shandilya A, Mehan S. Dysregulation of IGF-1/GLP-1 signaling in the progression of ALS: potential target activators and influences on neurological dysfunctions. Neurol Sci. 21 maggio 2021;

227. Cooper C, Burden ST, Cheng H, Molassiotis A. Understanding and managing cancer-related weight loss and anorexia: insights from a systematic review of qualitative research. J Cachexia Sarcopenia Muscle. marzo 2015;6(1):99–111.

228. Chen J-A, Splenser A, Guillory B, Luo J, Mendiratta M, Belinova B, et al. Ghrelin prevents tumour- and cisplatin-induced muscle wasting: characterization of multiple mechanisms involved. J Cachexia Sarcopenia Muscle. giugno 2015;6(2):132–43.

229. Bresciani E, Rizzi L, Molteni L, Ravelli M, Liantonio A, Ben Haj Salah K, et al. JMV2894, a novel growth hormone secretagogue, accelerates body mass recovery in an experimental model of cachexia. Endocrine. ottobre 2017;58(1):106–14.

230. Conte E, Camerino GM, Mele A, De Bellis M, Pierno S, Rana F, et al. Growth hormone secretagogues prevent dysregulation of skeletal muscle calcium homeostasis in a rat model of cisplatin-induced cachexia. J Cachexia Sarcopenia Muscle. giugno 2017;8(3):386–404.

231. Granado M, Priego T, Martín AI, Villanúa MA, López-Calderón A. Ghrelin receptor agonist GHRP-2 prevents arthritis-induced increase in E3 ubiquitin-ligating enzymes MuRF1 and MAFbx gene expression in skeletal muscle. Am J Physiol Endocrinol Metab. dicembre 2005;289(6):E1007-1014.

232. Sugiyama M, Yamaki A, Furuya M, Inomata N, Minamitake Y, Ohsuye K, et al. Ghrelin improves body weight loss and skeletal muscle catabolism associated with angiotensin II-induced cachexia in mice. Regul Pept. 10 ottobre 2012;178(1–3):21–8.

233. Porporato PE, Filigheddu N, Reano S, Ferrara M, Angelino E, Gnocchi VF, et al. Acylated and unacylated ghrelin impair skeletal muscle atrophy in mice. J Clin Invest. febbraio 2013;123(2):611–22.

234. Sirago G, Conte E, Fracasso F, Cormio A, Fehrentz J-A, Martinez J, et al. Growth hormone secretagogues hexarelin and JMV2894 protect skeletal muscle from mitochondrial damages in a rat model of cisplatin-induced cachexia. Sci Rep. 12 2017;7(1):13017.

235. Zhang Y, Pan X, Sun Y, Geng Y-J, Yu X-Y, Li Y. The Molecular Mechanisms and Prevention Principles of Muscle Atrophy in Aging. Adv Exp Med Biol. 2018;1088:347–68.

236. Kamiji MM, Inui A. The role of ghrelin and ghrelin analogues in wasting disease. Curr Opin Clin Nutr Metab Care. luglio 2008;11(4):443–51.

237. Frago LM, Baquedano E, Argente J, Chowen JA. Neuroprotective actions of ghrelin and growth hormone secretagogues. Front Mol Neurosci. 2011;4:23.

238. Liantonio A, Gramegna G, Carbonara G, Sblendorio VT, Pierno S, Fraysse B, et al. Growth hormone secretagogues exert differential effects on skeletal muscle calcium homeostasis in male rats depending on the peptidyl/nonpeptidyl structure. Endocrinology. ottobre 2013;154(10):3764–75.

239. Pang J-J, Xu R-K, Xu X-B, Cao J-M, Ni C, Zhu W-L, et al. Hexarelin protects rat cardiomyocytes from angiotensin II-induced apoptosis in vitro. Am J Physiol Heart Circ Physiol. marzo 2004;286(3):H1063-1069.

240. Müller TD, Nogueiras R, Andermann ML, Andrews ZB, Anker SD, Argente J, et al. Ghrelin. Mol Metab. giugno 2015;4(6):437–60.

241. Seminara RS, Jeet C, Biswas S, Kanwal B, Iftikhar W, Sakibuzzaman M, et al. The Neurocognitive Effects of Ghrelin-induced Signaling on the Hippocampus: A Promising Approach to Alzheimer's Disease. Cureus. 11 settembre 2018;10(9):e3285.

242. Moulin A, Demange L, Bergé G, Gagne D, Ryan J, Mousseaux D, et al. Toward potent ghrelin receptor ligands based on trisubstituted 1,2,4-triazole structure. 2. Synthesis and pharmacological in vitro and in vivo evaluations. J Med Chem. 15 novembre 2007;50(23):5790–806.

243. Demange L, Boeglin D, Moulin A, Mousseaux D, Ryan J, Bergé G, et al. Synthesis and pharmacological in vitro and in vivo evaluations of novel triazole derivatives as ligands of the ghrelin receptor. 1. J Med Chem. 19 aprile 2007;50(8):1939–57.

244. Bresciani E, Rizzi L, Molteni L, Ravelli M, Liantonio A, Ben Haj Salah K, et al. JMV2894, a novel growth hormone secretagogue, accelerates body mass recovery in an experimental model of cachexia. Endocrine. ottobre 2017;58(1):106–14.

245. Muccioli G, Papotti M, Locatelli V, Ghigo E, Deghenghi R. Binding of 125I-labeled ghrelin to membranes from human hypothalamus and pituitary gland. J Endocrinol Invest. marzo 2001;24(3):RC7-9.

246. Davenport AP, Bonner TI, Foord SM, Harmar AJ, Neubig RR, Pin J-P, et al. International Union of Pharmacology. LVI. Ghrelin receptor nomenclature, distribution, and function. Pharmacol Rev. dicembre 2005;57(4):541–6.

247. Lucchi C, Costa AM, Giordano C, Curia G, Piat M, Leo G, et al. Involvement of PPARγ in the Anticonvulsant Activity of EP-80317, a Ghrelin Receptor Antagonist. Front Pharmacol. 2017;8:676.

248. Biagini G, Torsello A, Marinelli C, Gualtieri F, Vezzali R, Coco S, et al. Beneficial effects of desacyl-ghrelin, hexarelin and EP-80317 in models of status epilepticus. European Journal of Pharmacology. 16 novembre 2011;670(1):130–6.

249. Cásedas G, Les F, Choya-Foces C, Hugo M, López V. The Metabolite Urolithin-A Ameliorates Oxidative Stress in Neuro-2a Cells, Becoming a Potential Neuroprotective Agent. Antioxidants. 21 febbraio 2020;9(2):177.

250. Sathya S, Shanmuganathan B, Devi KP. Deciphering the anti-apoptotic potential of α-bisabolol loaded solid lipid nanoparticles against Aβ induced neurotoxicity in Neuro-2a cells. Colloids and Surfaces B: Biointerfaces. giugno 2020;190:110948.

251. Corradin SB, Mauël J, Donini SD, Quattrocchi E, Ricciardi-Castagnoli P. Inducible nitric oxide synthase activity of cloned murine microglial cells. Glia. marzo 1993;7(3):255–62.

252. Losurdo M, Pedrazzoli M, D'Agostino C, Elia CA, Massenzio F, Lonati E, et al. Intranasal delivery of mesenchymal stem cell-derived extracellular vesicles exerts immunomodulatory and neuroprotective effects in a 3xTG model of Alzheimer's disease. STEM CELLS Transl Med. settembre 2020;9(9):1068–84.

253. Morrison H, Young K, Qureshi M, Rowe RK, Lifshitz J. Quantitative microglia analyses reveal diverse morphologic responses in the rat cortex after diffuse brain injury. Sci Rep. dicembre 2017;7(1):13211.

254. Fernández-Arjona M del M, Grondona JM, Granados-Durán P, Fernández-Llebrez P, López-Ávalos MD. Microglia Morphological Categorization in a Rat Model of Neuroinflammation by Hierarchical Cluster and Principal Components Analysis. Front Cell Neurosci. 8 agosto 2017;11:235.

255. Théry C, Amigorena S, Raposo G, Clayton A. Isolation and characterization of exosomes from cell culture supernatants and biological fluids. Curr Protoc Cell Biol. aprile 2006;Chapter 3:Unit 3.22.

256. D'Aloia A, Molteni L, Gullo F, Bresciani E, Artusa V, Rizzi L, et al. Palmitoylethanolamide Modulation of Microglia Activation: Characterization of Mechanisms of Action and Implication for Its Neuroprotective Effects. IJMS. 17 marzo 2021;22(6):3054.

257. Yune TY, Park HG, Lee JY, Oh TH. Estrogen-induced Bcl-2 expression after spinal cord injury is mediated through phosphoinositide-3-kinase/Akt-dependent CREB activation. J Neurotrauma. settembre 2008;25(9):1121–31.

258. Nanetti L, Raffaelli F, Vignini A, Perozzi C, Silvestrini M, Bartolini M, et al. Oxidative stress in ischaemic stroke. Eur J Clin Invest. dicembre 2011;41(12):1318–22.

259. Ramalingam M, Kim S-J. Reactive oxygen/nitrogen species and their functional correlations in neurodegenerative diseases. J Neural Transm (Vienna). agosto 2012;119(8):891–910.

260. Niedzielska E, Smaga I, Gawlik M, Moniczewski A, Stankowicz P, Pera J, et al. Oxidative Stress in Neurodegenerative Diseases. Mol Neurobiol. 2016;53(6):4094–125.

261. Uttara B, Singh AV, Zamboni P, Mahajan RT. Oxidative stress and neurodegenerative diseases: a review of upstream and downstream antioxidant therapeutic options. Curr Neuropharmacol. marzo 2009;7(1):65–74.

262. Barber SC, Shaw PJ. Oxidative stress in ALS: key role in motor neuron injury and therapeutic target. Free Radic Biol Med. 1 marzo 2010;48(5):629–41.

263. Lin MT, Beal MF. Mitochondrial dysfunction and oxidative stress in neurodegenerative diseases. Nature. ottobre 2006;443(7113):787–95.

264. Saccon RA, Bunton-Stasyshyn RKA, Fisher EMC, Fratta P. Is SOD1 loss of function involved in amyotrophic lateral sclerosis? Brain. agosto 2013;136(Pt 8):2342–58.

265. Dupuis L, Gonzalez de Aguilar J-L, Oudart H, de Tapia M, Barbeito L, Loeffler J-P. Mitochondria in amyotrophic lateral sclerosis: a trigger and a target. Neurodegener Dis. 2004;1(6):245–54.

266. Smith EF, Shaw PJ, De Vos KJ. The role of mitochondria in amyotrophic lateral sclerosis. Neurosci Lett. 25 settembre 2019;710:132933.

267. Gutteridge JM. Lipid peroxidation and antioxidants as biomarkers of tissue damage. Clin Chem. dicembre 1995;41(12 Pt 2):1819–28.

268. Kassie F, Parzefall W, Knasmüller S. Single cell gel electrophoresis assay: a new technique for human biomonitoring studies. Mutat Res. luglio 2000;463(1):13–31.

269. Kannan null, Jain null. Oxidative stress and apoptosis. Pathophysiology. settembre 2000;7(3):153–63.

270. Enari M, Sakahira H, Yokoyama H, Okawa K, Iwamatsu A, Nagata S. A caspase-activated DNase that degrades DNA during apoptosis, and its inhibitor ICAD. Nature. 1 gennaio 1998;391(6662):43–50.

271. Fernandez PC, Machado J, Heussler VT, Botteron C, Palmer GH, Dobbelaere DA. The inhibition of NF-kappaB activation pathways and the induction of apoptosis by dithiocarbamates in T cells are blocked by the glutathione precursor N-acetyl-L-cysteine. Biol Chem. dicembre 1999;380(12):1383–94.

272. Duangjan C, Rangsinth P, Zhang S, Gu X, Wink M, Tencomnao T. Neuroprotective Effects of Glochidion zeylanicum Leaf Extract against H2O2/Glutamate-Induced Toxicity in Cultured Neuronal Cells and Aβ-Induced Toxicity in Caenorhabditis elegans. Biology (Basel). 19 agosto 2021;10(8):800.

273. Sala G, Beretta S, Ceresa C, Mattavelli L, Zoia C, Tremolizzo L, et al. Impairment of glutamate transport and increased vulnerability to oxidative stress in neuroblastoma SH-SY5Y cells expressing a Cu,Zn superoxide dismutase typical of familial amyotrophic lateral sclerosis. Neurochemistry International. febbraio 2005;46(3):227–34.

274. Kumar KH, Khanum F. Hydroalcoholic extract of cyperus rotundus ameliorates H2O2-induced human neuronal cell damage via its anti-oxidative and anti-apoptotic machinery. Cell Mol Neurobiol. gennaio 2013;33(1):5–17.

275. Ghaffari H, Ghassam BJ, Chandra Nayaka S, Ramachandra Kini K, Prakash HS. Antioxidant and neuroprotective activities of Hyptis suaveolens (L.) Poit. against oxidative stress-induced neurotoxicity. Cell Mol Neurobiol. aprile 2014;34(3):323–31.

276. Liu B, Gao H-M, Wang J-Y, Jeohn G-H, Cooper CL, Hong J-S. Role of nitric oxide in inflammation-mediated neurodegeneration. Ann N Y Acad Sci. maggio 2002;962:318–31.

277. Kim PKM, Zamora R, Petrosko P, Billiar TR. The regulatory role of nitric oxide in apoptosis. International Immunopharmacology. agosto 2001;1(8):1421–41.

278. Kim S-J, Han Y. Insulin inhibits AMPA-induced neuronal damage via stimulation of protein kinase B (Akt). J Neural Transm (Vienna). febbraio 2005;112(2):179–91.

279. Mahesh R, Bhuvana S, Begum VMH. Effect of Terminalia chebula aqueous extract on oxidative stress and antioxidant status in the liver and kidney of young and aged rats. Cell Biochem Funct. agosto 2009;27(6):358–63.

280. Bulgarelli I, Tamiazzo L, Bresciani E, Rapetti D, Caporali S, Lattuada D, et al. Desacyl-ghrelin and synthetic GH-secretagogues modulate the production of inflammatory cytokines in mouse microglia cells stimulated by beta-amyloid fibrils. J Neurosci Res. settembre 2009;87(12):2718–27.

281. Torsello A, Bresciani E, Ravelli M, Rizzi L, Bulgarelli I, Ricci G, et al. Novel domain-selective ACE-inhibiting activity of synthetic growth hormone secretagogues. Pharmacol Res. ottobre 2012;66(4):317–24.

282. Johansson I, Destefanis S, Aberg ND, Aberg MAI, Blomgren K, Zhu C, et al. Proliferative and protective effects of growth hormone secretagogues on adult rat hippocampal progenitor cells. Endocrinology. maggio 2008;149(5):2191–9.

283. Brywe KG, Leverin A-L, Gustavsson M, Mallard C, Granata R, Destefanis S, et al. Growth Hormone-Releasing Peptide Hexarelin Reduces Neonatal Brain Injury and Alters Akt/Glycogen Synthase Kinase-3β Phosphorylation. Endocrinology. 1 novembre 2005;146(11):4665–72.

284. Barlind A, Karlsson N, Åberg ND, Björk-Eriksson T, Blomgren K, Isgaard J. The growth hormone secretagogue hexarelin increases cell proliferation in neurogenic regions of the mouse hippocampus. Growth Hormone & IGF Research. 1 febbraio 2010;20(1):49–54.

285. Fetler L, Amigorena S. Neuroscience. Brain under surveillance: the microglia patrol. Science. 15 luglio 2005;309(5733):392–3.

286. Griffin WS, Sheng JG, Royston MC, Gentleman SM, McKenzie JE, Graham DI, et al. Glial-neuronal interactions in Alzheimer's disease: the potential role of a «cytokine cycle» in disease progression. Brain Pathol. gennaio 1998;8(1):65–72.

287. Agbo E, Li M-X, Wang Y-Q, Saahene R-O, Massaro J, Tian G-Z. Hexarelin protects cardiac H9C2 cells from angiotensin II-induced hypertrophy via the regulation of autophagy. Pharmazie. 1 agosto 2019;74(8):485–91.

288. Carson JA, Hardee JP, VanderVeen BN. The emerging role of skeletal muscle oxidative metabolism as a biological target and cellular regulator of cancer-induced muscle wasting. Semin Cell Dev Biol. giugno 2016;54:53–67.

289. Zoccal KF, Gardinassi LG, Bordon KCF, Arantes EC, Marleau S, Ong H, et al. EP80317 Restrains Inflammation and Mortality Caused by Scorpion Envenomation in Mice. Front Pharmacol. 2019;10:171.

290. Bessi VL, Labbé SM, Huynh DN, Ménard L, Jossart C, Febbraio M, et al. EP 80317, a selective CD36 ligand, shows cardioprotective effects against post-ischaemic myocardial damage in mice. Cardiovasc Res. 1 ottobre 2012;96(1):99–108.

291. Bujold K, Mellal K, Zoccal KF, Rhainds D, Brissette L, Febbraio M, et al. EP 80317, a CD36 selective ligand, promotes reverse cholesterol transport in apolipoprotein E-deficient mice. Atherosclerosis. agosto 2013;229(2):408–14.

292. Ashkenazi A, Salvesen G. Regulated cell death: signaling and mechanisms. Annu Rev Cell Dev Biol. 2014;30:337–56.

293. Kwon S-H, Kim J-A, Hong S-I, Jung Y-H, Kim H-C, Lee S-Y, et al. Loganin protects against hydrogen peroxide-induced apoptosis by inhibiting phosphorylation of JNK, p38, and ERK 1/2 MAPKs in SH-SY5Y cells. Neurochem Int. marzo 2011;58(4):533–41.

294. He MT, Lee AY, Park CH, Cho EJ. Protective effect of Cordyceps militaris against hydrogen peroxide-induced oxidative stress in vitro. Nutr Res Pract. agosto 2019;13(4):279–85.

295. Ramalingam M, Kim S-J. Insulin involved Akt/ERK and Bcl-2/Bax pathways against oxidative damages in C6 glial cells. J Recept Signal Transduct Res. 2016;36(1):14–20.

296. Zhang R, Chae S, Lee JH, Hyun JW. The cytoprotective effect of butin against oxidative stress is mediated by the up-regulation of manganese superoxide dismutase expression through a PI3K/Akt/Nrf2-dependent pathway. J Cell Biochem. giugno 2012;113(6):1987–97.

297. Chong ZZ, Li F, Maiese K. Oxidative stress in the brain: novel cellular targets that govern survival during neurodegenerative disease. Prog Neurobiol. febbraio 2005;75(3):207–46.

298. Hui L, Pei D-S, Zhang Q-G, Guan Q-H, Zhang G-Y. The neuroprotection of insulin on ischemic brain injury in rat hippocampus through negative regulation of JNK signaling pathway by PI3K/Akt activation. Brain Res. 2 agosto 2005;1052(1):1–9.

299. Turturici G, Tinnirello R, Sconzo G, Geraci F. Extracellular membrane vesicles as a mechanism of cell-to-cell communication: advantages and disadvantages. Am J Physiol Cell Physiol. 1 aprile 2014;306(7):C621-633.